Pontifícia Universidade Católica
do Rio de Janeiro

**Maurício da Silva Cunha Galvão**

# Analytical Models for Thermal Wellbore Effects on Pressure Transient Testing

**Dissertação de Mestrado**

Dissertation presented to the Programa de Pós-graduação em Engenharia Mecânica of PUC-Rio in partial fullfillment of the requirements for the degree of Mestre em Engenharia Mecânica

Advisor: Prof. Márcio da Silveira Carvalho

Co-Advisor: Prof. Abelardo Borges Barreto Jr.

Rio de Janeiro
August 2018

Pontifícia Universidade Católica
do Rio de Janeiro

**Maurício da Silva Cunha Galvão**

# Analytical Models for Thermal Wellbore Effects on Pressure Transient Testing

Dissertation presented to the Programa de Pós-graduação em Engenharia Mecânica of PUC-Rio in partial fulfillment of the requirements for the degree of Mestre em Engenharia Mecânica. Approved by the undersigned Examination Committee.

**Prof. Márcio da Silveira Carvalho**
Advisor
Departamento de Engenharia Mecânica – PUC-Rio

**Prof. Abelardo Borges Barreto Jr.**
Co-Advisor
Departamento de Engenharia Mecânica – PUC-Rio

**Prof. Alvaro Marcello Marco Peres**
Centro de Ciências Exatas e Tecnologia – UENF

**Dr. Daniel Nunes de Miranda Filho**
PETROBRAS - Petróleo Brasileiro S.A.

**Prof. Sinesio Pesco**
Departamento de Matemática – PUC-Rio

**Dr. Mustafa Onur**
University of Tulsa – TU

**Prof. Márcio da Silveira Carvalho**
Vice Dean of Graduate Studies
Centro Técnico Científico – PUC-Rio

Rio de Janeiro, August 3rd, 2018

**Maurício da Silva Cunha Galvão**

The author graduated in Industrial Engineering from PUC-Rio – 2007. The author has worked at ExxonMobil, PricewaterhouseCoopers and PUC-Rio between the years of 2006 and 2010. In 2010, the author has been admitted to Petrobras at the position of Petroleum Engineer. The author holds a postgraduate degree in petroleum engineering from Petrobras Corporate University (2011, Brazil). The author holds a postgraduate degree in Reservoir Geo-Engineering from the consortium formed by UNICAMP, UNESP, University of Aveiro, IST school of engineering of the University of Lisbon and the Faculty of Sciences of the University of Lisbon (2012, Brazil and Portugal).



Bibliographic data

Galvão, Maurício da Silva Cunha

Analytical models for thermal wellbore effects on pressure transient testing / Maurício da Silva Cunha Galvão ; advisor: Márcio da Silveira Carvalho ; co-advisor: Abelardo Borges Barreto Jr. – 2018.
166 f. : il. color. ; 30 cm

Dissertação (mestrado) – Pontifícia Universidade Católica do Rio de Janeiro, Departamento de Engenharia Mecânica, 2018.
Inclui bibliografia

1. Engenharia Mecânica – Teses. 2. Teste de Pressão em Poços de Petróleo. 3. Transientes de Temperatura. 4. Coeficiente Joule-Thomson. 5. Acoplamento Poço/ Reservatório. 6. Transformada de Laplace. I. Carvalho, Márcio da Silveira. II. Barreto Junior, Abelardo Borges. III Pontifícia Universidade Católica do Rio de Janeiro. Departamento de Engenharia Mecânica. IV. Título.

CCD: 621

To my parents, for all support
and encouragement.

## Acknowledgements

I would like to thank my advisor Prof. Márcio da Silveira Carvalho and my co-advisor Prof. Abelardo Borges Barreto Jr. for their advice and guidance through the course of this work. I also would like to express my gratitude to the engineer Priscila Magalhães Ribeiro for all her assistance during this research.

I want to thank Petrobras for giving me opportunity to perform this study and for providing the field data analyzed in this research. I am thankful to the well-test group from Petrobras, especially to the engineer Christiane de Camargo, for all support throughout my career.

I am also grateful to my committee members, Prof. Mustafa Onur, Prof. Alvaro Peres, Prof. Sinesio Pesco and Dr. Daniel Miranda, for dedicating their time and expertise to evaluate and enrich this work.

Most especially, I want to thank my family for all support. My parents, my brother and my wife have always encouraged me to go further.

Lastly, I would like to thank PUC-Rio and CAPES for the financial support.

## Abstract

Galvão, Maurício da Silva Cunha; Carvalho, Márcio da Silveira (Advisor); Barreto Jr., Abelardo Borges (Co-Advisor). **Analytical Models for Thermal Wellbore Effects on Pressure Transient Testing.** Rio de Janeiro, 2018. 166p. Dissertação de Mestrado – Departamento de Engenharia Mecânica, Pontifícia Universidade Católica do Rio de Janeiro.

This work presents a new coupled transient-wellbore/reservoir thermal analytical model, consisting of a reservoir/casing/tubing combined system. The analytical solutions consider flow of a slightly compressible, single-phase fluid in a homogeneous infinite-acting reservoir system and provide temperature- and pressure-transient data for drawdown and buildup tests at any gauge location along the wellbore, accounting for Joule-Thomson, adiabatic fluid-expansion, conduction and convection effects. The wellbore fluid mass density is modeled as a function of temperature and the analytical solution makes use of the Laplace transformation to solve the transient heat-flow differential equation, accounting for a rigorous transient wellbore-temperature gradient $\partial T/\partial z$. Regarding pressure transient analysis (PTA), thermal impacted pressure data may lead to the interpretation of false geological heterogeneities, since the heat loss during the buildup period provides an increase in the pressure exerted by the wellbore-fluid column, due to an increase in the oil mass density, and a change in tubing length, consequently causing a change in the gauge location. These effects can make a homogeneous reservoir be wrongly interpreted as a double-porosity reservoir, yielding invalid conclusions to geological modeling. Results are compared to the response of a commercial non-isothermal simulator and thermal impacts on PTA interpretations are thoroughly investigated. In addition, a field case study is also provided to verify the proposed analytical solutions. The proposed model provides more accurate transient temperature flow profiles along the wellbore when compared to previous models in Literature.



## Keywords

Pressure Transient Analysis; Transient Temperature Data; Joule-Thomson Coefficient; Coupled Wellbore/Reservoir System; Laplace Transformation.

# Resumo

Galvão, Maurício da Silva Cunha; Carvalho, Márcio da Silveira (Orientador); Barreto Jr., Abelardo Borges (Co-Orientador). **Modelos Analíticos de Efeitos Térmicos em Testes de Pressão Transiente** Rio de Janeiro, 2018. 166p. Dissertação de Mestrado – Departamento de Engenharia Mecânica, Pontifícia Universidade Católica do Rio de Janeiro.

Este trabalho apresenta um novo modelo térmico analítico que acopla poço e reservatório, constituído por um sistema combinado de reservatório, revestimento e coluna de produção. As soluções analíticas consideram fluxo monofásico de fluido pouco compressível em um reservatório homogêneo e infinito e fornecem dados transitórios de temperatura e pressão ao longo do poço para testes de fluxo e de crescimento de pressão, considerando efeitos Joule-Thomson, de expansão adiabática, de condução e convecção. A massa específica do fluido é modelada como função da temperatura e a solução analítica faz uso da transformada de Laplace para resolver a equação diferencial de fluxo de calor transiente, assumindo o termo $\partial T/\partial z$ totalmente transiente. Com relação à análise de transientes de pressão (PTA), dados de pressão impactados por variações térmicas podem levar à interpretação de falsas heterogeneidades geológicas, pois a perda de calor durante a estática proporciona um aumento da pressão exercida pela coluna de fluido, devido ao incremento de sua massa específica, além de uma contração da coluna de produção, provocando uma mudança na posição do registrador. Esses efeitos podem fazer com que um reservatório homogêneo seja erroneamente interpretado como um reservatório de dupla porosidade, resultando em conclusões inválidas para a modelagem geológica. Os resultados deste trabalho são comparados com a resposta de um simulador comercial não-isotérmico e impactos nas interpretações são extensivamente investigados. Adicionalmente, um estudo de caso de campo é fornecido para validar as soluções analíticas propostas. Comparado à Literatura, o modelo proposto fornece perfis transientes de temperatura mais acurados.



## Palavras-chave

Teste de Pressão em Poços de Petróleo; Transientes de Temperatura; Coeficiente Joule-Thomson; Acoplamento Poço/Reservatório; Transformada de Laplace.

## Table of Contents

## List of Figures

## List of Tables

## Nomenclature

$a$ = Parameter defined by Eq. (3.12)
$a_o$ = Constant defined by Eq. (2.23)
$A$ = Cross-sectional area of the pipe
$B$ = Formation volume factor
$c$ = Isothermal compressibility
$C_1$ = Conversion factor
$C_2$ = Conversion factor
$C_3$ = Constant defined by Eq. (2.53)
$C_4$ = Conversion factor
$C_5$ = Conversion factor
$C_{iso}$ = Conversion factor
$c_p$ = Specific heat capacity
$c_{pR}$ = Ratio of volumetric-heat capacity of fluid to volumetric heat-capacity of fluid-saturated porous medium, defined by Eq. (2.7)
CPG1 = First coefficient in gas-phase heat-capacity correlation used in the CMG-STARS simulator
CPG2 = Second coefficient in gas-phase heat-capacity correlation used in the CMG-STARS simulator
$C_T$ = Thermal-storage coefficient
$E_f$ = Energy of the fluid per length
$E_w$ = Energy of the wellbore per length
$g$ = Gravitational acceleration
$g_c$ = Conversion factor, 1 kg.m/(N.s²)
$g_G$ = Geothermal gradient
$g$ = Gravitational acceleration
$h$ = Reservoir thickness
$H$ = Specific enthalpy
$J$ = Conversion factor, 1 N.m/J
$k$ = Permeability
$L_0$ = Pipe length between the gauge and the fixed point at shut-in
$L_R$ = Relaxation distance, defined by Eq. (3.4)
$L_\beta$ = Relaxation distance considering the fluid property $\beta_o \varepsilon_{JTo} \gamma_{oi}$, defined by Eq. (3.27)
$p$ = Pressure
$p_c$ = Critical pressure
$Q$ = Volumetric-flow rate at standard conditions
$q$ = Volumetric-flow rate at bottomhole conditions
$r$ = Radius

$r_w$ = Wellbore radius
$s$ = Fluid saturation
$S$ = Skin factor
SNR = Signal-to-noise ratio defined by Eq. (4.36)
$t$ = Time
$T$ = Temperature
$T_c$ = Critical temperature
$T_{eibh}$ = Earth temperature at $z = 0$ and $t = 0$
$u$ = Laplace variable
$u_c$ = Velocity of convective-heat transfer
$U_t$ = Overall heat-transfer coefficient
$v$ = Darcy's velocity
$z_c$ = Distance from the producing horizon to the bottom of the tubing string
$z_g$ = Gauge location (distance from the producing horizon)
$\alpha$ = Thermal diffusivity
$\alpha_{LTE}$ = Pipe linear thermal expansion coefficient
$\beta$ = Isobaric-thermal-expansion coefficient
$\gamma$ = Fluid specific weight or the Euler-Mascheroni constant
$\delta(x)$ = Dirac Delta function
$\Delta L$ = Change in pipe length
$\Delta t$ = Buildup (or shut-in) time
$\Delta T_z^{(0+)}$ = Wellbore buildup initial condition defined by Eq. (3.59)
$\varepsilon_{JT}$ = Joule-Thomson-expansion coefficient
$\eta$ = Hydraulic diffusivity
$\theta$ = Wellbore angle with the horizontal
$\Theta(x)$ = Heaviside Step function
$\lambda$ = Thermal conductivity
$\mu$ = Fluid viscosity
$\xi$ = Boltzmann transformation variable defined by Eq. (2.40)
$\rho$ = Mass Density
$\tau$ = Parameter defined by Eqs. (4.29) and (4.30)
$\phi$ = Porosity
$\varphi$ = Adiabatic-expansion coefficient
$\Phi$ = Function defined by Eq. (3.9)
$\psi$ = Parameter defined by Eq. (3.26)
$\omega$ = Acentric factor used in the CMG-STARS simulator
$\Omega$ = Parameter defined by Eq. (3.28)

**Superscripts**

$*$ = Effective
$BC$ = Boundary condition
$res$ = Reservoir

**Subscripts**

$a$ = Adjustable gauge location
$an$ = Annulus
$bh$ = Bottomhole
$BU$ = Buildup
$c$ = Casing
$cem$ = Cement
$ci$ = Inside-casing
$co$ = Outside-casing
$D$ = Dimensionless
$DD$ = Drawdown
$e$ = Formation adjacent to the wellbore or outer radius
$f$ = Fluid between the gauge and the producing horizon
$g$ = Gauge
$gc$ = Gauge placed in a casing string
$gt$ = Gauge placed in a tubing string
$i$ = Initial conditions
$o$ = Oil
$p$ = Producing condition prior to shut-in, isobaric or pipe
$r$ = Rock or radial direction
$S$ = Skin zone
$sf$ = Sandface
$t$ = Total system (rock plus fluid) or tubing/test string
$T$ = Isothermal
$ti$ = Inside-tubing
$to$ = Outside-tubing
$w$ = Water or wellbore
$wall$ = Pipe wall
$wp$ = Well condition during the producing period
$ws$ = Well condition during the shut-in period

# 1
# Introduction

The process of flowing a well and monitoring pressure, temperature and flow rate data, followed by the interpretation of these data, is called well testing. The available interpretation methods assume the isothermal hypothesis, i.e., they do not consider the influence of temperature on pressure data. This assumption is valid for several cases, nonetheless it may not be reasonable under some well-testing operational conditions and reservoir parameters. In particular, the pressure response measured far above the producing horizon in high transmissibility reservoirs can be severely affected by temperature effects.

This work develops a new coupled transient-wellbore/reservoir thermal analytical model designed to provide temperature-transient data for drawdown and buildup tests at any gauge location in the wellbore. The wellbore fluid mass density is modeled as a function of temperature and the wellbore-temperature gradient $\partial T/\partial z$ is not a known input to solve the transient problem. The analytical solution makes use of the Laplace transformation to solve the heat-flow differential equation and the resulting model accounts for a fully coupled reservoir/casing/tubing system. The analytical model considers a slightly compressible fluid under single-phase flow in an infinite-acting reservoir, accounting for Joule-Thomson (J-T), adiabatic fluid-expansion, conduction and convection effects. Moreover, the pipe-contraction effect due to temperature changes during buildup is taken into account.

Results are compared to the rigorous response of a commercial non-isothermal simulator (CMG STARS, 2017). In addition, a field case study is provided.

## 1.1.
## Well-Testing Operations

Well testing can be defined as a group of planned procedures and equipment designed to acquire the necessary data to enable the understanding of the potential

of a reservoir. Both near-wellbore and far-field parameters can be determined, providing valuable information for reservoir characterization. Together with geological, geophysical and petrophysical data, well-test analysis is used to build reservoir models designed to predict field performance, such as the evolution of pressure depletion and fluid saturation. In essence, well testing comprises the monitoring of flow rates, pressure, and temperature while the reservoir is in a transient state. Due to recent studies, the acquisition and interpretation of downhole temperature has gained special attention.

A typical well test lasts about 2 - 7 days, however in the case of reservoir limit testing several months of data may be required. This kind of test is known as Extended Well Test (EWT). One of the main differences of well-test data from other data sources (e.g., core plugs) is that they provide a description of the reservoir in dynamic conditions and at a larger scale. Pressure transient analysis (PTA) consists of applying mathematical models together with measured rates and pressures to determine well and reservoir properties. The main outcomes are:

1. Productivity index (PI) and skin factor S;
2. Radial and vertical permeabilities;
3. Reservoir heterogeneities, such as flow barriers;
4. Reservoir initial/average pressure, reservoir boundaries and volume.

Additionally, well tests also enable downhole fluid sampling at reservoir conditions.



### 1.1.1. Types of Transient Well Tests

The execution of a well test consists of measuring the reservoir response in the form of pressure and temperature changes due to an input impulse, being a change in flow rate. The reservoir response depends on a series of rock and fluid parameters, such as fluid viscosity, permeability, skin factor and flow barriers.

There are several types of transient tests. The most common ones are:

- **Drawdown test**: a shut-in well in stable condition is opened to flow at a constant production rate and the flowing bottomhole pressure is used for analysis. In practice, it is difficult to keep a well producing at a constant rate, hence drawdown data are often not conclusive.

- **Buildup test**: In this type of test, a well flowing at a nearly constant rate is shut in and the increase of bottomhole pressure is used for analysis. The main advantage of buildup tests is that the surface rate can be kept at a constant value (zero). This is by far the most common well-test configuration.
- **Injection test and fall-off test**: these tests are analogous to those previously described, however, instead of producing, a flow rate is imposed upon the well. Multiphase flow may occur, providing a more complex behavior of pressure transient data.
- **Interference test**: while another well is producing or injecting, the changes in bottomhole pressure are observed in a shut-in well. The main outcome of this test is to evaluate communication between wells.

### 1.1.2. Well-Testing Data Acquisition

The flow rate is measured at surface, and the pressure and temperature data are measured at a downhole gauge, placed relatively close to perforations. Some wells may not be completed with a downhole gauge, hence measurements are taken at the wellhead.

A special case occurs when the well is completed temporarily with a downhole tester valve, and a drill stem test (DST) is conducted. Frequently the well is already cased, and the test string is instrumented with a downhole gauge.

Some well tests may be designed to run a production logging tool (PLT), which is used to measure rate, fluid density, pressure, and temperature at the producing zones. The main outcome of this operation is the flow distribution across the perforations, being of special importance in cases of thick and heterogeneous reservoirs.

### 1.1.3. Well-Test Interpretation Methods

Well-test interpretation is an inverse problem, since inputs and outputs are known and the system has to be determined. Interpretation methods combine pressure and flow rate data to estimate wellbore and reservoir parameters. In

essence, pressure-data interpretation entails matching real data to a mathematical model, from which reservoir parameters can be inferred.

The most usual technique for analyzing variable pressure and rate problems is to apply *Superposition-Time functions*, e.g., *Agarwal Equivalent Time* (Agarwal, 1980). The work of van Everdingen and Hurst (1949) addressed the superposition principle to solve the variable terminal rate case. In essence, the authors made use of Duhamel's principle, which had been previously used to solve heat-flow and electric-circuit problems, and successfully applied it to pressure diffusivity in porous medium. They presented a solution in terms of a convolution integral for the pressure drop in a continuously varying flow scenario.

Horner (1951) made use of the superposition principle to evaluate pressure buildup tests (PBU), presenting a method based on the solution of the infinite-acting radial flow, for a single and constant flow rate period followed by a shut-in period. The method calculates reservoir permeability, skin factor, and initial pressure through straight-line analysis.

Russell (1963) applied the superposition principle to the two-rate test case. The author developed a method capable of estimating formation permeability, skin factor, and average reservoir pressure. Odeh and Jones (1965) then extended this solution for multi-rate tests.

The type curve analysis technique was introduced by Ramey (1970) and provided a way to identify the proper theoretical reservoir model to match real data. Gringarten et al. (1979) presented a type curve commonly known as the *Gringarten type curve*, which plotted $p_D$ against $t_D/C_D$ for different values of $C_D e^{2S}$, with great importance for well-test analysis. Agarwal (1980) presented a method that copes with producing time effects and allows the use of drawdown type curves for analyzing pressure buildup data.

The introduction of the derivative method by Bourdet et al. (1989) was a turning point in well-test analysis. The method made it possible to understand and recognize heterogeneous behaviors, such as double-permeability and composite reservoirs, and handle a wide range of boundary effects (Gringarten, 2006). The pressure derivative method comprises plotting both the pressure change and the pressure derivative with respect to the natural logarithm of time against the logarithm of time. The method has greater diagnosis capabilities in comparison to the analysis of the change in pressure itself, enabling the identification of several

flow regimes at early, middle and late times. Moreover, this method is the most common tool for verification and incorporation of well-test data into reservoir models.

Later, von Schroeter et al. (2001) introduced an effective algorithm for variable rate pressure data deconvolution. This technique converts variable-rate pressure data into a constant single-rate drawdown with a duration equal to the total duration of the test. The result provides an extension of the radius of investigation, and the application of the derivative method to deconvolved data allows the identification of additional geological features not seen in individual flow periods.

## 1.2. Literature Review

Wellbore heat transfer has been a subject of study in the oil and gas industry over the past decades and gained special attention in recent years due to the improvement in temperature measurement technologies. Downhole temperature monitoring devices can now provide high accuracy and a resolution better than 0.01 K (Duru and Horne, 2011a; Muradov and Davies, 2012; Sidorova et al., 2015). Due to this technological advance, several studies have proposed combined analyses of transient pressure and temperature data to enhance the information obtained from downhole gauges, in order to better characterize near-wellbore and far-field reservoir parameters. Literature provides analytical, semi-analytical, and numerical models for predicting both sandface and wellbore temperatures.

The classical work of Ramey (1962) provided an approximate solution to the transient heat-conduction problem in a vertical injection well, where the temperature of the wellbore system (fluids, tubing and casing) is a function of depth and time. The solution assumes a steady-state thermal energy balance in the wellbore, while the heat transfer to the rock formation occurs under transient radial conduction. The well is modeled as a line source and the net heat flow resistance in the wellbore caused by the fluid inside the tubing, tubing wall, fluid in the annulus, casing wall and cement is modeled by an overall heat transfer coefficient. Ramey's model provides reasonably accurate results after sufficient long elapsed times, nevertheless it may introduce substantial deviations from reality, especially at early times (Hasan and Kabir, 1991). Willhite (1967) developed a method to determine

the value of the overall heat-transfer coefficient, considering the radial thermal resistances of each of the aforementioned wellbore elements.

Curtis and Witterholt (1973) presented a method for determining individual zone flow rates in producing wells using dynamic temperature logging data. The method comprised an adaptation of Ramey's solution for producing wells. Horne and Shinohara (1979) presented another modification of Ramey's model for both production and injection wells to calculate heat losses along the wellbore to evaluate reservoir temperature.

Sagar et al. (1991) provided a multiphase flow model, accounting for kinetic energy and Joule-Thomson (J-T) effects. Hasan and Kabir (1991) studied the early-time thermal behavior and proposed a transient-diffusion temperature function considering a finite-size wellbore. The authors represented the heat transfer at the formation/wellbore interface by the Fourier law of heat conduction. The model provided more accurate results at early times when compared to Ramey's model.

Alves et al. (1992) developed a general model for predicting flow temperature profiles in wellbores and pipelines in a multiphase flow condition, accounting for conduction, convection and Joule-Thomson effects. Moreover, the model can be applied to any wellbore inclination angle.

Hasan et al. (1997) stated that wellhead pressure (WHP) cannot be translated into bottomhole pressure (BHP) by simply adding the hydrostatic head to it. The authors concluded that transient thermal effects must be taken into account for the correct pressure translation. The authors have developed a numerical wellbore model and assumed a steady-state fluid-temperature profile.

A method to compute the bottomhole pressure (BHP) from wellhead pressure (WHP) was proposed by Hasan et al. (2005). An analytical single-phase flow wellbore-temperature equation was developed to predict transient temperature profiles along the wellbore for drawdown and buildup tests, accounting for J-T effects and conserving momentum iteratively. Regarding transient well testing, the authors concluded that high transmissibility reservoirs might not yield representative translations of WHP to BHP data. Moreover, the authors concluded that flow capacity ($kh$) is the most important parameter to be considered in the context of transient testing and quality of results are improved with increasing flow rates.

Izgec et al. (2007) presented a wellbore simulator coupled with a semi-analytical temperature formulation for transient drawdown and buildup tests. The authors concluded that a numerical differentiation procedure can be used to overcome the limitation imposed by assuming a constant overall heat-transfer coefficient, especially for early-time transients.

The models previously discussed considered the heat transfer along the wellbore with fluid entering the well at a constant temperature from the reservoir. Sui et al. (2008a, 2008b) proposed a single-phase coupled wellbore-reservoir thermal model, assuming that pressure and temperature equations are decoupled. The temperature equation accounts for J-T effects and adiabatic expansion/compression by using a finite-difference method. The pressure is obtained from analytical solutions considering isothermal flow of slightly compressible fluid with constant isothermal compressibility and viscosity. Later, Sui et al. (2010) extended the model to single-phase gas flow. The authors proposed a multilayer testing method intended to investigate formation properties in commingled multilayered reservoirs, including damaged zone permeability and radius.

App (2009, 2010) presents field cases of non-isothermal behavior due to J-T and transient fluid expansion/compression effects, where either a cooling or a heating response is observed after rate changes. The author evaluates the impact of thermal effects considering a high drawdown scenario using a single-phase thermal simulator in which the oil viscosity depends on both temperature and pressure. The author concludes that a significant increase in well the productivity index may occur due to the improved mobility in the near-wellbore region. Besides, conventional well-test analysis considers constant viscosity, hence an overestimation of the near-wellbore permeability and an underestimation of the skin factor may occur.

Duru and Horne (2010a, 2010b, 2011a, 2011b) developed a thermal model in which pressure and temperature equations are decoupled, accounting for heat convection and conduction, J-T and adiabatic effects. The authors use a semi-analytical method to estimate reservoir and fluid parameters and conclude that temperature provides an additional source of information in transient analysis in comparison to conventional well-test analysis. Near-wellbore features, such as fracture network permeability, skin-zone permeability and skin-zone radius, can be

obtained. Furthermore, the authors present a well-test design that addresses the necessary procedures to guarantee useful temperature data.

Ribeiro and Horne (2013) investigated the application of transient temperature analysis in the context of hydraulic fracturing operations. The authors developed a coupled well-fracture-reservoir thermal model, which accounts for heat convection and conduction, J-T and adiabatic effects. The energy balance is coupled with the mass balance and geomechanical relationships. The authors concluded that transient temperature analysis is capable of reducing the uncertainty related to fracture length and reservoir permeability. Ribeiro and Horne (2016) extended the model to the case of multiple fractures along a horizontal well. The authors demonstrated that temperature data can provide valuable information regarding the existence of multiple fractures and any eventual crossflow between them.

Sidorova et al. (2014) investigated the impact of downhole gauge location on conventional pressure transient analysis in the case of high-productivity reservoirs. The authors used a transient thermal reservoir numerical model, which considers heat convection and conduction, J-T and adiabatic effects. The model also accounts for mixing of fluids in the well, heat transfer between wellbore fluid and formation, and heat caused by friction. The authors show the effects of temperature changes on pressure during buildup periods, when downhole temperature decreases. The increase of wellbore fluid mass density and tubing contraction lead to a decrease in the hydrostatic pressure over time between the gauge and the perforations. The authors provide a procedure for translating the recorded pressure to a corresponding isothermal condition. Nonetheless, the authors conclude that the resulting reconstructed data carry high uncertainty from the viewpoint of transient testing interpretation. Sidorova et al. (2015) used the same reservoir numerical model to evaluate the application of temperature transient data in different testing scenarios. In particular, the authors show the effects on wellbore temperature data caused by mud circulation, fluid losses, and cementing.

An analytical solution was presented by Chevarunotai et al. (2015) to calculate the temperature distribution in a reservoir under a constant-rate single-phase flow, incorporating the energy exchange from the reservoir to the over-burden and under-burden formations. The energy balance accounts for convection and J-T effects and neglects radial heat conduction and adiabatic expansion effects.

Mao and Zeidouni (2017) presented a method to incorporate fluid property variations in analytical solutions of temperature transient analysis. According to the authors, assuming constant fluid properties can result in significant errors when modeling transient temperature data in the case of high drawdown conditions. The authors identified that viscosity causes the largest impact on temperature data and the correct treatment of this fluid property by the application of the proposed method provides better results to the existing analytical solutions.

In a series of papers, Onur and Cinar (2016, 2017a), Palabiyik et al. (2016) and Onur et al. (2016a) presented semilog straight line and temperature logarithmic-time derivative methods for interpreting temperature transient data jointly with pressure transient analysis. Solutions for both constant-rate drawdown and buildup tests are provided considering a line-sink well in a single-layer infinite-acting homogeneous reservoir under single-phase flow of a slightly compressible fluid of constant compressibility and viscosity. The proposed analytical solution for the thermal energy-balance equation is decoupled from the pressure solution, and it is expressed explicitly in terms of temperature and J-T coefficients of oil and connate water. Early- and late-time approximate solutions for the buildup period are provided, whereas a complete solution for the drawdown period is derived. Results successfully reproduce the response of a commercial non-isothermal simulator and it is shown that decoupling pressure and temperature equations is a valid assumption. Therefore, sandface transient-pressure data under non-isothermal flow can be interpreted by conventional methods. Sandface-temperature responses for both drawdown and buildup periods are thoroughly investigated. The authors show that drawdown-sandface temperature at early times presents a cooling behavior, dominated by the fluid adiabatic expansion. During late times, the sandface temperature is dominated by the Joule-Thomson effect, providing a heating response for oil flow. The buildup-sandface temperature presents an increase at early times due to the compression of the fluid near the wellbore. As for late-time data, temperature is dominated by Joule-Thomson and conduction effects, yielding a cooling response. Another important conclusion shows that the presence of a skin zone has a dominant effect on drawdown- and buildup-sandface temperatures at early and intermediate times, when temperature is controlled by skin-zone properties. Among other important contributions, the authors provide a

methodology to estimate skin-zone permeability and skin-zone radius, consisting of semilog and derivative analyses of drawdown and buildup temperatures.

Onur et al. (2016b, 2017) extended the previous study by developing analytical and semi-analytical thermal models, considering a coupled wellbore-reservoir system. This important improvement allowed the investigation of transient-temperature measurements along the wellbore during drawdown and buildup tests, accounting for sandface-temperature changes. Moreover, the proposed semi-analytical non-isothermal model accounts for wellbore storage and momentum effects.

Onur and Cinar (2017b) extended the solutions to account for heat losses to strata in the reservoir. Besides, the authors presented solutions for the general case of variable surface-rate production history. Onur (2017) reviewed the interpretation methods and provided additional analyses regarding the previous results.

## 1.3. Conceptual Model

Classical well-test analysis assumes an isothermal wellbore/reservoir system. Nonetheless, the real system is non-isothermal, and the influence of temperature in pressure data may induce PTA to indicate false geological features.

The most significant impact of temperature changes on pressure data occurs during a buildup test. After a stabilized flow period, the wellbore-temperature distribution is higher than the Earth original temperature in depth. When the well is shut in, the wellbore fluid does not take long to start cooling due to thermal radial diffusion to the surroundings. The heat loss causes the wellbore fluid mass density to vary with time, consequently the pressure exerted by the static fluid between the downhole gauge and the perforations also varies with time. Moreover, depending on the type of well completion, expansion joints may allow the tubing to contract during buildup, changing the gauge location.

The classical assumption of a constant static-fluid pressure, which is the base of conventional PTA interpretation methods, may fail for some wellbore/reservoir systems.

Figure 1.1 illustrates a simplified wellbore/reservoir system with a gauge placed above the perforations.

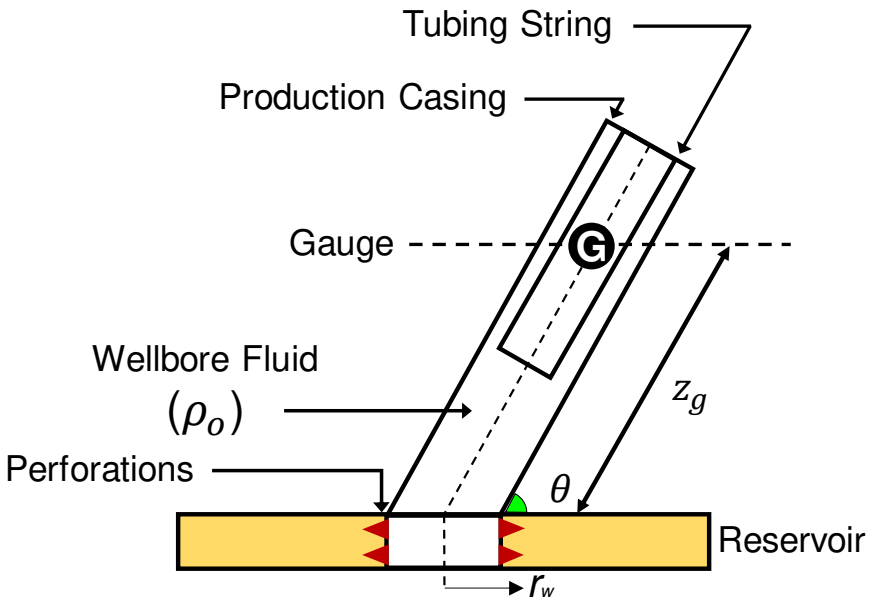


Figure 1.1: Simplified Wellbore/Reservoir System

For an isothermal system, the pressure at the gauge located in a slanted wellbore is described by the well-known hydrostatic expression (assuming negligible effect of pressure on the fluid mass density)

$$p_g(z_g, t) = p_{sf}(t) - \rho_o g z_g \sin\theta, \tag{1.1}$$

where $p_{sf}$ refers to the sandface pressure, $g$ is the acceleration of gravity, $z_g$ is the gauge distance from perforations, $\rho_o$ is the fluid mass density and $\theta$ is the inclination angle with the horizontal.

Under the isothermal hypothesis, the hydrostatic pressure is constant. Consequently, the derivative of pressure gauge data used for interpretation is equal to the sandface pressure derivative.

$$\left(\frac{\partial p_g}{\partial \ln t}\right)_{isothermal} = \frac{\partial p_{sf}}{\partial \ln t}. \tag{1.2}$$

Yet, under the real non-isothermal condition, the gauge derivative data in Eq. (1.2) may fail to describe the reservoir, since the fluid mass density is a function of temperature and pressure, which are functions of time and depth. Moreover, the gauge location may change due to tubing expansion or contraction. Hence, the generalized non-isothermal expression for pressure gauge data is given by

$$p_g(z_g,t) = p_{sf}(t) - \int_0^{z_g+\Delta L(t)} \rho_o(z,t) g \sin\theta \, dz, \tag{1.3}$$

where $\Delta L(t)$ represents the change in tubing length over time. The logarithmic-time derivative of Eq. (1.3) is given by

$$\frac{\partial p_g}{\partial \ln t} = \frac{\partial p_{sf}}{\partial \ln t} - g \sin\theta \frac{\partial}{\partial \ln t}\left(\int_0^{z_g+\Delta L(t)} \rho_o(z,t) dz\right). \tag{1.4}$$

The result in Eq. (1.4) leads to the conclusion that Eq. (1.2) is only valid when

$$\frac{\partial p_{sf}}{\partial \ln t} \gg g \sin\theta \frac{\partial}{\partial \ln t}\left(\int_0^{z_g+\Delta L(t)} \rho_o(z,t) dz\right). \tag{1.5}$$

In high transmissibility reservoirs, the sandface-pressure derivative is small, hence the isothermal hypothesis is not valid. Moreover, it is also clear in Eq. (1.5) that a gauge placed far from perforations also discredits the isothermal hypothesis. Therefore, the use of isothermal methods depends on an intrinsic relation between the reservoir transmissibility and the gauge location. Among other results, this work provides an analytical expression to calculate the maximum gauge distance given a specific non-isothermal wellbore/reservoir system.

## 1.4. Research Objectives

The main objective of this research is to solve the integral in Eq. (1.3), thus providing the means to understand and interpret well tests under non-isothermal conditions.

A fully coupled transient reservoir/casing/tubing thermal analytical model will be provided, accounting for Joule-Thomson, adiabatic fluid-expansion, conduction and convection effects. The wellbore fluid mass density will be modeled as function of temperature and the wellbore-temperature gradient $\partial T/\partial z$ is not a known input for the transient problem. Moreover, the change in pipe length will be taken into account.

Once the transient thermal analytical model is derived, an analytical solution for the integral in Eq. (1.3) can be obtained, which is the pressure exerted by the wellbore fluid as a function of time and depth. As a result, the wellbore cooling behavior during buildup tests can be analytically determined, hence permitting a thorough assessment of thermal impacts on PTA interpretations.

## 1.5. Dissertation Outline

This dissertation is organized in eight chapters, including the Introduction and the Conclusions.

Chapter 2 describes the mathematical modeling of the energy balance in the reservoir. This chapter derives a new analytical solution for the reservoir buildup temperature that applies from early to late shut-in times.

Chapter 3 describes the mathematical modeling of the energy balance for a fully coupled reservoir/casing/tubing system. This chapter derives new analytical solutions for both drawdown and buildup transient-wellbore temperatures. The solutions account for a temperature-dependent fluid mass density $\rho_o(T)$ and do not assume any approximation for the transient wellbore-temperature gradient $\partial T/\partial z$ to solve the partial-differential equation that describes the transient-wellbore-temperature distribution.

Chapter 4 uses the derived transient-wellbore solutions to describe the variation of the fluid mass density and the change in tubing length over time and depth. The integral in Eq. (1.3) is solved, yielding a fully analytical solution for the time dependent pressure exerted by the wellbore-fluid column during the buildup period. Moreover, practical and easy to compute metrics are derived for evaluating whether a particular wellbore/reservoir system fails under the isothermal hypothesis.

Chapter 5 presents the verification of results. Verifications are performed by comparing the derived analytical solutions to the response of a commercial non-isothermal simulator (CMG-STARS, 2017).

Chapter 6 presents synthetic case studies, where thermal impacts on PTA interpretations are investigated. It will be shown how the thermal effects can affect interpretation results.

Chapter 7 presents a field case study, where thermal impacts on pressure data are assessed at two different depths during a real DST operation. The proposed analytical solution in this work was able to reproduce the real data and to provide the true reservoir characterization, mitigating the risk of interpreting false heterogeneities. All wellbore, reservoir and fluid properties are provided, allowing

replication of results. Moreover, the production logging flow profile and the associated temperature curve are also provided.

Chapter 8 summarizes the results of this work, presents conclusions and outlines recommendations for further work.

# 2
# Analytical Reservoir-Temperature Solutions

This chapter presents analytical reservoir temperature solutions for both drawdown and buildup tests. First, the analytical single-rate drawdown solution developed by Onur and Cinar (2017a) is presented. Regarding the buildup period, the authors did not provide a complete solution, instead they derived analytical early- and late-time approximations.

At the end of this chapter, the mathematical formulation proposed by Onur and Cinar (2017a) is used as the basis to derive the proposed reservoir buildup-temperature solution, which applies from early to late shut-in times.



## 2.1.
## Pressure-Diffusion Equation

The well-known pressure-diffusion partial-differential equation is given by

$$\frac{1}{r}\frac{\partial}{\partial r}\left(r\frac{\partial p}{\partial r}\right) = \frac{\phi\mu_o c_t}{k_o}\frac{\partial p}{\partial t}, \tag{2.1}$$

where $\phi$ is the reservoir porosity, $\mu_o$ is the oil phase viscosity, $k_o$ is the effective oil permeability and $c_t$ is the fluid-saturated rock isothermal compressibility, defined by

$$c_t = s_o c_o + s_w c_w + c_r, \tag{2.2}$$

where the parameter $c$ is the isothermal compressibility and the subscripts $o, w$ and $r$ refer to the oil phase, aqueous phase and solid rock, respectively.

The derivation of Eq. (2.1) comprises the following assumptions:

1. The reservoir is homogeneous and isotropic;
2. Single-phase radial flow (oil with immobile connate water saturation);
3. Oil and water are slightly compressible fluids and are immiscible;
4. Fluid flow is governed by Darcy's law;
5. Rock and fluid properties are constant;
6. Well is vertical in the reservoir, fully penetrating the entire formation thickness;

7. Gravity and capillary effects are negligible;
8. The pressure and temperature equations are decoupled.

The next sections evaluate Eq. (2.1) under the appropriate initial and boundary conditions, in order to serve as a known input to the energy-balance equation.

## 2.2. Reservoir Energy-Balance Equation

In addition to the aforementioned assumptions, the non-isothermal reservoir model is based on the following assumptions (Onur and Cinar, 2017a):

1. Thermal properties of fluid and rock do not vary with pressure and temperature;
2. The solid matrix, oil and connate water are in local thermal equilibrium;
3. There exists no heat transfer to over- and under-burden strata from the reservoir.



The energy-balance partial-differential equation, which describes the temperature behavior for radial flow, is given by (Onur and Cinar 2017a)

$$\left(\rho c_p\right)_t \frac{\partial T}{\partial t} - \left(\rho c_p \varphi\right)_t \frac{\partial p}{\partial t} + \rho_o c_{po} \nu_{ro} \frac{\partial T}{\partial r} - \rho_o c_{po} \nu_{ro} \varepsilon_{JTo} \frac{\partial p}{\partial r} - \frac{1}{r}\frac{\partial}{\partial r}\left(\lambda_t \frac{\partial T}{\partial r}\right) = 0, \tag{2.3}$$

where the subscript $t$ refers to total system (fluid plus rock) properties. The parameter $\nu_{ro}$ represents the oil phase radial velocity, given by Darcy's equation,

$$\nu_{ro} = -\frac{k_o}{\mu_o}\frac{\partial p}{\partial r}. \tag{2.4}$$

The authors treat all physical and thermal properties of rock and fluid in Eqs. (2.3) and (2.4) as constant, hence the energy-balance equation can be expressed as

$$\frac{\partial T}{\partial t} + u_{co}(r,t)\frac{\partial T}{\partial r} - \frac{\alpha_t}{r}\frac{\partial}{\partial r}\left(r\frac{\partial T}{\partial r}\right) = \varphi_t^* \frac{\partial p}{\partial t} + \varepsilon_{JTo} u_{co}(r,t)\frac{\partial p}{\partial r}, \tag{2.5}$$

where $u_{co}$ is referred to as the velocity of convective heat transfer, defined by

$$u_{co}(r,t) = c_{pRo}\nu_{ro} = -c_{pRo}\frac{k_o}{\mu_o}\frac{\partial p}{\partial r}. \tag{2.6}$$

The parameter $c_{pRo}$ is the ratio of the volumetric-heat capacity of oil to the volumetric-heat capacity of the fluid-saturated porous medium, given by

$$c_{pRo} = \frac{\rho_o c_{po}}{(\rho c_p)_t}, \tag{2.7}$$

where $(\rho c_p)_t$ is the volumetric-heat capacity of the fluid-saturated porous medium, defined by

$$(\rho c_p)_t = \phi(s_o \rho_o c_{po} + s_w \rho_w c_{pw}) + (1-\phi)\rho_r c_{pr}\,. \tag{2.8}$$

In Eq. (2.5), $\alpha_t$ and $\varphi_t^*$ represent the thermal diffusivity and the effective adiabatic-expansion coefficient of the fluid-saturated rock, respectively, defined by

$$\alpha_t = \frac{\lambda_t}{(\rho c_p)_t}, \tag{2.9}$$

and

$$\varphi_t^* = \frac{(\rho c_p \varphi)_t}{(\rho c_p)_t}, \tag{2.10}$$

where $\lambda_t$ is the thermal conductivity of the fluid-saturated porous medium. The authors did not provide an explicit expression to calculate this parameter. Hence, this work adopts the default expression used by the non-isothermal simulator (CMG-STARS, 2017)

$$\lambda_t = \phi(s_w \lambda_w + s_o \lambda_o) + (1-\phi)\lambda_r, \tag{2.11}$$

where $\lambda$ is the thermal conductivity. The term $(\rho c_p \varphi)_t$ is referred to as the adiabatic-expansion coefficient of the fluid system, defined by

$$(\rho c_p \varphi)_t = \phi(s_o \rho_o c_{po} \varphi_o + s_w \rho_w c_{pw} \varphi_w). \tag{2.12}$$

The parameters $\rho, s, c_p$ and $\varphi$ represent the mass density, fluid saturation, isobaric-heat capacity and adiabatic-thermal expansion coefficient of fluid, respectively. The parameter $\varepsilon_{JTo}$ represents the oil phase Joule-Thomson coefficient.

The first term in the left-hand side (LHS) of Eq. (2.5) is the accumulation term and the third term refers to the conduction effect. The second term in the LHS and the second term in the right-hand side (RHS) of Eq. (2.5) refer to convection effects. The latter entails the Joule-Thomson expansion effect. The first term in the RHS of Eq. (2.5) refers to the fluid adiabatic expansion effect.

## 2.3. Constant-Rate Drawdown-Temperature Solution

Onur and Cinar (2017a) considered a line-sink well producing at a constant rate, in absence of wellbore effects, in an infinite-acting homogeneous reservoir with uniform thickness. The appropriate initial and boundary conditions for pressure are given by

$$\text{IC: } p(r, t = 0) = p_i, \tag{2.13}$$

$$\text{IBC: } \lim_{r \to 0} \left( r \frac{\partial p}{\partial r} \right) = C_2 \frac{Q_o B_o \mu_o}{k_o h}, \tag{2.14}$$

$$\text{OBC: } \lim_{r \to \infty} p(r, t) = p_i. \tag{2.15}$$

The parameter $C_2$ is a unit conversion factor (see Appendix A) and the oil rate at standard conditions is represented by the parameter $Q_o$.

The solution of Eq. (2.1) subject to the described conditions is the well-known expression

$$\Delta p(r, t) = p_i - p(r, t) = -\frac{1}{2} C_2 \frac{Q_o B_o \mu_o}{k_o h} \text{Ei}\left( -\frac{r^2}{4 C_1 \eta_o t} \right). \tag{2.16}$$

The parameter $C_1$ is a unit conversion factor (see Appendix A), $\eta_o$ is the effective oil hydraulic-diffusivity, defined by

$$\eta_o = \frac{k_o}{\phi \mu_o c_t}, \tag{2.17}$$

and $\text{Ei}(-x)$ is the exponential integral function.

Under the adopted assumptions, the solution for pressure is independent of temperature and the result in Eq. (2.16) is used to solve the energy-balance differential equation. The appropriate initial and boundary conditions for temperature are given by (Onur and Cinar, 2017a)

$$\text{IC: } T(r, t = 0) = T_i, \tag{2.18}$$

$$\text{IBC: } \lim_{r \to 0} \left( r \frac{\partial T}{\partial r} \right) = 0, \tag{2.19}$$

$$\text{OBC: } \lim_{r \to \infty} T(r, t) = T_i. \tag{2.20}$$

The inner-boundary condition in Eq. (2.19) describes an insulated wellbore at perforations. For the drawdown energy balance, Onur and Cinar (2017a) neglected the conduction term in Eq. (2.5) (third term in the LHS). The result is a first-order partial-differential equation, given by

$$\frac{\partial T}{\partial t} + u_{co}(r,t)\frac{\partial T}{\partial r} = \varphi_t^* \frac{\partial p}{\partial t} + \varepsilon_{JTo} u_{co}(r,t)\frac{\partial p}{\partial r}. \tag{2.21}$$

To solve Eq. (2.21) the authors decouple the pressure solution by using the result of Eq. (2.16), hence the RHS is a known input. Further, the authors applied the Boltzmann transformation to obtain the single-rate drawdown solution:

$$T(r,t) = T_i + \frac{1}{2}C_2\frac{Q_o B_o \mu_o}{k_o h}\left[\varepsilon_{JTo}\mathrm{Ei}\left(-\frac{r^2}{4C_1\eta_o t}\right) + \left(\varphi_t^* - \varepsilon_{JTo}\right)\mathrm{Ei}\left(-\frac{r^2}{4C_1\eta_o t} - a_o e^{\left(-\frac{r^2}{4C_1\eta_o t}\right)}\right)\right], \tag{2.22}$$

where $a_o$ is a constant defined by

$$a_o = \frac{1}{2}C_2\frac{c_{pRo}Q_o B_o}{\eta_o h}. \tag{2.23}$$

The sandface-temperature change is obtained by evaluating Eq. (2.22) at $r = r_w$. In presence of skin effects, the authors show that a good approximation for the sandface-temperature solution at early and intermediate times is obtained by using the skin zone altered permeability ($k_S$) in Eq. (2.22).



## 2.4. Buildup-Temperature Solution

Regarding the buildup period, Onur and Cinar (2017a) neglected the convective terms in Eq. (2.5), by assuming the fluid velocity to be negligible during the shut-in period. Therefore, the buildup energy balance can be expressed by the following second-order partial-differential equation:

$$\frac{\partial T}{\partial t} - \frac{\alpha_t}{r}\frac{\partial}{\partial r}\left(r\frac{\partial T}{\partial r}\right) = \varphi_t^*\frac{\partial p}{\partial t}. \tag{2.24}$$

The initial and boundary conditions are given by

$$\text{IC: } T\left(r, t = t_p\right) = T_p(r), \tag{2.25}$$

$$\text{IBC: } \lim_{r\to 0}\left(r\frac{\partial T}{\partial r}\right) = 0, \tag{2.26}$$

$$\text{OBC: } \lim_{r\to\infty} T(r,t) = T_i, \tag{2.27}$$

where $t_p$ is the producing time before shut-in and $T_p(r)$ represents the temperature distribution in the reservoir at shut-in, computed from Eq. (2.22) at $t = t_p$.

The authors propose a more convenient way to approach the problem, defining time and temperature differences, where $\Delta t$ represents the elapsed time

since the beginning of shut-in ($\Delta t = t - t_p$) and $\Delta T$ is the temperature difference for buildup, defined by

$$\Delta T(r, \Delta t) = T(r, \Delta t) - T_p(r). \tag{2.28}$$

The energy balance in Eq. (2.24) and the initial and boundary conditions can be rewritten as follows (Onur and Cinar, 2017a):

$$\text{PDE: } \frac{\partial \Delta T}{\partial \Delta t} - \frac{\alpha_t}{r}\frac{\partial}{\partial r}\left(r\frac{\partial \Delta T}{\partial r}\right) - \frac{\alpha_t}{r}\frac{\partial}{\partial r}\left(r\frac{\partial T_p}{\partial r}\right) = \varphi_t^*\frac{\partial p}{\partial \Delta t}, \tag{2.29}$$

$$\text{IC: } \Delta T(r, \Delta t = 0) = 0, \tag{2.30}$$

$$\text{IBC: } \lim_{r\to 0}\left(r\frac{\partial \Delta T}{\partial r}\right) = \lim_{r\to 0}\left(r\frac{\partial T}{\partial r}\right) - \lim_{r\to 0}\left(r\frac{\partial T_p}{\partial r}\right) = -C_2\frac{Q_o B_o \mu_o}{k_o h}\varepsilon_{JTo}, \tag{2.31}$$

$$\text{OBC: } \lim_{r\to\infty}\Delta T(r, \Delta t) = 0. \tag{2.32}$$

The inner-boundary condition in Eq. (2.31) is obtained from the combination of Eq. (2.26) and Eq. (2.22) evaluated at $t = t_p$.

Onur and Cinar (2017a) did not provide a complete solution, instead they derived asymptotic early- and late-time approximate solutions.

The early-time approximate solution considers that the temperature change is mainly caused by adiabatic compression, yielding the following expression at sandface:

$$\Delta T(r = r_w, \Delta t) = -\frac{1}{2}C_2\frac{Q_o B_o \mu_o}{k_o h}\varphi_t^*\text{Ei}\left(-\frac{r_w^2}{4C_1\eta_o \Delta t}\right). \tag{2.33}$$

For the late-time approximate solution, the authors neglected the adiabatic compression term and considered only the conduction terms. Moreover, the authors set the third term in the LHS of Eq. (2.29) as zero. The next subsection evaluates when this simplification may fail.

The late-time approximate solution is given by

$$\Delta T(r, \Delta t) = -\frac{1}{2}C_2\frac{Q_o B_o \mu_o}{k_o h}\varepsilon_{JTo}\text{Ei}\left(-\frac{r^2}{4\alpha_t \Delta t}\right), \tag{2.34}$$

where the sandface-temperature change is obtained by evaluating Eq. (2.34) at $r = r_w$.

All mathematical treatment and results up to this point were obtained from the formulations proposed by Onur and Cinar (2017a). The following subsection presents the novel solution for the buildup period.

### 2.4.1. Proposed Buildup-Temperature Solution

The proposed line-sink analytical solution in this work for the buildup initial boundary problem has been developed considering well-testing operational conditions, where producing and shut-in times are in the order of hours and flow rates range from hundreds to few thousands of m³/d. Furthermore, the solution does not take into account skin effects and assumes the porous medium not to be a low-permeability reservoir. These assumptions allow the derivation of a complete analytical solution that applies from early to late shut-in times. The verification of the solution is presented in Chapter 5.

The pressure difference for a buildup test after a constant production rate can be obtained by superimposing two constant-rate drawdown solutions (Horner, 1951)

$$p_i - p(r,\Delta t) = \Delta p\big(r, t_p + \Delta t\big) - \Delta p(r,\Delta t), \tag{2.35}$$

where $\Delta p$ is given by the constant-rate drawdown solution in Eq. (2.16).

Assuming a sufficiently long drawdown period, the derivative of Eq. (2.35) with respect to $\Delta t$ can approximated by:

$$\frac{\partial p(r,\Delta t)}{\partial \Delta t} \approx \frac{\partial \Delta p(r,\Delta t)}{\partial \Delta t} = \frac{1}{2} C_2 \frac{Q_o B_o \mu_o}{k_o h} \frac{1}{\Delta t} e^{\left(-\frac{r^2}{4C_1 \eta \Delta t}\right)}. \tag{2.36}$$

Eq. (2.36) neglects the pressure superposition effect. Indeed, for pressure analysis this assumption is not reasonable, nevertheless this approximation entails negligible impacts for the buildup-temperature problem, even for relatively long shut-in times. Therefore, the expression in Eq. (2.36) will be used to describe the pressure-derivative term in the RHS of Eq. (2.29).

Regarding the third term in the LHS of Eq. (2.29), it can be expanded into the following expression (adapted from Onur and Cinar, 2017a):

$$\frac{\alpha_t}{r}\frac{\partial}{\partial r}\left(r\frac{\partial T_p}{\partial r}\right) = \frac{1}{(\eta_o t_p)}\left[\frac{\alpha_t}{r}\frac{1}{2} C_2 \frac{Q_o B_o \mu_o e^{\left(-\frac{r^2}{4C_1 \eta_o t_p}\right)}}{4k_o h C_1}\right] \times \mathrm{Y}(r), \tag{2.37}$$

where

$$\mathrm{Y}(r) = -4\varepsilon_{JTo} r + \frac{4\left(\varphi_t^* - \varepsilon_{JTo}\right)\left[r a_o \left(4C_1\eta_o t_p\right) e^{\left(-\frac{r^2}{4C_1\eta_o t_p}\right)} - r^5\right]}{\left[\left(\frac{r^2}{4C_1\eta_o t_p}\right) + a_o e^{\left(-\frac{r^2}{4C_1\eta_o t_p}\right)}\right]^2}. \tag{2.38}$$

Following the same approach proposed by Onur and Cinar (2017a), this term will be set to zero. It is important to state that this assumption may fail for low flow capacity (*kh*) reservoirs and short drawdown times.

Under the adopted assumptions, the buildup energy-balance differential equation is given by

$$\frac{\partial \Delta T}{\partial \Delta t} - \frac{\alpha_t}{r}\frac{\partial}{\partial r}\left(r\frac{\partial \Delta T}{\partial r}\right) = \varphi_t^* \frac{1}{2} C_2 \frac{Q_o B_o \mu_o}{k_o h}\frac{1}{\Delta t} e^{\left(-\frac{r^2}{4C_1\eta \Delta t}\right)}. \tag{2.39}$$

Eq. (2.39) is a second-order linear partial-differential equation. The initial and boundary conditions are the same presented in Eqs. (2.30) through (2.32). The Boltzmann transformation will be used to solve the described problem.

The Boltzmann variable is defined by

$$\xi = \frac{r^2}{4\eta_o C_1 \Delta t}. \tag{2.40}$$

The transformation of the first term in the LHS of Eq. (2.39) is given by

$$\frac{\partial \Delta T}{\partial \Delta t} = \frac{\partial \Delta T}{\partial \xi}\left(\frac{r^2}{4\eta C_1}\right)\left(\frac{-1}{\Delta t^2}\right) = -\frac{\partial \Delta T}{\partial \xi}\xi\frac{1}{\Delta t}. \tag{2.41}$$

The second term in the LHS of Eq. (2.39) can be split into two terms:

$$\frac{\alpha_t}{r}\frac{\partial}{\partial r}\left(r\frac{\partial \Delta T}{\partial r}\right) = \frac{\alpha_t}{r}\frac{\partial \Delta T}{\partial r} + \alpha_t \frac{\partial^2 \Delta T}{\partial r^2}. \tag{2.42}$$

The transformation of each term in the RHS of Eq. (2.42) is given by, respectively,

$$\frac{\alpha_t}{r}\frac{\partial \Delta T}{\partial r} = \frac{\alpha_t}{r}\frac{\partial \Delta T}{\partial \xi}\frac{2r}{4\eta_o C_1 \Delta t} = \frac{\partial \Delta T}{\partial \xi}\left(\frac{\alpha_t}{2\eta_o C_1}\right)\frac{1}{\Delta t}, \tag{2.43}$$

and

$$\alpha_t \frac{\partial^2 \Delta T}{\partial r^2} = \frac{\partial^2 \Delta T}{\partial \xi^2}\xi\left(\frac{\alpha_t}{C_1\eta_o \Delta t}\right) + \frac{\partial \Delta T}{\partial \xi}\frac{1}{2}\left(\frac{\alpha_t}{C_1\eta_o \Delta t}\right). \tag{2.44}$$

Finally, the transformation of the RHS of Eq. (2.39) is given by

$$\varphi_t^* \frac{\partial p}{\partial \Delta t} = \varphi_t^* \frac{1}{2} C_2 \frac{Q_o B_o \mu_o}{k_o h}\frac{1}{\Delta t} e^{-\xi}. \tag{2.45}$$

The energy balance expressed in Eq. (2.39) can be rewritten as

$$-\frac{\partial \Delta T}{\partial \xi}\xi\frac{1}{\Delta t}-\frac{\partial \Delta T}{\partial \xi}\frac{1}{2}\frac{\alpha_t}{C_1\eta_o}\frac{1}{\Delta t}-\frac{\partial^2 \Delta T}{\partial \xi^2}\xi\frac{\alpha_t}{C_1\eta_o}\frac{1}{\Delta t}-\frac{\partial \Delta T}{\partial \xi}\frac{1}{2}\frac{\alpha_t}{C_1\eta_o}\frac{1}{\Delta t}=$$
$$=\varphi_t^*\frac{1}{2}C_2\frac{Q_oB_o\mu_o}{k_oh}\frac{1}{\Delta t}e^{-\xi}. \tag{2.46}$$

The transformations of the initial and outer-boundary conditions are given by

$$\Delta T(r,\Delta t=0)=\lim_{\xi\to\infty}\Delta T=0, \tag{2.47}$$

$$\lim_{r\to\infty}\Delta T(r,\Delta t)=\lim_{\xi\to\infty}\Delta T=0. \tag{2.48}$$

Note that the transformation of the initial condition is identical to the transformation of the outer-boundary condition. As for the inner-boundary condition,

$$\lim_{r\to 0}\left(r\frac{\partial \Delta T}{\partial r}\right)=\lim_{\xi\to 0}2\xi\frac{d\Delta T}{d\xi}=-C_2\frac{Q_oB_o\mu_o}{k_oh}\varepsilon_{JT}. \tag{2.49}$$

The multiplication of Eq. (2.46) by $(-\Delta t)$ and rearranging its terms yields the following second-order linear ordinary-differential equation:

$$\text{ODE: }\left(\xi\frac{\alpha_t}{C_1\eta_o}\right)\frac{d^2\Delta T}{d\xi^2}+\left(\frac{\alpha_t}{C_1\eta_o}+\xi\right)\frac{d\Delta T}{d\xi}=-C_3\varphi_t^*e^{-\xi}. \tag{2.50}$$

The appropriate boundary conditions for the transformed problem are given by

$$\text{BC: }\lim_{\xi\to\infty}\Delta T=0, \tag{2.51}$$

$$\text{BC: }\lim_{\xi\to 0}\xi\frac{d\Delta T}{d\xi}=-C_3\varepsilon_{JT}, \tag{2.52}$$

where the constant $C_3$ is defined by

$$C_3=\frac{1}{2}C_2\frac{Q_oB_o\mu_o}{k_oh}. \tag{2.53}$$

The solution of Eq. (2.50) subject to the conditions presented in Eqs. (2.51) and (2.52) is given by

$$\Delta T(\xi)=C_3\left\{\frac{\varphi_t^*}{\left(\frac{\alpha_t}{C_1\eta_o}-1\right)}\text{Ei}(-\xi)\right.$$
$$\left.-\left[\frac{\varphi_t^*}{\left(\frac{\alpha_t}{C_1\eta_o}-1\right)}+\varepsilon_{JTo}\right]\text{Ei}\left(-\frac{\xi}{\frac{\alpha_t}{C_1\eta_o}}\right)\right\}. \tag{2.54}$$

Finally, the solution expressed in terms of the original variables $r$ and $\Delta t$ is given by

$$\Delta T(r,\Delta t) = C_2 \frac{Q_o B_o \mu_o}{k_o h} \frac{1}{2} \times \left\{ \frac{\varphi_t^*}{\left(1-\frac{\alpha_t}{C_1 \eta_o}\right)} \left[ -\mathrm{Ei}\left(-\frac{r^2}{4C_1\eta_o \Delta t}\right) + \mathrm{Ei}\left(-\frac{r^2}{4\alpha_t \Delta t}\right) \right] - \varepsilon_{JTo} \mathrm{Ei}\left(-\frac{r^2}{4\alpha_t \Delta t}\right) \right\}. \quad (2.55)$$

In the RHS of Eq. (2.55), the first term inside the braces refers to the adiabatic-compression effect and provides a heating response, since the hydraulic-diffusion coefficient is much greater than the thermal-diffusion coefficient. Conversely, the second term entails a cooling behavior for oil flow, related to conduction and J-T effects. The solution is valid from early to late well-testing shut-in times and the temperature change is a result of the balance between the aforementioned heating and cooling effects.

The sandface-temperature change is obtained by evaluating Eq. (2.55) at $r = r_w$:

$$\Delta T(r_w,\Delta t) = C_2 \frac{Q_o B_o \mu_o}{k_o h} \frac{1}{2} \times \left\{ \frac{\varphi_t^*}{\left(1-\frac{\alpha_t}{C_1 \eta_o}\right)} \left[ -\mathrm{Ei}\left(-\frac{r_w^2}{4C_1\eta_o \Delta t}\right) + \mathrm{Ei}\left(-\frac{r_w^2}{4\alpha_t \Delta t}\right) \right] - \varepsilon_{JTo} \mathrm{Ei}\left(-\frac{r_w^2}{4\alpha_t \Delta t}\right) \right\}. \quad (2.56)$$

The logarithmic approximation of the exponential integral function yields

$$\Delta T(r_w,\Delta t) = C_2 \frac{Q_o B_o \mu_o}{k_o h} \frac{1}{2} \left\{ \frac{\varphi_t^*}{\left(1-\frac{\alpha_t}{C_1 \eta_o}\right)} \ln\left(\frac{\eta_o C_1}{\alpha_t}\right) + \varepsilon_{JTo} \ln\left(\frac{4\alpha_t \Delta t}{r_w^2 e^{\gamma}}\right) \right\}. \quad (2.57)$$

Note that only the J-T/conduction term is time dependent in this approximation. The adiabatic-compression effect occurs instantaneously at shut-in.

It is noteworthy to state that when $\Delta t \to \infty$ the solution given by Eq. (2.56) fails to describe the buildup-sandface temperature

$$\lim_{\Delta t \to \infty} \Delta T(r_w,\Delta t) = -\infty. \quad (2.58)$$

Nonetheless, in Chapter 5 the proposed solution is compared to the response of a commercial non-isothermal simulator and it is shown that the solution is valid from early to late shut-in times in the context of well testing.

# 3
# Analytical Transient-Wellbore-Temperature Solutions

This chapter presents a novel solution for the transient-wellbore-temperature distribution, where the fluid mass density is a function of temperature, and the wellbore comprises a fully coupled reservoir/casing/tubing system. Moreover, the wellbore-heat-flow partial-differential equation is modeled not making use of the classical approximation of using the wellbore-temperature gradient $\partial T/\partial z$ from the steady-state regime to solve the transient problem. This work will present complete transient analytical solutions for both drawdown and buildup tests.

The coupled non-isothermal wellbore/reservoir model is based on the following assumptions:

1. The wellbore accounts for an inclination angle $\theta$ above the perforations;
2. The volumetric rate along the wellbore is uniform, therefore wellbore storage (WBS) and momentum effects are neglected;
3. Fluid properties along the wellbore are constant, except for the fluid mass density, which depends on temperature;
4. There is cement between the formation adjacent to the wellbore and the outside-casing wall;
5. The casing-tubing annulus is filled with fluid (or an insulation material);
6. Tubing and casing account for finite walls and a packer isolates the casing-tubing annulus from the formation;
7. Wellbore components have constant thermal conductivities;
8. The gauge can be placed at any depth, including a location in the production casing below the bottom of the tubing string;
9. There is no friction loss along the wellbore;
10. Viscous dissipation effects are neglected;
11. Heat transfer to the surroundings occurs due to radial diffusion. There is no axial heat transfer;

12. The model accounts for Joule-Thomson and gravity effects;
13. Initial thermal equilibrium responds to the geothermal gradient;
14. Perforations are assumed to be a point source;
15. Tubing may contract or expand due to thermal effects, letting the gauge location be adjusted.

Regarding the last assumption, the wellbore completion may comprise expansion joints between the gauge and the packer used to compensate for tubing movement due to temperature changes. This work provides an analytical continuous solution that encompasses the effect of tubing contraction during shut-in. First, the solution for a fixed gauge location is obtained and then the effect of change in tubing length is incorporated. This effect will be addressed in Chapter 4.

Figure 3.1 shows a schematic of the coupled non-isothermal wellbore/reservoir system considered in this work. The wellbore is cased, cemented and completed with a production tubing. Moreover, there is a packer isolating the casing-tubing annulus, filled with annular fluid.



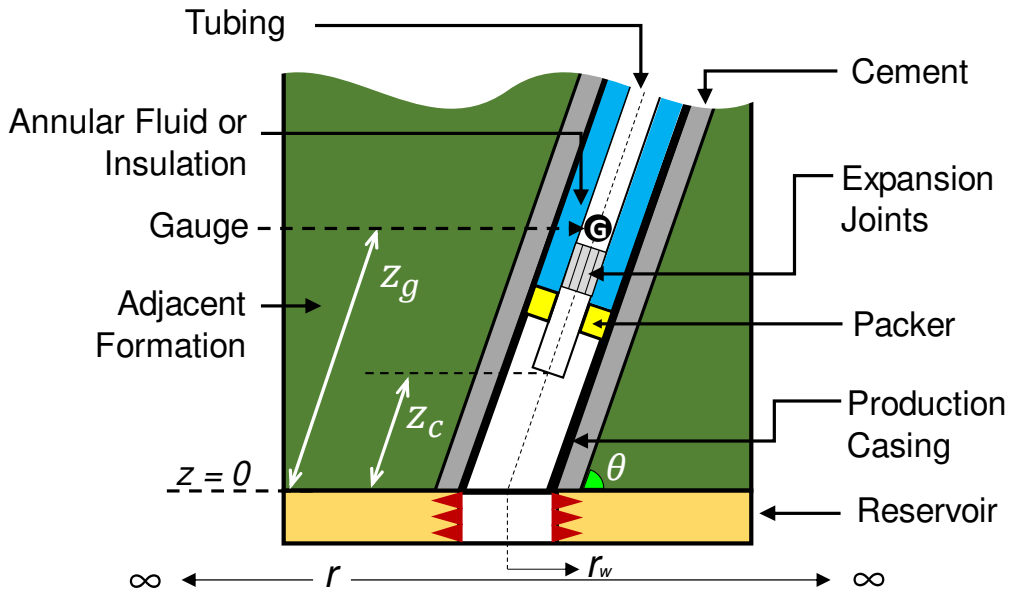


Figure 3.1: Schematic of the Coupled Wellbore/Reservoir System

In Figure 3.1, perforations are assumed to be a point source and the parameter $z_c$ is the distance between the producing horizon and the bottom of the tubing string. A finite perforated interval is out of the scope of this work, nonetheless the field case study in Chapter 7 provides an approach to circumvent this limitation.

## 3.1. Wellbore-Heat-Flow Model

The transient-wellbore-temperature distribution can be modeled by the following partial-differential equation (adapted from Hasan et al. (2005) and Onur et al. (2017)):

$$A(1+C_T)\frac{\partial T_w}{\partial t} = q_o L_R[T_{ei}(z) - T_w(z,t)] - q_o\left[\frac{\partial T_w}{\partial z} - \Phi(p_w, T_w) + \frac{g\sin\theta}{g_c c_{p_o} J}\right], \quad (3.1)$$

where $q_o$ is the volumetric oil rate at bottomhole conditions, $A$ is the cross-sectional area of the pipe and the subscript $w$ refers to properties inside the wellbore.

Eq. (3.1) considers the coordinate axis $z$ positive in the upward direction and the value of $z = 0$ is set at the producing horizon. The first term in the in the RHS of Eq. (3.1) refers to the heat loss to the formation and the second term represents the convective energy transport into and out of the control volume. The LHS of Eq. (3.1) refers to the accumulation term, where $C_T$ is the thermal-storage coefficient, defined by

$$C_T = \frac{E_w}{E_f}, \quad (3.2)$$

where $E_w$ is the energy of the wellbore per length and $E_f$ is the energy of the fluid per length. The thermal-storage represents the wellbore capacity to store or release heat and its value depends on a series of thermal, dimensional and operational parameters (Hasan et al., 2005).

$T_{ei}(z)$ is the initial Earth temperature distribution due to the geothermal gradient, defined by

$$T_{ei}(z) = T_{eibh} - z g_G \sin\theta, \quad (3.3)$$

where $T_{eibh}$ is the Earth temperature at $z = 0$ and $t = 0$. The geothermal gradient $g_G$ adopted in this study is the same value of $0.03$ K/m used by Onur et al. (2017). In Eq. (3.1), $g_c$ and $J$ are unit conversion factors and $L_R$ is the relaxation-distance parameter, defined by

$$L_R = \frac{2\pi r_{to} U_t \lambda_e}{\rho_o C_4 q_o c_{po}[\lambda_e + r_{to} U_t f_D(t_D)]}, \quad (3.4)$$

where $C_4$ is a unit conversion factor (see Appendix A), $U_t$ is the overall heat-transfer coefficient and $\lambda_e$ is the thermal conductivity of the formation adjacent to the

wellbore. For flow inside a cased tubing, the overall heat-transfer coefficient is defined by (Sagar et al., 1991)

$$U_t = \frac{1}{r_{ti}}\left[\frac{\ln(r_{ci}/r_{to})}{\lambda_{an}} + \frac{\ln(r_w/r_{co})}{\lambda_{cem}}\right]^{-1}. \tag{3.5}$$

In absence of a tubing, $U_t$ is defined by (Sagar et al., 1991)

$$U_t = \frac{1}{r_{ci}}\left[\frac{\ln(r_w/r_{co})}{\lambda_{cem}}\right]^{-1}. \tag{3.6}$$

In Eqs. (3.5) and (3.6), $r_{ti}$ is the inside-tubing radius, $r_{to}$ is the outside-tubing radius, $r_{ci}$ is the inside-casing radius, $r_{co}$ is the outside-casing radius, $\lambda_{an}$ is the thermal conductivity of the annular fluid and $\lambda_{cem}$ is the thermal conductivity of cement.

In this work, the finite wellbore model comprises a cased tubing (see Figure 3.1), therefore the parameters $A$ and $L_R$ vary with depth. In Eq. (3.4), $r_{to}$ is replaced by $r_{co}$ in the wellbore section without a tubing string.

In Eq. (3.4), $f_D(t_D)$ is the dimensionless heat-transfer function. Onur et al. (2017) uses the approximation proposed by Hasan and Kabir (2002). This work adopts the same expression, given by

$$f_D(t_D) = \ln\left[e^{-0.2t_D} + (1.5 - 0.3719e^{-t_D})\sqrt{t_D}\,\right], \tag{3.7}$$

where $t_D$ represents the dimensionless time, defined by (Onur et al., 2017)

$$t_D = \frac{\alpha_e}{r_{co}^2}t\,, \tag{3.8}$$

where $\alpha_e$ is the thermal-diffusivity coefficient of the formation adjacent to the wellbore. It is noteworthy to state that Hasan and Kabir (2002) define the dimensionless time $t_D$ with respect to the wellbore radius $r_w$.

The overall heat-transfer coefficient $U_t$ models the resistances to heat flow in the wellbore, and the relaxation distance $L_R$ can be viewed as the overall resistance for the formation/wellbore system (Hasan and Kabir, 2002). This parameter is the inverse of the parameter $A$ defined by Ramey (1962).

The parameter $\Phi(z,t)$ combines the Joule-Thomson effect and kinetic-energy contribution (Hasan et al., 2005). The parameter is given by (Onur et al., 2017)

$$\Phi(p_w, T_w) = \varepsilon_{JTo}\frac{\partial p_w}{\partial z} - \frac{q_o}{A^2 c_{po} g_c J}\frac{\partial q_o}{\partial z}. \tag{3.9}$$

The results to be given in this study are derived for a constant volumetric rate and viscous dissipation effects are neglected. Hence, Eq. (3.9) reduces to

$$\Phi(p_w, T_w) = \varepsilon_{JTo}\left(-\frac{\rho_o(p_w, T_w)g}{g_c}\right) = -\varepsilon_{JTo}\gamma_o(p_w, T_w), \tag{3.10}$$

where $g$ is the gravitational acceleration and $\gamma_o$ is the oil specific weight, which depends on pressure and temperature, therefore depends on $z$ and $t$.

The wellbore energy balance presented in Eq. (3.1) can be rewritten as

$$\frac{1}{a}\frac{\partial T_w}{\partial t} = L_R[T_{ei}(z) - T_w(z,t)] - \left[\frac{\partial T_w}{\partial z} + \varepsilon_{JTo}\gamma_o(z,t) + \frac{g\sin\theta}{g_c c_{p_o} J}\right], \tag{3.11}$$

where the constant $a$ is defined by (Onur et al., 2017)

$$a = \frac{C_4 q_o}{A(1 + C_T)}. \tag{3.12}$$

It is more convenient to work with the temperature difference, now defined by

$$\Delta T_w(z,t) = T_w(z,t) - T_{ei}(z). \tag{3.13}$$

The combination of Eqs. (3.3) and (3.13) yields

$$\Delta T_w(z,t) = T_w(z,t) - T_{eibh} + z g_G \sin\theta. \tag{3.14}$$

The temporal and spatial derivatives of $\Delta T_w$ are given by, respectively,

$$\frac{\partial \Delta T_w}{\partial t} = \frac{\partial T_w}{\partial t} - \frac{\partial T_{eibh}}{\partial t} + \frac{\partial (z g_G \sin\theta)}{\partial t} = \frac{\partial T_w}{\partial t}, \tag{3.15}$$

and

$$\frac{\partial \Delta T_w}{\partial z} = \frac{\partial T_w}{\partial z} - \frac{\partial T_{eibh}}{\partial z} + \frac{\partial (z g_G \sin\theta)}{\partial z} = \frac{\partial T_w}{\partial z} + g_G \sin\theta. \tag{3.16}$$

Then, the energy balance expressed in Eq. (3.11) can be rewritten as

$$\frac{1}{a}\frac{\partial \Delta T_w}{\partial t} = -L_R \Delta T_w - \left[\frac{\partial \Delta T_w}{\partial z} - g_G \sin\theta + \varepsilon_{JTo}\gamma_o(z,t) + \frac{g\sin\theta}{g_c c_{p_o} J}\right]. \tag{3.17}$$

The next subsection will provide an expression for the oil specific weight as a function of temperature. Then, the final expression for the energy-balance equation will be presented.

### 3.1.1. Oil Mass Density as a Function of Temperature

The oil specific weight $\gamma_o(z,t)$ in Eq. (3.17) is a direct function of the oil mass density, which depends on both pressure and temperature:

$$\gamma_o(p_w,T_w) = \rho_o(p_w,T_w)\frac{g}{g_c}. \tag{3.18}$$

The mass density can be related to the isothermal compressibility $c_o$ and the isobaric-thermal-expansion coefficient $\beta_o$, as described by the following equations:

$$c_o = \frac{1}{\rho_o}\left(\frac{\partial \rho_o}{\partial p}\right)_T, \tag{3.19}$$

and

$$\beta_o = -\frac{1}{\rho_o}\left(\frac{\partial \rho_o}{\partial T}\right)_p. \tag{3.20}$$

The combination of Eqs. (3.18) through (3.20) provides the expression for the oil specific weight

$$\gamma_o(p_w,T_w) = \gamma_{oi}e^{[c_o\Delta p-\beta_o(T_w-T_{eibh})]}, \tag{3.21}$$

where $\gamma_{oi}$ is a reference oil specific weight, evaluated at initial temperature $T_{eibh}$ and initial pressure $p_i$ at $z = 0$.

In this work, the adopted oil properties and well-testing operational features provide a product $\beta(T - T_{eibh})$ having a magnitude of 1E-2, being much greater than the product $c_o\Delta p$, which ranges from 1E-4 to 1E-3. Therefore, the pressure dependency will be neglected and the expression for the oil specific weight will be given by

$$\gamma_o(T_w) = \gamma_{oi}e^{[-\beta_o(T_w-T_{eibh})]}. \tag{3.22}$$

It is convenient to apply the Taylor series approximation to the expression in the form

$$e^{(-x)} \approx 1 - x. \tag{3.23}$$

Then, Eq. (3.22) can be written as

$$\gamma_o(T) = \gamma_{oi}[1 - \beta_o(T - T_{eibh})]. \tag{3.24}$$

The use of Eq. (3.14) in Eq. (3.24) provides the final expression for the oil specific weight:

$$\gamma_o(z,t) = \gamma_{oi}[1 - \beta_o(\Delta T_w - zg_G\sin\theta)]. \tag{3.25}$$

The next subsection provides the final expression for the wellbore energy-balance equation used to derive all transient-wellbore-temperature solutions.

### 3.1.2. Transient-Wellbore-Temperature Differential Equation

Regarding the terms in the energy-balance equation presented in Eq. (3.17), let the parameter $\psi$ be defined by (adapted from Onur et al., 2017)

$$\psi = g_G \sin\theta - \frac{\varepsilon_{JTo}\gamma_{oi}}{C_5} - \frac{g \sin\theta}{g_c c_{p_o} J}, \tag{3.26}$$

where $C_5$ is a unit conversion factor (see Appendix A). Due to the adopted assumptions, $\psi$ is constant.

It is convenient to define a new relaxation-distance parameter $L_\beta$, which accounts for the fluid thermal property $\beta_o \varepsilon_{JTo}\gamma_{oi}$, now defined by

$$L_\beta = L_R - \frac{\beta_o \varepsilon_{JTo}\gamma_{oi}}{C_5}. \tag{3.27}$$

Another important parameter defined in this work is Ω, given by

$$\Omega = \frac{g_G \beta_o \varepsilon_{JTo}\gamma_{oi} \sin\theta}{C_5}. \tag{3.28}$$

Finally, combining Eqs. (3.17), (3.25), (3.26), (3.27) and (3.28), the expression for the wellbore energy balance is given by

$$\frac{1}{a}\frac{\partial \Delta T_w}{\partial t} = -L_\beta \Delta T_w - \frac{\partial \Delta T_w}{\partial z} - z\Omega + \psi. \tag{3.29}$$

For well-testing applications, the parameter $L_R$ can be assumed constant, since $f_D(t_D)$ is a weak function of time (Hasan and Kabir, 2002) and changes in the oil mass density can be neglected for this parameter. Izgec et al. (2007) showed that this assumption is particularly reasonable for buildup tests. This approach follows the works of several authors, e.g., Hasan et al. (2005) and Onur et al. (2017). Consequently, the parameter $L_\beta$ is also constant.

Under the adopted assumptions, Eq. (3.29) is a first-order linear partial-differential equation. The appropriate initial and boundary conditions depend on the flow period, i.e., drawdown or buildup, and on the wellbore configuration.

The following sections derive the coupled analytical wellbore/reservoir temperature solutions.

## 3.2. Transient-Wellbore-Temperature Solutions: Drawdown Period

The wellbore-heat-flow drawdown problem considers the following initial condition:

$$\Delta T_w(z, t = 0) = 0. \tag{3.30}$$

Eq. (3.30) states that the wellbore is in thermal equilibrium with the formation at $t = 0$.

The boundary condition depends on whether there is a tubing in the wellbore. The solution for flow in a production casing and the solution for flow in a cased tubing are presented in this work.

The use of the Laplace transformation in Eq. (3.29) takes the problem to the Laplace domain with the Laplace-transform variable $u$ with respect to time $t$. The overbars denote the Laplace transformed quantities.

$$\mathcal{L}_t\{\Delta T_w(z,t)\}(u) = \overline{\Delta T}_w(z,u), \tag{3.31}$$

$$\frac{1}{a}\left(u\overline{\Delta T}_w - \Delta T_w(0^+)\right) = -L_\beta \overline{\Delta T}_w - \frac{d\overline{\Delta T}_w}{dz} - \frac{z\Omega}{u} + \frac{\psi}{u}. \tag{3.32}$$

The use of Eq. (3.30) in Eq. (3.32) reduces the expression to

$$\frac{1}{a}u\overline{\Delta T}_w = -L_\beta \overline{\Delta T}_w - \frac{d\overline{\Delta T}_w}{dz} - \frac{z\Omega}{u} + \frac{\psi}{u}. \tag{3.33}$$

Eq. (3.33) is a first-order linear ordinary-differential equation. The solution is given by

$$\overline{\Delta T}_w(z,u) = \mathrm{M}e^{-\frac{uz}{a} - zL_\beta} + \frac{a}{\left(aL_\beta + u\right)^2}\left(-z\Omega\left(\frac{aL_\beta}{u} + 1\right) + \frac{a\Omega}{u} + \frac{a\psi L_\beta}{u} + \psi\right), \tag{3.34}$$

where M is a constant of integration and depends on the problem's boundary condition.

The following two subsections present the solutions for the flow in a production casing and flow in a cased tubing, respectively. It will be shown that the wellbore solution is fully coupled with the reservoir response.

### 3.2.1. Flow in a Production Casing: Drawdown-Temperature Solution

In this particular case, the appropriate boundary condition is given by

$$\Delta T_w(z=0,t) = \Delta T_{sf}(t), \tag{3.35}$$

where $\Delta T_{sf}(t)$ is the drawdown sandface-temperature solution, obtained by evaluating Eq. (2.22) at $r = r_w$. Eq. (3.35) states that the wellbore temperature at the producing horizon ($z = 0$) is in equilibrium with the sandface temperature.

The transformation of Eq. (3.35) to the Laplace domain is given by

$$\mathcal{L}_t\{\Delta T_w(z=0,t)\}(u) = \overline{\Delta T}_{sf}(u). \tag{3.36}$$

It will be shown that there is no need to explicitly transform the result in Eq. (2.22), due to an important Laplace transform property.

The combination of Eqs. (3.34) and (3.36) provides the solution for the production casing drawdown temperature in the Laplace domain:

$$\begin{aligned}\overline{\Delta T}_w(z,u) = e^{-\frac{uz}{a_c}}\Bigg[&\overline{\Delta T}_{sf}(u) - \frac{a_c}{\left(a_c L_{\beta c} + u\right)^2} \\ &\times \left(\frac{a_c\Omega}{u} + \frac{a_c\psi L_{\beta c}}{u} + \psi\right)\Bigg] e^{-zL_{\beta c}} + \frac{a_c}{\left(a_c L_{\beta c} + u\right)^2} \\ &\times \left(-z\Omega\left(\frac{a_c L_{\beta c}}{u} + 1\right) + \frac{a_c\Omega}{u} + \frac{a_c\psi L_{\beta c}}{u} + \psi\right),\end{aligned} \tag{3.37}$$

where the subscript $c$ refers to production casing properties.

Regarding the analytical inversion of term dependent on the boundary condition in Eq. (3.37) $\left(\overline{\Delta T}_{sf}(u)e^{\left(-\frac{uz}{a_c} - zL_{\beta c}\right)}\right)$, the well-known Laplace transform *Time Delay* property can be used:

$$\mathcal{L}_u^{-1}\left\{F(u)e^{(-ua)}\right\}(t) = \Theta(t-a)f(t-a), \tag{3.38}$$

where $\Theta(x)$ is the Heaviside Step function, also known as the Unit Step function, defined by

$$\Theta(x) = \begin{cases} 0, x < 0 \\ 1, x \geq 0 \end{cases}. \tag{3.39}$$

Hence, the inversion of the boundary-condition term is given by

$$\mathcal{L}_u^{-1}\left\{\overline{\Delta T}_{sf}(u)e^{\left(-\frac{uz}{a_c} - zL_{\beta c}\right)}\right\}(t) = \Theta\left(t - \frac{z}{a_c}\right)e^{-zL_{\beta c}}\Delta T_{sf}\left(t - \frac{z}{a_c}\right). \tag{3.40}$$

As mentioned before, the explicit transformation of $\Delta T_{sf}(t)$ was not necessary. The analytical inversion of Eq. (3.37) provides the solution in the real space:

$$\Delta T_w(z,t) = F^{BC}_{(DD,c)}(z,t) + F_{(DD,c)}(z,t). \tag{3.41}$$

It is convenient to split the solution into these two functions, where $F^{BC}_{(DD,c)}(z,t)$ depends on the boundary condition and the function $F_{(DD,c)}(z,t)$ does not. For the specific case of flow in a production casing, these functions are given by, respectively,

$$F^{BC}_{(DD,c)}(z,t) = \Theta\left(t - \frac{z}{a_c}\right) e^{-zL_{\beta c}} \Delta T_{sf}\left(t - \frac{z}{a_c}\right), \tag{3.42}$$

and

$$\begin{aligned} F_{(DD,c)}(z,t) = \frac{e^{-L_{\beta c}(ta_c+z)}}{L^2_{\beta c}} \Bigg\{ & \Theta\left(t - \frac{z}{a_c}\right) \\ & \times \left[e^{zL_{\beta c}}\left(ta_c\Omega L_{\beta c} - z\Omega L_{\beta c} + \Omega + \psi L_{\beta c}\right)\right. \\ & \left. - e^{ta_cL_{\beta c}}\left(\Omega + \psi L_{\beta c}\right)\right] \\ & + e^{zL_{\beta c}}\Omega\left(\left(1 - zL_{\beta c}\right)e^{ta_cL_{\beta c}} - ta_cL_{\beta c} + zL_{\beta c} - 1\right) \\ & + e^{zL_{\beta c}}\psi L_{\beta c}(e^{ta_cL_{\beta c}} - 1)\Bigg\}. \end{aligned} \tag{3.43}$$

The function $F^{BC}_{(DD,c)}(z,t)$ carries all the information from the sandface-temperature solution, keeping the reservoir and the wellbore fully coupled. Note that the expression entails a time delay, which is expected, since reservoir temperature changes cannot be read instantaneously by the gauge.

The solution in Eq. (3.41) is fully analytical, requiring no iterative or numerical methods to be computed. It can be easily implemented in any software, since it only makes use of two fundamental mathematical functions, the exponential function and the Heaviside Step function.

As mentioned before, past studies have adopted the term $\partial T/\partial z$ from the steady-state regime to solve the transient problem, e.g., Hasan et al. (2005) and Onur et al. (2017). One of the main contributions of this work is to provide the transient expression for the wellbore-temperature gradient, which is given by the differentiation of Eq. (3.41) with respect to $z$:

$$\frac{\partial[\Delta T_w(z,t)]}{\partial z} = \frac{\partial\left[F^{BC}_{(DD,c)}(z,t)\right]}{\partial z} + \frac{\partial\left[F_{(DD,c)}(z,t)\right]}{\partial z}. \tag{3.44}$$

The explicit expression for flow in a production casing is given by

$$\frac{\partial[\Delta T_w(z,t)]}{\partial z} = -\frac{e^{(-zL_{\beta c})}}{a_c}\left\{\delta\left(t-\frac{z}{a_c}\right)\Delta T_{sf}\left(t-\frac{z}{a_c}\right)+\Theta\left(t-\frac{z}{a_c}\right)\right.$$
$$\left.\times\left(a_c L_{\beta c}\Delta T_{sf}\left(t-\frac{z}{a_c}\right)+\frac{\partial\left[\Delta T_{sf}\left(t-\frac{z}{a_c}\right)\right]}{\partial z}\right)\right\}$$
$$+\frac{1}{a_c L_{\beta c}^2}\left\{\delta\left(t-\frac{z}{a_c}\right)\right.$$
$$\times\left[L_{\beta c}\left(\Omega z e^{(-ta_c L_{\beta c})}+\psi\left(e^{(-zL_{\beta c})}-e^{(-ta_c L_{\beta c})}\right)\right)\right.$$
$$\left.+\Omega\left(e^{(-zL_{\beta c})}-e^{(-ta_c L_{\beta c})}\right)-ta_c L_{\beta c}\Omega e^{(-ta_c L_{\beta c})}\right]$$
$$+a_c L_{\beta c}\Theta\left(t-\frac{z}{a_c}\right)\left[\Omega\left(e^{(-zL_{\beta c})}-e^{(-ta_c L_{\beta c})}\right)\right.$$
$$\left.\left.+L_{\beta c}\psi e^{(-zL_{\beta c})}\right]\right\}+\frac{\Omega\left(e^{(-ta_c L_{\beta c})}-1\right)}{L_{\beta c}}, \tag{3.45}$$

where $\delta(x)$ is the well-known Dirac delta function defined by

$$\delta(x) = \frac{d}{dx}[\Theta(x)], \tag{3.46}$$

and the term $\left(\frac{\partial\left[\Delta T_{sf}\left(t-\frac{z}{a_c}\right)\right]}{\partial z}\right)$ is given by the partial derivative of the drawdown sandface-temperature solution, obtained by evaluating Eq. (2.22) at $r = r_w$ and substituting $t$ for $\left(t-\frac{z}{a_c}\right)$.

Indeed, computing the Dirac delta function is not an easy task. Nevertheless, the results in this study do not require the computation of Eq. (3.45). This expression has been derived to show that the wellbore-temperature gradient presents a strong transient behavior. The impact of assuming the steady-state temperature gradient to solve the transient problem is evaluated in Chapter 5, where the proposed analytical solution in this work is compared to other two analytical solutions that make use of this simplification, proposed by Hasan et al. (2005) and Onur et al. (2017). Moreover, the three analytical solutions are compared to the rigorous response of a commercial non-isothermal simulator.

### 3.2.2. Flow in a Cased Tubing: Drawdown-Temperature Solution

In this case, the appropriate boundary condition has to account for the flow transition between the production casing and the tubing string. It is convenient to define a new variable $z_t$, referenced at the bottom of the tubing string:

$$z_t = z - z_c. \tag{3.47}$$

The subscript $t$ refers to the tubing string and $z_c$ is the constant distance between the producing horizon and the bottom of the tubing (see Figure 3.1).

Since the solution is obtained by Laplace transformation, the boundary condition will be given in the Laplace domain by evaluating Eq. (3.37) at $z = z_c$

$$\mathcal{L}_t\{\Delta T_w(z_t = 0)\}(u) = \overline{\Delta T}_w(z_c, u) = \overline{\Delta T}_{z_c}\,, \tag{3.48}$$

where

$$\overline{\Delta T}_{z_c} = e^{-\frac{uz_c}{a_c}}\left[\overline{\Delta T}_{sf}(u) - \frac{a_c}{\left(a_c L_{\beta c} + u\right)^2} \times \left(\frac{a_c\Omega}{u} + \frac{a_c\psi L_{\beta c}}{u} + \psi\right)\right] e^{-z_c L_{\beta c}} + \frac{a_c}{\left(a_c L_{\beta c} + u\right)^2} \times \left(-z_c\Omega\left(\frac{a_c L_{\beta c}}{u} + 1\right) + \frac{a_c\Omega}{u} + \frac{a_c\psi L_{\beta c}}{u} + \psi\right). \tag{3.49}$$

The use of this boundary condition in Eq. (3.34) provides the cased-tubing solution in the Laplace domain:

$$\overline{\Delta T}_w(u, z_t) = e^{-\frac{uz_t}{a_t}}\left[\overline{\Delta T}_{z_c}(u, z_c) - \frac{a_t}{\left(a_t L_{\beta t} + u\right)^2} \times \left(\frac{a_t\Omega}{u} + \frac{a_t\psi L_{\beta t}}{u} + \psi\right)\right] e^{-z_t L_{\beta t}} + \frac{a_t}{\left(a_t L_{\beta t} + u\right)^2} \times \left(-z_t\Omega\left(\frac{a_t L_{\beta t}}{u} + 1\right) + \frac{a_t\Omega}{u} + \frac{a_t\psi L_{\beta t}}{u} + \psi\right), \tag{3.50}$$

where the subscript $t$ refers to tubing properties.

The analytical inversion of Eq. (3.50) is given by

$$\Delta T_w(z_t, t) = F^{BC}_{(DD,t)}(z_t, t) + F_{(DD,t)}(z_t, t). \tag{3.51}$$

In the same way as in the production-casing solution, the function $F^{BC}_{(DD,t)}(z_t, t)$ depends on the boundary condition and the function $F_{(DD,t)}(z_t, t)$ does not.

It is convenient to write the function $F^{BC}_{(DD,t)}(z_t,t)$ as a summation of four functions:

$$F^{BC}_{(DD,t)}(z_t,t) = f^{BC}_{1(DD,t)} + f^{BC}_{2(DD,t)} + f^{BC}_{3(DD,t)} + f^{BC}_{4(DD,t)}, \tag{3.52}$$

where

$$f^{BC}_{1(DD,t)}(z_t,t) = \frac{1}{a_t L^2_{\beta_C}}\left\{\Theta\left(t-\frac{z_t}{a_t}-\frac{z_c}{a_c}\right) \times\left(a_c\Omega L_{\beta c}\left(t-\frac{z_t}{a_t}\right)a_t e^{-a_c\left(t-\frac{z_t}{a_t}\right)L_{\beta c}-z_t L_{\beta t}}\right)\right\}, \tag{3.53}$$

$$f^{BC}_{2(DD,t)}(z_t,t) = \frac{1}{a_t L^2_{\beta_C}}\left\{\Theta\left(t-\frac{z_t}{a_t}-\frac{z_c}{a_c}\right) \times\left(-a_t\Omega\left(\left(e^{a_c t L_{\beta c}}-e^{\frac{a_c L_{\beta c} z_t}{a_t}+L_{\beta c}z_c}\right) \times e^{-a_c t L_{\beta c}-L_{\beta c}z_c-z_t L_{\beta t}}+L_{\beta c}z_c e^{-a_c\left(t-\frac{z_t}{a_t}\right)L_{\beta c}-z_t L_{\beta t}}\right)\right)\right\}, \tag{3.54}$$

$$f^{BC}_{3(DD,t)}(z_t,t) = \frac{1}{a_t L^2_{\beta_C}}\left\{\Theta\left(t-\frac{z_t}{a_t}-\frac{z_c}{a_c}\right) \times\left(-a_t L_{\beta c}\left(\psi\left(e^{a_c t L_{\beta c}}-e^{\frac{a_c L_{\beta c} z_t}{a_t}+L_{\beta c}z_c}\right) \times e^{-a_c t L_{\beta c}-L_{\beta c}z_c-z_t L_{\beta t}} - e^{-z_c L_{\beta c}-z_t L_{\beta t}}L_{\beta c}\Delta T_{sf}\left(t-\frac{z_t}{a_t}-\frac{z_c}{a_c}\right)\right)\right)\right\}, \tag{3.55}$$

and

$$f_{4(DD,t)}^{BC}(z_t,t)=\frac{1}{a_t L_{\beta_C}^2}\Bigg\{-\Theta\left(t-\frac{z_t}{a_t}\right)\times e^{-a_c\left(t-\frac{z_t}{a_t}\right)L_{\beta c}-z_t L_{\beta t}}\Bigg(a_t\left(\Omega\left(z_c L_{\beta c}-1\right)-\psi L_{\beta c}\right)\times\left(e^{a_c\left(t-\frac{z_t}{a_t}\right)L_{\beta c}}-1\right)+a_c\Omega L_{\beta c}a_t\left(t-\frac{z_t}{a_t}\right)\Bigg)\Bigg\}. \tag{3.56}$$

The function $F_{(DD,t)}(z_t,t)$ is analogous to the production casing result, with the substitution of the variable $z$ for the variable $z_t$ and tubing properties:

$$F_{(DD,t)}(z_t,t)=\frac{e^{-L_{\beta t}(ta_t+z_t)}}{L_{\beta_t}^2}\Bigg\{\Theta\left(t-\frac{z_t}{a_t}\right)\times\left[e^{z_t L_{\beta t}}\left(ta_t\Omega L_{\beta t}-z_t\Omega L_{\beta t}+\Omega+\psi L_{\beta t}\right)-e^{ta_t L_{\beta t}}\left(\Omega+\psi L_{\beta t}\right)\right]+e^{z_t L_{\beta t}}\Omega\left(\left(1-z_t L_{\beta t}\right)e^{ta_t L_{\beta t}}-ta_t L_{\beta t}+z_t L_{\beta t}-1\right)+e^{z_t L_{\beta t}}\psi L_{\beta t}(e^{ta_t L_{\beta t}}-1)\Bigg\}, \tag{3.57}$$

The function $F_{(DD,t)}^{BC}(z,t)$ provides the coupling with the sandface and production casing temperature changes at $z=z_c$, hence keeping the reservoir, casing and tubing as a fully coupled system.

Again, the solution is fully analytical and it can be easily implemented in any software, requiring only the exponential function and the Heaviside Step function to be computed. The transient-wellbore-temperature gradient for flow in a cased tubing can be obtained by the differentiation of the Eq. (3.51) with respect to $z_t$.

## 3.3. Transient-Wellbore-Temperature Solutions: Buildup Period

The results in this study do not consider WBS effects, hence the buildup bottomhole flow rate is zero. However, the buildup solution will be obtained for an approximate general case, where the differential equation is solved assuming a non-zero constant rate, allowing the use of wellbore-fluid-flow models (WBS or momentum) afterwards. Onur et al. (2017) adopted this approach to derive their drawdown and buildup solutions.

For the buildup case, it is convenient to keep the temperature difference referenced to the Earth initial temperature over depth

$$\Delta T_{ws}(z,\Delta t) = T_{ws}(z,\Delta t) - T_{ei}(z), \tag{3.58}$$

where the subscript $ws$ refers to the well shut-in period and $\Delta t$ represents the elapsed time since the beginning of shut-in ($\Delta t = t - t_p$).

The wellbore-heat-flow buildup problem has the following appropriate initial condition:

$$\Delta T_{ws}(z,\Delta t = 0^+) = \Delta T_{wp}\big(z,t_p\big) + \Delta T_{sf}(0^+) = \Delta T_z^{(0+)}. \tag{3.59}$$

Eq. (3.59) states that the wellbore-temperature distribution right after shut-in is described by the final flowing temperature distribution added to the immediate impact of shutting in the well, i.e., the heating response due to adiabatic fluid compression. For the production casing configuration, $\Delta T_{wp}$ is the well flowing temperature obtained by evaluating Eq. (3.41) at $t = t_p$, whereas in presence of a tubing it must be evaluated by Eq. (3.51). $\Delta T_{sf}(0^+)$ is obtained by evaluating Eq. (2.56) for a small $\Delta t$ (1 – 5 seconds).

The energy-balance equation is given by Eq. (3.29) and the boundary condition depends on whether there is a tubing in the wellbore. The use of the Laplace transformation in Eq. (3.29) takes the problem to the Laplace domain with the Laplace-transform variable $u$ with respect to the shut-in time $\Delta t$.

$$\mathcal{L}_{\Delta t}\{\Delta T_{ws}(z,\Delta t)\}(u) = \overline{\Delta T}_{ws}(z,u), \tag{3.60}$$

$$\frac{1}{a}\big(u\overline{\Delta T}_{ws} - \Delta T_{ws}(0^+)\big) = -L_\beta \overline{\Delta T}_{ws} - \frac{\partial \overline{\Delta T}_{ws}}{\partial z} - \frac{z\Omega}{u} + \frac{\psi}{u}. \tag{3.61}$$

The combination of Eqs. (3.59) and (3.61) gives

$$\frac{u}{a}\overline{\Delta T}_{ws} - \frac{\Delta T_z^{(0+)}}{a} = -L_\beta \overline{\Delta T}_{ws} - z\frac{\Omega}{u} - \frac{\partial \overline{\Delta T}_{ws}}{\partial z} + \frac{\psi}{u}. \tag{3.62}$$

Eq. (3.62) is a first-order linear ordinary-differential equation and the solution in the Laplace domain is given by

$$\begin{aligned}\overline{\Delta T}_{ws}(z,u) = {} & \mathrm{M} e^{-\frac{uz}{a} - zL_\beta} \\ & + \frac{a}{\big(aL_\beta + u\big)^2}\left[-z\Omega\left(\frac{aL_\beta}{u} + 1\right) + \frac{a\Omega}{u} + \frac{aL_\beta\psi}{u} + \psi \right. \\ & \left. + L_\beta \Delta T_z^{(0+)} + \frac{u\Delta T_z^{(0+)}}{a}\right],\end{aligned} \tag{3.63}$$

where M is a constant of integration and depends on the problem's boundary condition.

### 3.3.1. Production Casing: Buildup-Temperature Solution

In this particular case, the appropriate boundary condition is given by

$$\Delta T_{ws}(z=0,\Delta t) = \Delta T_{sf}(\Delta t), \tag{3.64}$$

where $\Delta T_{sf}(\Delta t)$ is the buildup sandface-temperature solution, given by Eq. (2.56). Eq. (3.64) states that the wellbore temperature at the producing horizon $(z=0)$ is in equilibrium with the sandface temperature. The transformation of the boundary condition to the Laplace domain is given by

$$\mathcal{L}_{\Delta t}\{\Delta T_{ws}(z=0,\Delta t)\}(u) = \overline{\Delta T}_{sf}(u). \tag{3.65}$$

Like in the drawdown case, there is no need to explicitly transform Eq. (2.56) due to the use of the *Time Delay* property afterwards.

The combination of Eqs. (3.63) and (3.65) provides the solution for the production casing buildup temperature in the Laplace domain:

$$\begin{aligned}\overline{\Delta T}_{ws}(z,u) = e^{-\frac{uz}{a_c}}\Bigg[&\overline{\Delta T}_{sf}(u) - \frac{a_c}{\left(a_c L_{\beta c}+u\right)^2}\\ &\times\left(\frac{a_c\Omega}{u}+\frac{a_c L_{\beta c}\psi}{u}+\psi+L_{\beta c}\Delta T_z^{(0+)}+\frac{u\Delta T_z^{(0+)}}{a_c}\right)\Bigg]\\ &\times e^{-zL_{\beta c}}+\frac{a_c}{\left(a_c L_{\beta c}+u\right)^2}\\ &\times\Bigg(-z\Omega\left(\frac{a_c L_{\beta c}}{u}+1\right)+\frac{a_c\Omega}{u}+\frac{a_c L_{\beta c}\psi}{u}+\psi\\ &+L_{\beta c}\Delta T_z^{(0+)}+\frac{u\Delta T_z^{(0+)}}{a_c}\Bigg).\end{aligned} \tag{3.66}$$

The analytical inversion of Eq. (3.66) provides the solution in the real space:

$$\Delta T_{ws}(z,\Delta t) = F_{(BU,c)}^{BC}(z,\Delta t) + F_{(BU,c)}(z,\Delta t). \tag{3.67}$$

Following the same approach as in the drawdown case, the function $F_{(BU,c)}^{BC}(z,\Delta t)$ depends on the boundary condition and the function $F_{(BU,c)}(z,\Delta t)$ does not.

$$F^{BC}_{(BU,c)}(z,\Delta t) = \Theta\left(\Delta t - \frac{z}{a_c}\right) e^{-zL_{\beta c}} \Delta T_{sf}\left(\Delta t - \frac{z}{a_c}\right), \tag{3.68}$$

and

$$\begin{aligned} F_{(BU,c)}(z,\Delta t) = \frac{e^{-L_{\beta c}(\Delta t a_c + z)}}{L^2_{\beta c}} \Big\{ & e^{zL_{\beta c}} \Big( \Omega \Big( \big(1 - zL_{\beta c}\big) e^{\Delta t a_c L_{\beta c}} \\ & - \Delta t a_c L_{\beta c} + zL_{\beta c} - 1 \Big) \\ & + L_{\beta c} \Big( \psi \big( e^{\Delta t a_c L_{\beta c}} - 1 \big) + L_{\beta c} \Delta T_z^{(0+)} \Big) \Big) - \Theta\left(\Delta t - \frac{z}{a_c}\right) \\ & \times \Big[ e^{zL_{\beta c}} \Big( \Omega \big( -\Delta t a_c L_{\beta c} + zL_{\beta c} - 1 \big) \\ & + L_{\beta c} \Big( L_{\beta c} \Delta T_z^{(0+)} - \psi \Big) \Big) + e^{\Delta t a_c L_{\beta c}} \big( \Omega + \psi L_{\beta c} \big) \Big] \Big\}. \end{aligned} \tag{3.69}$$

The function $F^{BC}_{(BU,c)}(z,\Delta t)$ carries all the information from the sandface-temperature solution, keeping the reservoir and the wellbore fully coupled. However, during the buildup period the rate rapidly reaches small values, regardless of the use of wellbore-fluid-flow models (WBS or momentum). Consequently, the argument of the Heaviside Step function in Eq. (3.68) tends to large negative values, yielding a null value for the function. Then, as expected, the reservoir and the wellbore become decoupled (except at $z = 0$), since there is no longer any available information in the form of convection to connect the reservoir to the gauge. From this moment, the temperature change is dominated by the radial heat loss to surroundings.

Once again, the solution in Eq. (3.67) is fully analytical and it only requires the exponential function and the Heaviside Step function to be computed.



### 3.3.2. Cased Tubing: Buildup-Temperature Solution

In this case, the appropriate boundary condition has to take into account the flow transition between the production casing and the tubing string. Since the solution is obtained by Laplace transformation, the boundary condition will be given in the Laplace domain by evaluating Eq. (3.66) at $z = z_c$.

It is convenient to use the variable $z_t$ defined by Eq. (3.47), therefore the boundary condition for the cased tubing in the Laplace domain is given by

$$\mathcal{L}_{\Delta t}\{\Delta T_{ws}(z_t = 0)\}(u) = \overline{\Delta T}_{ws}(z_c, u) = \overline{\Delta T}_{z_c}, \tag{3.70}$$

where the term $\overline{\Delta T}_{z_c}$ is the buildup solution for the production casing at $z = z_c$ in Eq. (3.66):

$$\overline{\Delta T}_{z_c} = e^{-\frac{uz_c}{a_c}}\left[\overline{\Delta T}_{sf}(u) - \frac{a_c}{\left(a_c L_{\beta c} + u\right)^2} \times \left(\frac{a_c \Omega}{u} + \frac{a_c L_{\beta c}\psi}{u} + \psi + L_{\beta c}\Delta T_z^{(0+)} + \frac{u\Delta T_z^{(0+)}}{a_c}\right)\right] \times e^{-zL_{\beta c}} + \frac{a_c}{\left(a_c L_{\beta c} + u\right)^2} \times \left(-z_c\Omega\left(\frac{a_c L_{\beta}}{u} + 1\right) + \frac{a_c \Omega}{u} + \frac{a_c L_{\beta c}\psi}{u} + \psi + L_{\beta c}\Delta T_z^{(0+)} + \frac{u\Delta T_z^{(0+)}}{a_c}\right). \tag{3.71}$$

The use of this boundary condition in Eq. (3.63) provides the cased-tubing solution in the Laplace domain. The analytical inversion yields

$$\Delta T_{ws}(z_t, \Delta t) = F_{(BU,t)}^{BC}(z_t, \Delta t) + F_{(BU,t)}(z_t, \Delta t). \tag{3.72}$$

Following the same approach as in the drawdown case, the function $F_{(BU,t)}^{BC}(z, \Delta t)$ depends on the boundary condition and the function $F_{(BU,t)}(z, \Delta t)$ does not.

$$F_{(BU,t)}^{BC}(z_t, \Delta t) = \frac{1}{a_t L_{\beta_c}^2}\left\{\Theta\left(\Delta t - \frac{z_c}{a_c} - \frac{z_t}{a_t}\right) f_{1(BU,t)}^{BC} - \Theta\left(\Delta t - \frac{z_t}{a_t}\right) f_{2(BU,t)}^{BC}\right\}, \tag{3.73}$$

where

$$f_{1(BU,t)}^{BC} = a_c\Omega L_{\beta c}(\Delta t a_t - z_t)e^{a_c\left(\frac{z_t L_{\beta c}}{a_t} - \Delta t L_{\beta c}\right) - z_t L_{\beta t}}$$
$$- a_t\Bigg(\Omega\Bigg(\left(e^{a_c \Delta t L_{\beta c}} - e^{\frac{a_c L_{\beta c} z_t}{a_t} + L_{\beta c} z_c}\right)$$
$$\times e^{-a_c \Delta t L_{\beta c} - L_{\beta c} z_c - z_t L_{\beta t}} + L_{\beta c} z_c e^{a_c\left(\frac{z_t L_{\beta c}}{a_t} - \Delta t L_{\beta c}\right) - z_t L_{\beta t}}\Bigg)$$
$$+ L_{\beta c}\Bigg(\psi\left(e^{a_c \Delta t L_{\beta c}} - e^{\frac{a_c L_{\beta c} z_t}{a_t} + L_{\beta c} z_c}\right)$$
$$\times e^{-a_c \Delta t L_{\beta c} - L_{\beta c} z_c - z_t L_{\beta t}}$$
$$+ L_{\beta c}\Bigg(\Delta T_z^{(0+)} e^{a_c\left(\frac{z_t L_{\beta c}}{a_t} - \Delta t L_{\beta c}\right) - z_t L_{\beta t}}$$
$$- \Delta T_{sf}\left(\Delta t - \frac{z_c}{a_c} - \frac{z_t}{a_t}\right)e^{-z_c L_{\beta c} - z_t L_{\beta t}}\Bigg)\Bigg)\Bigg), \tag{3.74}$$

and

$$f_{2(BU,t)}^{BC} = e^{a_c\left(\frac{z_t L_{\beta c}}{a_t} - \Delta t L_{\beta c}\right) - z_t L_{\beta t}}\Bigg[a_t\Bigg(\Omega\big(z_c L_{\beta c} - 1\big)$$
$$\times\left(e^{a_c\left(\Delta t L_{\beta c} - \frac{L_{\beta c} z_t}{a_t}\right)} - 1\right)$$
$$- L_{\beta c}\left(\psi\left(e^{a_c\left(\Delta t L_{\beta c} - \frac{L_{\beta c} z_t}{a_t}\right)} - 1\right) + L_{\beta c}\Delta T_z^{(0+)}\right)\Bigg)$$
$$+ a_c\Omega L_{\beta c}(a_t \Delta t - z_t)\Bigg]. \tag{3.75}$$

The function $F_{(BU,t)}$ is given by

$$F_{(BU,t)}(z_t, \Delta t) = \frac{e^{-L_{\beta t}(\Delta t a_t + z_t)}}{L_{\beta_t}^2}\Big\{e^{z_t L_{\beta t}}\Big(\Omega\Big(\big(1 - z_t L_{\beta t}\big)e^{\Delta t a_t L_{\beta t}}$$
$$- \Delta t a_t L_{\beta t} + z_t L_{\beta t} - 1\Big)$$
$$+ L_{\beta t}\Big(\psi\big(e^{\Delta t a_t L_{\beta t}} - 1\big) + L_{\beta t}\Delta T_z^{(0+)}\Big)\Big) - \Theta\left(\Delta t - \frac{z_t}{a_t}\right)$$
$$\times\Big[e^{z_t L_{\beta t}}\Big(\Omega\big(-\Delta t a_t L_{\beta t} + z_t L_{\beta t} - 1\big)$$
$$+ L_{\beta t}\Big(L_{\beta t}\Delta T_z^{(0+)} - \psi\Big)\Big) + e^{\Delta t a_t L_{\beta t}}\big(\Omega + \psi L_{\beta t}\big)\Big]\Big\}. \tag{3.76}$$

The function $F_{(BU,t)}^{BC}(z,\Delta t)$ provides the coupling with the sandface and production casing temperature changes at $z = z_c$, hence keeping the reservoir, casing and tubing as a fully coupled system. However, as mentioned before, regardless of the use of wellbore-fluid-flow models, the rate rapidly tends to small values. Therefore, the Heaviside Step functions yield null values and, as expected, the reservoir and the wellbore become decoupled (except at $z = 0$), since there is no longer any convection to feed the gauge with sandface-temperature data.

Like in the previous cases, the solution in Eq. (3.72) is fully analytical, requiring no iterative or numerical methods to be computed. It requires only the exponential function and the Heaviside Step function to be implemented.

The following section addresses an important solution for the buildup period, which is the zero-rate case.

### 3.3.3. Zero-Rate Case: A Buildup Particular Solution



When the rate is zero, the solution is considerably simpler. The particular solutions to be presented can be obtained by either solving the partial-differential equation in Eq. (3.29) considering the rate as zero, or by setting the rate to zero in the previously derived solutions.

Assuming the rate is zero, the energy balance is given by the following ordinary differential equation

$$\frac{d\Delta T_w}{dt} = -aL_R\Delta T_w\,. \tag{3.77}$$

For a null rate, the product $aL_\beta$ reduces to the product $aL_R$. The initial condition to solve the problem is expressed in Eq. (3.59).

In absence of a tubing string, the solution is given by

$$\Delta T_{ws}(z,\Delta t) = e^{-\Delta t a_c L_{Rc}}\Delta T_z^{(0+)}, \tag{3.78}$$

The solution in Eq. (3.78) is similar to the constant zero-rate buildup expressions presented by Hasan et al. (2005) and Onur et al. (2017), except that Eq. (3.78) accounts for the adiabatic compression effect at $\Delta t = 0^+$. The solution proposed by Onur et al. (2017) also accounts for this effect, but it requires a wellbore-fluid-flow model to keep the wellbore coupled with the reservoir.

In presence of a tubing string, the solution is given by

$$\Delta T_{ws}(z,\Delta t)=\begin{cases} e^{-\Delta t a_c L_{Rc}}\Delta T_z^{(0+)}, z \le z_c \\ e^{-\Delta t a_t L_{Rt}}\Delta T_z^{(0+)}, z > z_c \end{cases} \tag{3.79}$$

It is important to state that after $\Delta t = 0^+$ the wellbore-temperature changes are no longer coupled with the reservoir response (except at $z = 0$).

# 4
# Thermal Impacts on Wellbore Pressure: Non-Isothermal Well-Testing Solutions

This chapter investigates thermal impacts on pressure gauge data during buildup tests. Solutions are given in the form of buildup-pressure differences for different completion scenarios.

If the wellbore completion comprises expansion joints, the tubing string may compensate thermal effects during buildup in the form of pipe contraction, therefore the gauge location may be adjusted. This work provides three solutions:

**Constant Pipe-Length Solutions:**

1. Buildup-Pressure Difference in a Production Casing;
2. Buildup-Pressure Difference in a Cased Tubing;

**Variable Pipe-Length Solution:**

3. Buildup-Pressure Difference in a Cased Tubing.

In addition, metrics for evaluating the application of the isothermal hypothesis are also derived.



## 4.1.
## Pressure Gauge Data

The measured pressure at a gauge above the perforations can be expressed as

$$p_{gauge} = p_{sf} - p_f, \tag{4.1}$$

where $p_{sf}$ is the sandface pressure and $p_f$ refers to the pressure exerted by the wellbore-fluid column between the downhole gauge and the producing horizon.

Under the isothermal hypothesis, $p_f$ is the constant hydrostatic pressure given by (assuming negligible effect of pressure on the fluid mass density)

$$p_f = \gamma_o z_g \sin\theta, \tag{4.2}$$

where $z_g$ is the distance from the producing horizon and $\gamma_o$ is the wellbore-fluid specific weight.

Under the real non-isothermal condition, $p_f$ must be expressed in a generalized form as

$$p_f(z_g,t) = \int_0^{z_g+\Delta L(t)} \gamma_o(z,t)\sin\theta\, dz\,, \tag{4.3}$$

where $\Delta L(t)$ is the change in pipe length over time, which depends on temperature changes, and $z_g$ is the original gauge location. The wellbore-fluid specific weight is a function of temperature, therefore depends on time and depth.

The next subsection provides the constant pipe-length solutions. Then, the variable length configuration will be addressed.

## 4.2. Thermal Impacts on Buildup Pressure: Constant Pipe-Length Configuration

For a constant pipe length, Eq. (4.3) can be written as

$$p_f(z_g,t) = \int_0^{z_g} \gamma_o(z,t)\sin\theta\, dz\,, \tag{4.4}$$

where $\gamma_o$ is given by (see Eq. (3.25))

$$\gamma_o(z,t) = \gamma_{oi} - \gamma_{oi}\beta_o\Delta T_w(z,t) + \gamma_{oi}\beta_o z g_G \sin\theta. \tag{4.5}$$

The combination of Eqs. (4.4) and (4.5) yields

$$p_f(z_g,t) = z_g\gamma_{oi}\sin\theta - \beta_o\gamma_{oi}\sin\theta\int_0^{z_g}\Delta T_w(z,t)dz + \frac{z_g^2}{2}\gamma_{oi}\beta_o g_G(\sin\theta)^2. \tag{4.6}$$

Rewriting Eq. (4.1), the measured pressure under the non-isothermal condition is given by

$$p_g(z_g,t) = p_{sf}(t) - z_g\gamma_{oi}\sin\theta + \sin\theta\,\beta_o\gamma_{oi}\int_0^{z_g}\Delta T_w(z,t)dz - \frac{z_g^2}{2}\gamma_{oi}\beta_o g_G(\sin\theta)^2. \tag{4.7}$$

Note that under the non-isothermal condition, the pressure is not a linear function of depth. In particular, the initial pressure is a quadratic function of depth. At the end of this chapter, the initial pressure datum shifting procedure will be discussed.

In Eq. (4.7), the pressure at a gauge above the perforations responds to the sandface pressure $p_{sf}$ and to a time depending fluid pressure.

Recalling the purpose of this work, apart from the change in tubing length, Eq. (4.7) is equal to Eq. (1.3), where the integral of mass density has been converted

into an integral of the wellbore-temperature distribution. The pipe-contraction effect will be addressed afterwards to provide the complete final solution, which is the main objective of this work.

The following expression describes the flowing pressure at the moment of shut-in ($t = t_p$):

$$p_g(z_g, t_p) = p_{sf}(t_p) - z_g\gamma_{oi}\sin\theta + \beta_o\gamma_{oi}\sin\theta\int_0^{z_g}\Delta T_{wp}(z, t_p)dz - \frac{z_g^2}{2}\gamma_{oi}\beta_o g_G(\sin\theta)^2, \tag{4.8}$$

where $\Delta T_{wp}$ refers to the wellbore flowing temperature change at $t = t_p$.

After shut-in, the buildup pressure for a fixed gauge location is given by

$$p_g(z_g, \Delta t) = p_{sf}(\Delta t) - z_g\gamma_{oi}\sin\theta + \beta_o\gamma_{oi}\sin\theta\int_0^{z_g}\Delta T_{ws}(z, \Delta t)dz - \frac{z_g^2}{2}\gamma_{oi}\beta_o g_G(\sin\theta)^2. \tag{4.9}$$

Let the buildup-pressure difference at the gauge be defined by

$$\Delta p_g(z_g, \Delta t) = p_g(z_g, \Delta t) - p_g(z_g, t_p). \tag{4.10}$$

The calculation expressed in Eq. (4.10) is of paramount importance for well-test analysis, since it comprises the buildup-pressure data to be interpreted.

Combining Eqs. (4.8), (4.9) and (4.10), the pressure difference can be rewritten as

$$\Delta p_g(z_g, \Delta t) = \Delta p_{sf}(\Delta t) + \beta_o\gamma_{oi}\sin\theta\int_0^{z_g}\left[\Delta T_{ws}(z, \Delta t) - \Delta T_{wp}(z, t_p)\right]dz. \tag{4.11}$$

The integrand in Eq. (4.11) is composed by the analytical solutions derived in this work. Let the static-fluid buildup-pressure difference be defined by

$$\Delta p_f(z_g, \Delta t) = \beta_o\gamma_{oi}\sin\theta\int_0^{z_g}\left[\Delta T_{wp}(z, t_p) - \Delta T_{ws}(z, \Delta t)\right]dz. \tag{4.12}$$

Therefore, the buildup-pressure difference for a fixed gauge location is given by

$$\Delta p_g(z_g, \Delta t) = \Delta p_{sf}(\Delta t) - \Delta p_f(z_g, \Delta t). \tag{4.13}$$

The term $\Delta p_f$ in Eq. (4.13) represents the fluid thermal impact on gauge data during buildup, responsible for part of deviations in PTA interpretations. The total

impact must account for the additional effect of change in tubing length, to be addressed afterwards in this chapter.

The solution of the integral in Eq. (4.12) depends on whether there is a tubing in the wellbore. All results to be presented assume the buildup zero-rate case.

### 4.2.1. Production-Casing Solution: Thermal Impacts on Buildup Pressure (Constant Pipe Length)

The analytical expression for the buildup-pressure difference at a fixed gauge location in a production casing is given by

$$\Delta p_{gc}(z_g, \Delta t) = \Delta p_{sf}(\Delta t) - \Delta p_{fc}(z_g, \Delta t), \tag{4.14}$$

where the static-fluid pressure difference during the buildup period is given by

$$\begin{aligned}\Delta p_{f_c}(z_g, \Delta t) = &-z_g \beta_o \gamma_{oi} \sin\theta \, \Delta T_{sf}(0^+) e^{-\Delta t a_c L_{\beta c}} \\ &+ \beta_o \gamma_{oi} \sin\theta \left(1 - e^{-\Delta t a_c L_{\beta c}}\right) \\ &\times \left(\mathrm{W}^{BC}_{(DD,c)}(z_g, t_p) + \mathrm{W}_{(DD,c)}(z_g, t_p)\right).\end{aligned} \tag{4.15}$$

See Appendix B for the derivation of this solution.

### 4.2.2. Cased-Tubing Solution: Thermal Impacts on Buildup Pressure (Constant Pipe Length)

The expression for the buildup-pressure difference at a fixed gauge location in a cased tubing is given by

$$\Delta p_{gt}(z_g, \Delta t) = \Delta p_{sf}(\Delta t) - \Delta p_{ft}(z_g, \Delta t), \tag{4.16}$$

where the static-fluid pressure difference during the buildup period in this configuration is given by

$$\begin{aligned}\Delta p_{f_t}(z_g, \Delta t) = &\Delta p_{f_c}(z_c, \Delta t) \\ &- \beta_o \gamma_{oi} \sin\theta \, \Delta T_{sf}(0^+) e^{-\Delta t a_t L_{Rt}}(z_g - z_c) \\ &+ \beta_o \gamma_{oi} \sin\theta \, (1 - e^{-\Delta t a_t L_{Rt}}) \\ &\times \left(\mathrm{W}^{BC}_{(DD,t)}\left((z_g - z_c), t_p\right) + \mathrm{W}_{(DD,t)}\left((z_g - z_c), t_p\right)\right),\end{aligned} \tag{4.17}$$

where $\Delta p_{f_c}(z_c, \Delta t)$ is given by Eq. (4.15) evaluated at $z = z_c$.

For a constant tubing length, Eq. (4.17) comprises all thermal impacts on gauge data during shut-in. Like in the production-casing result, the solution is fully analytical. See Appendix B for the derivation of this solution.

The complete and final solution accounting for the additional pipe-contraction effect will be addressed in the following section.

## 4.3. Thermal Impacts on Buildup Pressure: Variable Pipe-Length Configuration

If the tubing string comprises expansion joints, the expression for the pressure exerted by the wellbore-fluid column between the gauge and the producing horizon during buildup is given by

$$p_{f,a}(z_g, \Delta t) = \int_0^{z_g+\Delta L(\Delta t)} \gamma_o(z, \Delta t) \sin\theta \, dz, \tag{4.18}$$

where $\Delta L(\Delta t)$ is the change in tubing length over the shut-in time, which depends on temperature changes, and $z_g$ is the gauge location at the end of the flowing period. The subscript $a$ refers to the adjustable gauge location.

The buildup-pressure difference at the gauge, accounting for the pipe-contraction effect, can be written as

$$\Delta p_{gt,a}(z_g, \Delta t) = \Delta p_{sf}(\Delta t) - \Delta p_{ft}(z_g, \Delta t) - \Delta p_{cont}(z_g, \Delta t), \tag{4.19}$$

where $\Delta p_{cont}$ is the transient pipe-contraction effect on pressure during the buildup period, given by

$$\Delta p_{cont}(z_g, \Delta t) = \Delta L(\Delta t)\left(\gamma_{oi} \sin\theta + \gamma_{oi} z_g \beta_o g_G (\sin\theta)^2\right). \tag{4.20}$$

The transient change in pipe length is given by

$$\begin{aligned}\Delta L(\Delta t) = \alpha_{LTE}\,(1 - e^{-\Delta t a_t L_{Rt}}) \\ \times \left[\mathrm{W}_{(DD,t)}(L_0, t_p) + \mathrm{W}^{BC}_{(DD,t)}(L_0, t_p)\right] \\ - \alpha_{LTE} \Delta T_{sf}(0^+) e^{-\Delta t a_t L_{Rt}} L_0.\end{aligned} \tag{4.21}$$

See Appendix B for the derivation Eqs. (4.19), (4.20) and (4.21).

The final expression for $\Delta p_{gt,a}(z_g, \Delta t)$ is given by the combination of Eqs. (4.17), (4.19), (4.20) and (4.21):

$$\begin{aligned}\Delta p_{gt,a}(z_g,\Delta t) = \Delta p_{sf}(\Delta t) \\ &- \Big\{\Delta p_{f_c}(z_c,\Delta t) \\ &- \beta_o\gamma_{oi}\sin\theta\,\Delta T_{sf}(0^+)e^{-\Delta t a_t L_{Rt}}\left(z_g - z_c\right) \\ &+ \beta_o\gamma_{oi}\sin\theta\,(1-e^{-\Delta t a_t L_{Rt}}) \\ &\times\Big(\mathrm{W}^{BC}_{(DD,t)}\Big(\left(z_g - z_c\right),t_p\Big) \\ &+ \mathrm{W}_{(DD,t)}\Big(\left(z_g - z_c\right),t_p\Big)\Big)\Big\} \\ &- \Big\{\left(\gamma_{oi}\sin\theta + \gamma_{oi}z_g\beta_o g_G(\sin\theta)^2\right) \\ &\times\Big\{\alpha_{LTE}\,(1-e^{-\Delta t a_t L_{Rt}}) \\ &\times\left[\mathrm{W}_{(DD,t)}(L_0,t_p) + \mathrm{W}^{BC}_{(DD,t)}(L_0,t_p)\right] \\ &- \alpha_{LTE}\Delta T_{sf}(0^+)e^{-\Delta t a_t L_{Rt}}L_0\Big\}\Big\},\end{aligned} \tag{4.22}$$

where $\Delta p_{f_c}(z_c,\Delta t)$ is given by Eq. (4.15) evaluated at $z = z_c$.

Eq. (4.22) is the solution of Eq. (1.3) in terms of pressure differences. The solution is fully analytical, requiring no iterative or numerical methods to be computed. It is noteworthy to state that after deriving the solution in Eq. (4.22), the main objective of this work has been accomplished.

## 4.4. Metrics for Evaluating the Isothermal Hypothesis

As mentioned before, the derivative method (Bourdet et al., 1989) is the most important interpretation tool for pressure transient analysis. It is desired to derive practical metrics to evaluate thermal impacts on pressure derivative curves.

The buildup-pressure derivative with respect to $\ln\Delta t$ at a gauge is given by:

$$\frac{\partial\Delta p_{gt,a}(z_g,\Delta t)}{\partial\ln\Delta t} = \frac{\partial\Delta p_{sf}(\Delta t)}{\partial\ln\Delta t} - \frac{\partial\Delta p_{f_t}(z_g,\Delta t)}{\partial\ln\Delta t} - \frac{\partial\Delta p_{cont}(z_g,\Delta t)}{\partial\ln\Delta t}, \tag{4.23}$$

where $\Delta p_{sf}$ is the reservoir response and

$$\frac{\partial \Delta p_{f_t}}{\partial \ln \Delta t} = \Delta t a_c L_{Rc} \beta_o \gamma_{oi} \sin\theta \, e^{-\Delta t a_c L_{Rc}} \times \left( z_c \Delta T_{sf}(0^+) + \mathrm{W}_{(DD,c)}^{BC}(z_c, t_p) + \mathrm{W}_{(DD,c)}(z_c, t_p) \right) + \Delta t a_t L_{Rt} \beta_o \gamma_{oi} \sin\theta \, e^{-\Delta t a_t L_{Rt}} \times \left( (z_g - z_c) \Delta T_{sf}(0^+) + \mathrm{W}_{(DD,t)}^{BC}(z_g - z_c, t_p) + \mathrm{W}_{(DD,t)}(z_g - z_c, t_p) \right), \quad (4.24)$$

and

$$\frac{\partial \Delta p_{cont}}{\partial \ln \Delta t} = \Delta t a_t L_{Rt} e^{-\Delta t a_t L_{Rt}} \, \alpha_{LTE} \left( \gamma_{oi} \sin\theta + \gamma_{oi} z_g \beta_o g_G (\sin\theta)^2 \right) \times \left( L_0 \Delta T_{sf}(0^+) + \mathrm{W}_{(DD,t)}(L_0, t_p) + \mathrm{W}_{(DD,t)}^{BC}(L_0, t_p) \right). \quad (4.25)$$

Eqs. (4.24) and (4.25) are the derivatives of Eqs. (4.17) and (4.20), respectively. All thermal impacts on the derivative method are enclosed in these two expressions, which can be viewed as the derivative "thermal noise" and $\Delta p_{sf}$ is the formation signal.

The following subsection will derive the shut-in time when impacts on pressure data are most significant. In addition, an important relation is derived to evaluate whether the isothermal hypothesis can be used during a well test. From these results, several operational parameters can be determined. First, the maximum gauge distance from the producing horizon will be derived. Then, analytical expressions for the required minimum drawdown rate and the associated signal-to-noise ratio (SNR) in a well test will be provided.



### 4.4.1. Time of Maximum Thermal Impact on Pressure $\Delta t_{mp}$

The logarithmic-time derivative of thermal noise, which is the sum of expressions in Eqs. (4.24) and (4.25), comprises a function with inflections, therefore presents local minimum and maximum values. The impact of local maxima on the signal of a homogeneous reservoir creates "valleys" in the pressure derivative data, which can be interpreted as false heterogeneities and lead to invalid conclusions.

For sufficiently long producing times, the buildup-pressure derivative with respect to $\ln \Delta t$ can be treated as constant in infinite-acting homogeneous

reservoirs. Under this condition, the temporal derivative of Eq. (4.23) can be written as

$$\frac{\partial}{\partial \Delta t}\left(\frac{\partial \Delta p_{gt,a}(z_g,\Delta t)}{\partial \ln \Delta t}\right) \approx -\frac{\partial}{\partial \Delta t}\left(\frac{\partial \Delta p_{f_t}}{\partial \ln \Delta t}+\frac{\partial \Delta p_{cont}}{\partial \ln \Delta t}\right). \tag{4.26}$$

Therefore, the shut-in times when inflections occur can be estimated by calculating the local minima and maxima of the derivative thermal noise, which are the roots of the following expression:

$$\begin{aligned}
-\frac{\partial}{\partial \Delta t}\left(\frac{\partial \Delta p_{f_t}}{\partial \ln \Delta t}+\frac{\partial \Delta p_{cont}}{\partial \ln \Delta t}\right) = \\
&= (\Delta t a_c L_{Rc}-1)e^{-\Delta t a_c L_{Rc}}\{a_c L_{Rc}\beta_o\gamma_{oi}\sin\theta \\
&\times \left[z_c \Delta T_{sf}(0^+)+\mathrm{W}^{BC}_{(DD,c)}(z_c,t_p)+\mathrm{W}_{(DD,c)}(z_c,t_p)\right]\} \\
&+ (\Delta t a_t L_{Rt}-1)e^{-\Delta t a_t L_{Rt}}\{a_t L_{Rt}\beta_o\gamma_{oi}\sin\theta \\
&\times \left[(z_g-z_c)\Delta T_{sf}(0^+)+\mathrm{W}^{BC}_{(DD,t)}(z_g-z_c,t_p)\right. \\
&\left.+\mathrm{W}_{(DD,t)}(z_g-z_c,t_p)\right]+a_t L_{Rt}\,\alpha_{LTE} \\
&\times \left(\gamma_{oi}\sin\theta+\gamma_{oi}z_g\beta_o g_G(\sin\theta)^2\right)\left[L_0\Delta T_{sf}(0^+)\right. \\
&\left.+\mathrm{W}_{(DD,t)}(L_0,t_p)+\mathrm{W}^{BC}_{(DD,t)}(L_0,t_p)\right]\}.
\end{aligned} \tag{4.27}$$

Eq. (4.27) can be rewritten as:

$$\begin{aligned}
-\frac{\partial}{\partial \Delta t}\left(\frac{\partial \Delta p_{f_t}}{\partial \ln \Delta t}+\frac{\partial \Delta p_{cont}}{\partial \ln \Delta t}\right) = \\
&= \tau_c(\Delta t a_c L_{Rc}-1)e^{-\Delta t a_c L_{Rc}} \\
&+ \tau_t(\Delta t a_t L_{Rt}-1)e^{-\Delta t a_t L_{Rt}},
\end{aligned} \tag{4.28}$$

where

$$\begin{aligned}
\tau_c = a_c L_{Rc}\beta_o\gamma_{oi}\sin\theta \\
&\times \left[z_c\Delta T_{sf}(0^+)+\mathrm{W}^{BC}_{(DD,c)}(z_c,t_p)+\mathrm{W}_{(DD,c)}(z_c,t_p)\right],
\end{aligned} \tag{4.29}$$

and

$$\begin{aligned}
\tau_t = a_t L_{Rt}\beta_o\gamma_{oi}\sin\theta \\
&\times \left[(z_g-z_c)\Delta T_{sf}(0^+)+\mathrm{W}^{BC}_{(DD,t)}(z_g-z_c,t_p)\right. \\
&\left.+\mathrm{W}_{(DD,t)}(z_g-z_c,t_p)\right]+a_t L_{Rt}\,\alpha_{LTE} \\
&\times \left(\gamma_{oi}\sin\theta+\gamma_{oi}z_g\beta_o g_G(\sin\theta)^2\right)\left[L_0\Delta T_{sf}(0^+)\right. \\
&\left.+\mathrm{W}_{(DD,t)}(L_0,t_p)+\mathrm{W}^{BC}_{(DD,t)}(L_0,t_p)\right].
\end{aligned} \tag{4.30}$$

Let the LHS of Eq. (4.28) be equal to zero:

$$0 = \tau_c(\Delta t a_c L_{Rc} - 1)e^{-\Delta t a_c L_{Rc}} + \tau_t(\Delta t a_t L_{Rt} - 1)e^{-\Delta t a_t L_{Rt}}. \quad (4.31)$$

Solving Eq. (4.31) for $\Delta t$ provides the shut-in times when valleys occur in the gauge derivative curve. In practical cases, only one valley is observed during well-testing times, since tubing and casing usually share similar pipe diameters and thermal-storage coefficients. Therefore, the expression in Eq. (4.31) reduces to

$$0 = \left(\Delta t a_p L_{Rp} - 1\right)e^{-\Delta t a_p L_{Rp}}, \quad (4.32)$$

where the subscript $p$ refers to properties of the pipe that governs the fluid flow. As a rule of thumb, for small values of $z_c$, tubing properties should be used, whereas for large values casing properties must be used.

The expression in Eq. (4.32) has two roots. The first root comprises a local maximum value, providing a drop in the gauge derivative signal. The second root occurs after long shut-in times $(\Delta t \to \infty)$, and it can be interpreted as the asymptotic fading of the thermal noise. Hence, under the adopted assumptions, thermal effects cause only one valley in the derivative curve and the *Time of Maximum Thermal Impact on Pressure* $(\Delta t_{mp})$ is given by

$$\Delta t_{mp} = \frac{1}{a_p L_{Rp}}, \quad (4.33)$$

where

$$a_p L_{Rp} = \frac{2\pi r_{po} U_{tp} \lambda_e}{\rho_{oi} c_{po}\left[\lambda_e + r_{po} U_{tp} f_D(t_D)\right] A_p (1 + C_{Tp})}. \quad (4.34)$$

Note that $\Delta t_{mp}$ does not depend on the gauge location, tubing length nor on reservoir properties. Moreover, it does not depend on the preceding production rate magnitude nor on the duration of the drawdown period. It only depends on the radial diffusion (heat loss) to surroundings and on some wellbore and fluid properties, such as inside-pipe radius and fluid heat capacity. The verification of this result is presented in Chapter 5.

Depending on wellbore and operational features, additional inflections may occur, as shown by Eq. (4.31). This condition will be addressed in Chapter 6.

The following metrics assume the same assumptions used to derive Eq. (4.33).

### 4.4.2. Isothermal Hypothesis Test

A metric for evaluating whether a well test is impacted by thermal effects can be easily drawn. In Eq. (4.23), when the sandface-pressure derivative is much greater than the thermal noise derivative, the isothermal hypothesis is valid.

Here the derivation of $\Delta t_{mp}$ turns out to be of paramount importance, since there is only the need to evaluate the thermal impacts at this specific time. In other words, if the gauge data are not impacted at $\Delta t_{mp}$, then the isothermal hypothesis is valid for all shut-in times. It will be assumed a typical well-test configuration, where $z_c$ is small, i.e., the test string is placed near the perforations. Hence, only test string properties are required for calculations.

The thermal noise derivative maximum value is given by the combination of Eqs. (4.24), (4.25) and (4.33):

$$\left(\frac{\partial\left(\Delta p_{f_t}+\Delta p_{cont}\right)}{\partial \ln \Delta t}\right)_{\Delta t_{mp}} = \\ = \frac{\beta_o \gamma_{oi} \sin\theta}{e}\Big(z_g \Delta T_{sf}(0^+) + \mathrm{W}^{BC}_{(DD,t)}\left(z_g, t_p\right) \\ + \mathrm{W}_{(DD,t)}\left(z_g, t_p\right)\Big) + \frac{\alpha_{LTE}\gamma_{oi}}{e}\left(\sin\theta + z_g \beta_o g_G (\sin\theta)^2\right) \\ \times \Big(L_0 \Delta T_{sf}(0^+) + \mathrm{W}_{(DD,t)}\left(L_0, t_p\right) + \mathrm{W}^{BC}_{(DD,t)}\left(L_0, t_p\right)\Big), \quad (4.35)$$

where $e$ is Euler's number.

Therefore, the thermal signal-to-noise ratio (SNR) can be defined by

$$(\mathrm{SNR}) = \frac{\left(\frac{\partial \Delta p_{sf}}{\partial \ln \Delta t}\right)_{\Delta t_{mp}}}{\left(\frac{\partial\left(\Delta p_{f_t}+\Delta p_{cont}\right)}{\partial \ln \Delta t}\right)_{\Delta t_{mp}}}. \quad (4.36)$$

Under the adopted assumptions, the expression for the buildup-sandface pressure in SI units is given by

$$\Delta p_{sf}(\Delta t) = p_{ws}\left(t_p+\Delta t\right) - p_{wf}\left(t_p\right) = \\ = \frac{1}{4\pi}\frac{Q_o B_o \mu_o}{k_o h}\left[\ln\left(\frac{t_p \Delta t}{t_p+\Delta t}\right) + \ln\left(\frac{4k_o}{\phi \mu_o c_t r_w^2 e^{\gamma}}\right) + S\right], \quad (4.37)$$

where the term $\left(\frac{t_p \Delta t}{t_p+\Delta t}\right)$ is the well-known *Agarwal Equivalent Time* (Agarwal, 1980) and $\gamma$ is the Euler-Mascheroni constant. The sandface-pressure derivative with respect to $\ln \Delta t$ is given by

$$\frac{\partial \Delta p_{sf}}{\partial \ln \Delta t} = \frac{1}{4\pi} \frac{Q_o B_o \mu_o}{k_o h} \left(\frac{t_p}{t_p + \Delta t}\right). \tag{4.38}$$

Eq. (4.38) evaluated at $\Delta t_{mp}$ gives

$$\left(\frac{\partial \Delta p_{sf}}{\partial \ln \Delta t}\right)_{\Delta t_{mp}} = \frac{1}{4\pi} \frac{Q_o B_o \mu_o}{k_o h} \left(\frac{a_t L_{Rt} t_p}{a_t L_{Rt} t_p + 1}\right). \tag{4.39}$$

For a generic unit system, Eq. (4.36) can be written as

$$\begin{aligned} &\frac{\frac{1}{C_5}}{\frac{1}{2} C_2 \frac{Q_o B_o \mu_o}{k_o h} \left(\frac{a_t L_{Rt} t_p}{a_t L_{Rt} t_p + 1}\right)} \left( \frac{\beta_o \gamma_{oi} \sin\theta}{e} \left( z_g \Delta T_{sf}(0^+) \right.\right. \\ &\qquad + \mathrm{W}^{BC}_{(DD,t)}(z_g, t_p) + \mathrm{W}_{(DD,t)}(z_g, t_p) \Big) \\ &\qquad + \frac{\alpha_{LTE} \gamma_{oi} \sin\theta}{e} \left(1 + z_g \beta_o g_G \sin\theta\right) \Big( L_0 \Delta T_{sf}(0^+) \\ &\qquad \left. + \mathrm{W}_{(DD,t)}(L_0, t_p) + \mathrm{W}^{BC}_{(DD,t)}(L_0, t_p) \Big) \right) = \frac{1}{(\mathrm{SNR})}. \end{aligned} \tag{4.40}$$

It is desired to develop a metric that evaluates whether the isothermal hypothesis can be applied. Therefore, a minimum signal-to-noise ratio is required and Eq. (4.40) will be expressed in the form of an inequality. Under the adopted assumptions, the sums in the LHS of Eq. (4.40) are governed by the $\mathrm{W}_{(DD,t)}$ functions. Further, the product $\left(z_g \beta_o g_G \sin\theta\right)$ is much smaller than the unity, even for $z_g$ in the order of kilometers. Then, Eq. (4.40) can be written as

$$\frac{\frac{1}{2} C_2 \frac{Q_o B_o \mu_o}{k_o h} \left(\frac{a_t L_{Rt} t_p}{a_t L_{Rt} t_p + 1}\right)}{\frac{\sin\theta}{C_5} \left( \frac{\beta_o \gamma_{oi}}{e} \left( \mathrm{W}_{(DD,t)}(z_g, t_p) \right) + \frac{\alpha_{LTE} \gamma_{oi}}{e} \left( \mathrm{W}_{(DD,t)}(L_0, t_p) \right) \right)} > (\mathrm{SNR}). \tag{4.41}$$

The appropriate minimum value for the SNR will be discussed afterwards. Rearranging the terms in Eq. (4.41), it is possible to isolate and verify reservoir properties against wellbore/fluid properties:

$$\frac{k_o h}{\mu_o} < \frac{\frac{1}{2}\frac{1}{\sin\theta}\, Q_o B_o \left(\frac{C_2 \times C_5}{(\mathrm{SNR})}\right)\left(\frac{a_t L_{Rt} t_p}{a_t L_{Rt} t_p + 1}\right)}{\frac{\beta_o \gamma_{oi}}{e}\left(\mathrm{W}_{(DD,t)}(z_g, t_p)\right) + \frac{\alpha_{LTE}\gamma_{oi}}{e}\left(\mathrm{W}_{(DD,t)}(L_0, t_p)\right)}. \tag{4.42}$$

The LHS of Eq. (4.42) accounts for reservoir properties, in the form of the effective oil transmissibility. The RHS describes the dependency on the operating drawdown rate, fluid thermal properties and wellbore thermal and dimensional properties. Among other wellbore features, the gauge depth $z_g$ is an explicit input to calculate $\mathrm{W}_{(DD,t)}(z_g, t_p)$ (see Eq. (B.18)).

A reasonable approximation for $\mathrm{W}_{(DD,t)}$ can be made when

$$t_p > \frac{L_0}{a_t}, \tag{4.43}$$

which is the argument of the Heaviside step function in Eq. (B.18), substituting $(z_g - z_c)$ for $L_0$. This condition is satisfied in a few hours of well flow, considering lengths in the order of few kilometers and downhole rates greater than 300 m³/d. Then, the function $\mathrm{W}_{(DD,t)}$ can be written as

$$\mathrm{W}_{(DD,t)}(x) = -\frac{\Omega x^2}{2L_{\beta t}} + \left(\frac{\Omega}{L_{\beta t}^3} + \frac{\psi}{L_{\beta t}^2}\right)\left(xL_{\beta t} + e^{(-xL_{\beta t})} - 1\right), \tag{4.44}$$

where $x$ is replaced by $z_g$ and $L_0$ in the arguments of the $\mathrm{W}_{(DD,t)}$ functions in Eq. (4.42).

Under the adopted assumptions, the terms $z_g L_{\beta t}$ and $L_0 L_{\beta t}$ yield small values. Hence, it is convenient to apply the Taylor series approximation in the form

$$x + e^{-x} \approx 1 + \frac{x^2}{2}. \tag{4.45}$$

Therefore, the expression in Eq. (4.44) can be rewritten as

$$\mathrm{W}_{(DD,t)}(x) = -\frac{\Omega x^2}{2L_{\beta t}} + \left(\frac{\Omega}{L_{\beta t}^3} + \frac{\psi}{L_{\beta t}^2}\right)\frac{\left(xL_{\beta t}\right)^2}{2}. \tag{4.46}$$

Rearranging the terms in Eq. (4.46), the expression reduces to

$$\mathrm{W}_{(DD,t)}(x) = x^2\frac{\psi}{2}. \tag{4.47}$$

The combination of Eqs. (4.42) and (4.47) yields

$$\frac{k_o h}{\mu_o} < \frac{\frac{Q_o B_o}{\sin\theta}\left(\frac{C_2 \times C_5}{(\mathrm{SNR})}\right)\left(\frac{a_t L_{Rt} t_p}{a_t L_{Rt} t_p + 1}\right)}{\frac{\beta_o \gamma_{oi}}{e} z_g^2 \psi + \frac{\alpha_{LTE}\gamma_{oi}}{e}(L_0)^2 \psi}. \tag{4.48}$$

Eq. (4.48) provides an important conclusion. It shows that thermal impacts on pressure gauge data respond to the square of the distance from the producing horizon.

The metric can be rearranged to calculate two important parameters that can be controlled in well-test design and operations. The following subsections provide the expressions for the maximum gauge distance from the producing horizon and the minimum drawdown rate, respectively. Then, the expression for the SNR will be addressed.

### 4.4.3. Maximum Gauge Distance from the Producing Horizon $\Delta z_{max}$

The inequality in Eq. (4.48) can be removed by adopting the concept of a maximum gauge distance from the producing horizon $\Delta z_{max}$. For a specific wellbore/reservoir system undergoing a well test, the gauge must be placed within $\Delta z_{max}$ to allow the use of isothermal interpretations methods.

$$\frac{k_o h}{\mu_o} = \frac{\frac{Q_o B_o}{\sin\theta}\left(\frac{C_2 \times C_5}{(\mathrm{SNR})}\right)\left(\frac{a_t L_{Rt} t_p}{a_t L_{Rt} t_p + 1}\right)}{\frac{\beta_o \gamma_{oi}}{e}(\Delta z_{max})^2 \psi + \frac{\alpha_{LTE}\gamma_{oi}}{e}(L_0)^2 \psi}. \tag{4.49}$$

Eq. (4.49) can be rearranged as

$$\Delta z_{max} = \sqrt{\frac{Q_o B_o \mu_o}{k_o h \sin\theta}\frac{1}{\psi}\frac{e}{\beta_o \gamma_{oi}}\left(\frac{C_2 \times C_5}{(\mathrm{SNR})}\right)\left(\frac{a_t L_{Rt} t_p}{a_t L_{Rt} t_p + 1}\right) - \frac{\alpha_{LTE}(L_0)^2}{\beta_o}}. \tag{4.50}$$

Eq. (4.50) states that for a specific wellbore/reservoir system, the isothermal hypothesis is only valid when the gauge is placed below $\Delta z_{max}$. It is important to state that all inputs in Eq. (4.50) are commonly known fluid and wellbore parameters.

Further approximations for usual property values and operational conditions can be made. The product $\beta_o \gamma_{oi}$ typically ranges from 6 to 8 $(kg/m^3/K)$ and the value of the term $\left(\frac{a_t L_{Rt} t_p}{a_t L_{Rt} t_p + 1}\right)$ lies between 0.80 and 0.99 in well-testing operations. Moreover, for a vertical well and typical fluid thermal properties, the constant $\psi$ can be approximated by 90% of the geothermal gradient (see Eq. (3.26)), and the dimensionless ratio $\frac{\alpha_{LTE}}{\beta_o}$ has a magnitude of 1.0E-2.

With the aforementioned considerations, the expression for $\Delta z_{max}$ is given by (in SI units)

$$(\Delta z_{max})_{90^\circ} = \sqrt{\left(\frac{9}{4}\frac{e}{\pi}\right)\frac{Q_o B_o \mu_o}{k_o h}\frac{1}{(\mathrm{SNR})} - \frac{(L_0)^2}{100}}. \tag{4.51}$$

For a different unit system,

$$(\Delta z_{max})_{90^\circ} = \sqrt{(C_{iso})^2\frac{Q_o B_o \mu_o}{k_o h}\frac{1}{(\mathrm{SNR})} - \frac{(L_0)^2}{100}}, \tag{4.52}$$

where $C_{iso}$ is a unit conversion factor. The value of $C_{iso}$ is 11,322 in Oil Field units and 4,778 for the adopted unit system in this work (see Appendix A). The value of SNR should range between 4 and 6.

In the particular case of constant pipe length, the term dependent on tubing length $(L_0)$ in Eqs. (4.50), (4.51) and (4.52) must be set to zero.

The expression in Eq. (4.52) is a powerful result and easy to compute. If the pressure gauge is placed below $\Delta z_{max}$, then the isothermal hypothesis is valid. If the gauge is placed above $\Delta z_{max}$, then the well test must be considered non-isothermal and be interpreted considering the influence of thermal effects.

The expression in Eq. (4.52) is useful for quick analyses. For a more accurate result, one must perform calculations with Eq. (4.50). Chapter 5 will verify the results presented in this section.



### 4.4.4. Minimum Operating Drawdown Rate

Given the gauge location $z_g$, there is a minimum drawdown rate prior to shut-in that must be imposed to allow the application of the isothermal hypothesis. Rearranging Eq. (4.50), the expression for the minimum rate is given by

$$Q_{min} = \left(\frac{k_o h}{\mu_o B_o}\right)\left(\beta_o z_g^2 + \alpha_{LTE}(L_0)^2\right) \times \psi\frac{\gamma_{oi}\sin\theta}{e}\left(\frac{(\mathrm{SNR})}{C_2 \times C_5}\right)\left(\frac{a_t L_{Rt} t_p + 1}{a_t L_{Rt} t_p}\right). \tag{4.53}$$

Following the same idea to derive the approximate expression for $\Delta z_{max}$ in Eq. (4.52), the expression for the minimum rate in a vertical well is given by

$$(Q_{min})_{90^\circ} = \left(\frac{k_o h}{\mu_o B_o}\right)\frac{z_g^2 + \frac{(L_0)^2}{100}}{(C_{iso})^2}(\text{SNR}). \tag{4.54}$$

For a specific wellbore/reservoir system, the isothermal hypothesis is only valid when the drawdown rate prior to shut-in is greater than $Q_{min}$.

### 4.4.5. Signal-to-Noise Ratio (SNR)

Eq. (4.53) can be rearranged to provide an easy to compute expression for the SNR, given a particular wellbore/reservoir system undergoing a well test.

$$(\text{SNR}) = \frac{\left(\frac{Q_o B_o \mu_o}{k_o h}\right)}{\left(\beta_o z_g^2 + \alpha_{LTE}(L_0)^2\right)}\left(\frac{e}{\psi}\right)\left(\frac{C_2 \times C_5}{\gamma_{oi}\sin\theta}\right)\left(\frac{a_t L_{Rt} t_p}{a_t L_{Rt} t_p + 1}\right). \tag{4.55}$$

It is noteworthy the inverse relation with the parameters $\beta_o$, $\alpha_{LTE}$ and $\gamma_{oi}$ and with the square of $z_g$.

Eq. (4.54) can also be rearranged to provide an expression for quick analyses:

$$(\text{SNR})_{90^\circ} = \frac{\left(\frac{Q_o B_o \mu_o}{k_o h}\right)(C_{iso})^2}{z_g^2 + \frac{(L_0)^2}{100}}. \tag{4.56}$$

As mentioned before, the value of SNR should range between 4 and 6.

## 4.5. Non-Isothermal Initial Pressure

The initial pressure is computed from Eq. (4.7) evaluated at $t = 0$.

$$p_g(z_g, t=0) = p_{sf}(t=0) - z_g\gamma_{oi}\sin\theta + \sin\theta\,\beta_o\gamma_{oi}\int_0^{z_g}\Delta T_w(z, t=0)dz - \frac{z_g^2}{2}\gamma_{oi}\beta_o g_G(\sin\theta)^2. \tag{4.57}$$

The value of $\Delta T_w$ at $t = 0$ is zero. Then, it becomes clear that the expression for the initial pressure at a gauge is a quadratic function of depth:

$$p_i(z_g) = p_i^{res} - z_g\gamma_{oi}\sin\theta - \frac{z_g^2}{2}\gamma_{oi}\beta_o g_G(\sin\theta)^2, \tag{4.58}$$

where $p_i^{res}$ refers to the initial pressure at $z = 0$.

As mentioned before, one of the main outcomes of a well test is to determine the reservoir initial pressure. Under the isothermal hypothesis, the initial pressure

measured at a gauge is simply shifted to the desired datum by using the fluid specific weight. The error associated to this procedure under a non-isothermal condition can be easily determined. The pressure-shift relative error (PSRE) is given by:

$$\mathrm{PSRE}(z_g) = 1 - \frac{\left(p_i^{res} - p_i(z_g)\right)_{iso}}{\left(p_i^{res} - p_i(z_g)\right)_{non-iso}} = 1 - \frac{2}{2 + z_g \beta_o g_G \sin\theta}. \qquad (4.59)$$

Note that the error does not depend on the fluid mass density. For a vertical well and typical values, the resulting initial pressure encompasses an error ranging from 0.1% to 2% when the isothermal hypothesis is assumed.

# 5
# Validation of Analytical Solutions

This chapter compares the derived analytical solutions to the rigorous response of a commercial non-isothermal simulator (CMG-STARS, 2017). All synthetic examples used to verify the proposed analytical solutions consider an oil/water system, where the only flowing phase is oil with presence of connate water.

The rigorous non-isothermal simulator model accounts for a finite wellbore coupled to the reservoir grid. The model consists of 200 gridblocks in the *r*-direction and 41 gridblocks in the *z*-direction. The finite wellbore is cased, cemented and completed with a production tubing. The reservoir comprises only the bottom layer, which is fully perforated, and the other 40 layers represent the formation adjacent to the wellbore. Layers may exchange heat between them, but no fluid flow occurs.

Figure 5.1 illustrates the schematic of the wellbore/reservoir system to be used in the examples.

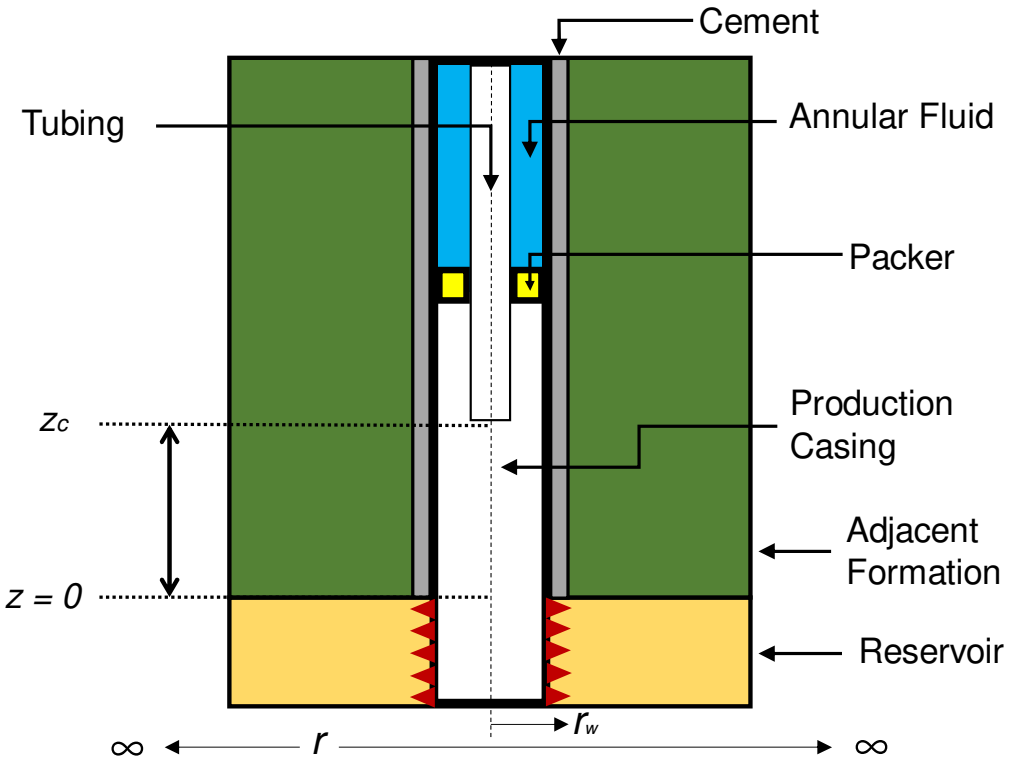


Figure 5.1: Schematic of Wellbore/Reservoir System

The non-isothermal simulator model comprises a finite perforated interval, whereas the proposed analytical solution assumes perforations to be a point source. Hence, the location of $z = 0$ at the top of the completed interval in Figure 5.1 is merely schematic.

The parameter $z_c$ is the distance between the producing horizon and the bottom of the tubing string. In the simulator, fluid flows from perforations through the production casing between $z = 0$ and $z = z_c$. Above $z_c$, flow occurs only through the tubing string, because a packer has been placed in the casing-tubing annulus. Likewise, the analytical solution assumes no flow in the annulus.

Reservoir properties are presented in Table 5.1.

Table 5.1: Reservoir Properties

| Property | Value |
|---|---|
| $p_i$ (kgf/cm²) | 500.0 |
| $T_i$ (K) | 334.0 |
| $k_{radial}$ (mD) | *depends on the example* |
| $k_{vertical}$ (mD) | 0 |
| $h$ (m) | *depends on the example* |
| $r_e$ (m) | 25,000.00 |
| $\phi$ (fraction) | 0.12 |
| $c_r$ (cm²/kgf) | 3.0E-5 |
| $s_w$ (fraction) | 0.15 |
| $g_G$ (K/m) | 0.03 |
| $c_{pr}$(J/m³/K) | 2.347E+6 |
| $\lambda_r$ (J/m/h/K) | 1.396E+4 |
| $\lambda_e$ (J/m/h/K) | 1.383E+4 |
| $\alpha_e$(m²/h) | 5.894E-3 |

The results in this study consider only single-phase-liquid flow, therefore the adopted fluid model in the simulator only accounts for one water and one dead oil. When modeling pressure and temperature in the simulator, the following properties are variable with temperature and pressure:

- Fluid mass densities;
- Specific heat capacities;
- Joule-Thomson coefficients;
- Adiabatic-expansion coefficients.

All other properties have been set as constants to the simulator. The Joule-Thomson coefficients, heat capacities and adiabatic-expansion coefficients cannot be explicitly entered into the simulator. The software calculates these parameters from other input fluid properties, making use of the Lee-Kesler (1975) method to include the Joule-Thomson effect on the temperature transients. It requires critical properties of oil as input data, including critical pressure ($p_c$), critical temperature ($T_c$), molecular weight (MW), acentric factor ($\omega$) and two correlation gas-phase heat-capacity coefficients (CPG1 and CPG2). The simulator generates heat-capacity and enthalpy tables, which allow the calculation of the aforementioned properties as functions of pressure and temperature over time.

The proposed analytical solution in this work models the oil mass density as function of temperature in the wellbore. All other physical and thermal properties of oil, water and rock are assumed constant, including the oil mass density in the porous medium. In order to be consistent with the simulator, the constant values for these properties are obtained from output tables generated by the software, evaluated at initial pressure and temperature.

The input fluid properties are presented in Table 5.2.

Table 5.2: Input Fluid Properties

| Property | Oil | Water |
|---|---|---|
| $B$ (m³/std m³) | 1.4 | 1.0 |
| $c$ (cm²/kgf) | 1.10E-4 | 3.96E-5 |
| $\mu$ (cP) | 0.9 | 1.0 |
| MW (kg/gmol) | 0.102 | 0.01802 |
| $T_c$ (K) | 513.15 | 647.35 |
| $p_c$ (kgf/cm²) | 30.0 | 224.83 |
| $\omega$, acentric factor | 0.3506 | - |
| CPG1 (J/gmole/K) | 8.845 | - |
| CPG2 (J/gmole/K²) | 0.5067 | - |
| $\lambda$ (J/m/h/K) | 5.833E+2 | 2.229E+3 |
| $\rho_{oi}$ (kg/m³) | 770.0 | 998.2 |
| $\beta$ (K$^{-1}$) | 1.11E-3 | 5.27E-4 |

The adopted formation volume factor is 1.4 for oil and 1.0 for water. Though the non-isothermal simulator is not a black-oil simulator, it permits the modeling of

$B_o$ with a pressure/temperature cross term for liquid density (Onur and Cinar, 2017a).

The simulator uses the data in Table 5.1 and Table 5.2 to generate several fluid property tables. The output data will be interpolated to obtain the constant values for the Joule-Thomson coefficients, adiabatic-expansion coefficients and heat capacities at initial conditions.

Table 5.3 presents a portion of the oil heat capacity table generated by the non-isothermal simulator.

Table 5.3: Oil Heat Capacity at Initial Pressure

| **Temperature (K)** (Reduced Temperature) | **Heat Capacity (J/kg/K)** |
|---|---|
| **274.0** (0.5340) | 2,008.38 |
| **374.0** (0.7288) | 2,415.90 |

The interpolation of Table 5.3 data provides an oil heat capacity at initial pressure and temperature of 2,252.9 J/kg/K.

Table 5.4 presents a portion of the oil specific enthalpy data generated by the non-isothermal simulator. These data are used to calculate both Joule-Thomson and adiabatic-expansion coefficients.

Table 5.4: Specific Enthalpy Table (kJ/kg)

| | **Pressure (kgf/cm²)** (Reduced Pressure) | | |
|---|---|---|---|
| **Temperature (K)** (Reduced Temperature) | **250.0** (8.33) | **500.0** (16.67) | **1,000.0** (33.33) |
| **274.0** (0.5340) | -423.733 | -403.233 | -362.127 |
| **374.0** (0.7288) | -199.036 | -181.089 | -145.091 |

The required thermodynamic relationships to calculate the coefficients are given by

$$\varepsilon_{JTo} = -\frac{1}{c_{po}}\left(\frac{\partial H}{\partial p}\right)_T, \tag{5.1}$$

and

$$\varphi_o = \frac{1}{\rho_{oi} c_{po}} + \varepsilon_{JTo}, \tag{5.2}$$

where $H$ is the specific enthalpy.

The interpolation of Table 5.4 data combined with the thermodynamic relationships in Eqs. (5.1) and (5.2) provide an oil Joule-Thomson coefficient at initial conditions of -0.03374 K/(kgf/cm²) and an adiabatic-expansion coefficient of 0.02279 K/(kgf/cm²).

Water coefficients have been obtained by a similar procedure. Table 5.5 summarizes the calculated fluid properties to be used in the analytical solutions.

Table 5.5: Fluid Thermal Properties at Initial Conditions

| Property | Oil | Water |
|---|---|---|
| $c_p$ (J/kg/K) | 2252.90 | 4209.35 |
| $\varepsilon_{JT}$ (K/(kgf/cm²)) | -3.374E-2 | -1.921E-2 |
| $\varphi$ (K/(kgf/cm²)) | 2.279E-2 | 4.132E-3 |

Shown in Table 5.6 are the saturated porous medium properties. The expressions to calculate $\lambda_t$, $\alpha_t$ and $\varphi_t^*$ are presented in Eqs. (2.9), (2.10) and (2.11), respectively.

Table 5.6: Saturated Porous-Medium Properties

| Property | Value |
|---|---|
| $\lambda_t$ (J/m/h/K) | 1.238E+4 |
| $\varphi_t^*$ (K/(kgf/cm²)) | 1.874E-3 |
| $\alpha_t$ (m²/h) | 5.342E-3 |

The gauge location depends on the example. Wellbore parameters are presented in Table 5.7.

Table 5.7: Wellbore Parameters

| Property | Value |
|---|---|
| $r_w$ (m) | 0.156 |
| $r_{co}$ (m) | 0.12224 |
| $r_{ci}$ (m) | 0.10839 |
| $r_{to}$ (m) | 0.06985 |
| $r_{ti}$ (m) | 0.05931 |
| $\lambda_{cem}$ (J/m/h/K) | 6.833E+3 |
| $\lambda_{wall}$ (J/m/h/K) | 1.617E+5 |
| $\lambda_{wall-cem}$ (J/m/h/K) | 9.995E+3 |
| $\lambda_{an}$ (J/m/h/K) | 5.833E+2 |
| Skin Factor | 0 |
| $\theta$ (degree) | 90° |
| $z_c$ (m) | 100 |
| $z_{gauge}$ (m) | *depends on the example* |
| $C_{Tc}$ (dimensionless) | *depends on the example* |
| $C_{Tt}$ (dimensionless) | *depends on the example* |

The parameters $\psi$ and $\Omega$ are computed from Eqs. (3.26) and (3.28), yielding the values of 2.825 E-2 K/m and -8.652 E-8 K/m², respectively.

It has been adopted an infinitesimal thickness for both casing and tubing walls in the simulation model. Besides, the casing wall/cement system has been modeled in the simulator as a single wellbore cylindrical layer,

$$\lambda_{wall-cem} = \ln\left(r_w/r_{ci}\right)\left[\frac{\ln\left(r_w/r_{co}\right)}{\lambda_{cem}} + \frac{\ln\left(r_{co}/r_{ci}\right)}{\lambda_{wall}}\right]^{-1}. \tag{5.3}$$

Gauges will be located below and above the packer, placed 87.5 m from the bottom of the tubing string. Therefore, to allow easy comparisons at different locations, the tubing string is not insulated. To model this condition, the proposed analytical solution assumes the same thermal conductivity for the annular fluid and the oil phase.

The proposed analytical solution makes use of the relaxation distance $L_\beta$ to model the formation/wellbore overall resistance to heat flow. During the drawdown period, this parameter is computed from the combination of Eqs. (3.4) and (3.27). After shut-in, the parameter is set as constant, evaluated at $t = t_p$.

The following subsections present three examples. Except for the effective oil flow capacity (*kh*) and gauge locations, all examples share the data presented in this section.

The examples are used to verify the proposed analytical transient solutions derived in this work, which are:

- Buildup sandface-temperature solution (Chapter 2);
- Wellbore-temperature solutions (Chapter 3);
- Solutions for thermal impacts on wellbore pressure (Chapter 4).

## 5.1. Validation of Analytical Buildup Sandface-Temperature Solution

The proposed buildup sandface-temperature solution is presented in Eq. (2.56). Buildup tests usually comprise a 24-hour drawdown followed by a 24 to 48-hour buildup period. To analyze and verify the proposed solution, the shut-in time will be 5 times greater than the producing period. Therefore, the simulated test sequence comprises 24 hours of production followed by a 120-hour buildup. The constant oil production downhole rate was set at 800 m³/d and the reservoir is 50 meters thick.

To evaluate the sandface temperature in absence of wellbore axial conduction effects, the casing wall was not considered in the finite wellbore simulation model of Example 1.

By changing the reservoir permeability, the solution has been evaluated for different values of transmissibility. Table 5.8 presents the effective oil permeabilities for each case.

Table 5.8: Effective Oil Permeabilities for Example 1

| Case | Effective Oil Permeability $k_o$(mD) | Effective Oil Transmissibility (mD.m/cP) |
|---|---|---|
| Case 1.1 | 1400 | 77,778 |
| Case 1.2 | 35 | 1,944 |

Each case presents a Cartesian plot of the entire testing time (drawdown + buildup) and a semilog plot of the buildup period. Results are presented as follows.

**Case 1.1 ($k_o$ = 1400 mD)**

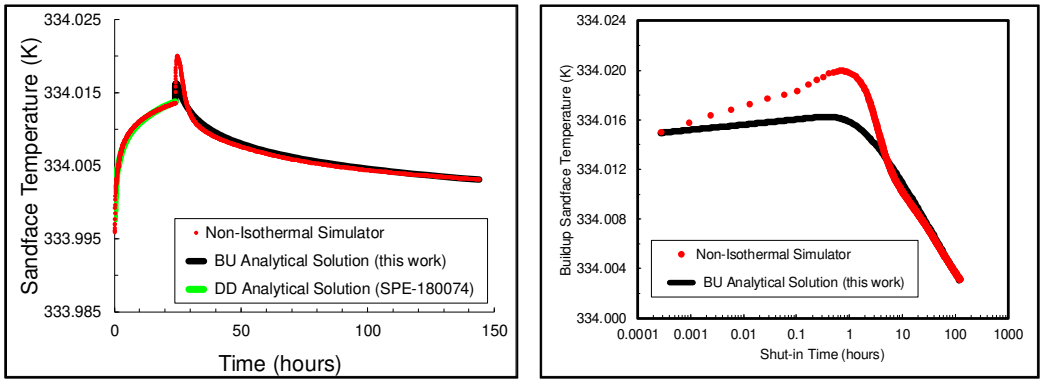


(a) (b)

Figure 5.2: Case 1.1 – (a) Cartesian Plot; (b) Semilog Plot

The Cartesian plot in Figure 5.2 (a) is composed by three temperature curves:

1. Non-isothermal simulator drawdown + buildup curve (in red);
2. Onur and Cinar (2017a) analytical drawdown-sandface solution (in blue);
3. The proposed analytical buildup-sandface solution in this work (in black).

Onur and Cinar (2017a) drawdown sandface-temperature solution is used as the initial condition for the buildup problem (see Eqs. (2.28) and (2.30)). However, any other drawdown-sandface solution could be used. Nevertheless, this work recommends the use of the expression proposed by Onur and Cinar (2017a), since it presented a good match with the non-isothermal simulator in all analyses performed in this study.

The semilog plot in Figure 5.2 (b) presents the buildup curves computed from the simulator (in red) and from the proposed solution (in black).

In both plots, there is an evident deviation in early shut-in times. In this case, the difference between the maximum temperatures is 0.004 K. This difference will be discussed at the end of this subsection and it will be shown that it is systematic. Apart from that, the proposed solution presents a good match with the non-isothermal simulator in both plots.

It is interesting to note that the initial reservoir temperature is 334 K and the cooling response at initial drawdown times is due to the adiabatic expansion effect.

**Case 1.2 ($k_o$ = 35 mD)**

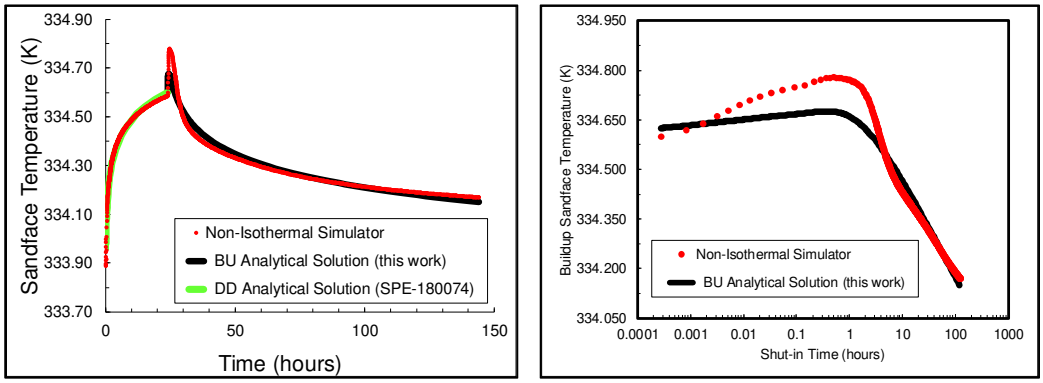


(a) (b)

Figure 5.3: Case 1.2 – (a) Cartesian Plot; (b) Semilog Plot

The previous comments apply to this case and the early-time deviation is 0.1 K. Two other cases with permeabilities of 700 mD and 350 mD have been run, providing deviations of 0.007 K and 0.013 K, respectively. In all cases the deviation occurred between 0.01 – 3.0 hours. Besides that, buildup temperatures computed from Eq. (2.56) match well with the corresponding simulator temperatures.

The explanation for the mismatch lies on analyzing the early-time pressure response. When the well is shut in, the analytical solution considers the downhole rate to be zero, whereas the non-isothermal simulator presents a non-zero rate. The result on wellbore pressure is the well-known wellbore storage (WBS) effect, which implies a higher $\partial\Delta p/\partial\Delta t$ at early times. As for temperature, the impact comes in the form of a stronger adiabatic compression effect. This early-time thermal effect lasts longer than WBS effects, because in practical cases thermal conduction dominating the buildup period is a much slower process than pressure diffusion.

The energy balance expressed in Eq. (5.4), which is the early-time approximation of Eq. (2.29), illustrates the relation between early-time pressure and temperature,

$$\Delta T(r,\Delta t) = \int \left(\varphi_t^* \frac{\partial \Delta p}{\partial \Delta t}\right) d\Delta t \,. \tag{5.4}$$

The solution of Eq. (5.4) with the appropriate boundary conditions is given by Eq. (2.33), where temperature responds to the inverse of permeability (assuming a weak contribution of the exponential integral function). Hence, as expected, the absolute early-time temperature deviation also responds to the inverse of permeability, as shown by the negative slope close to $-1$ in Figure 5.4.

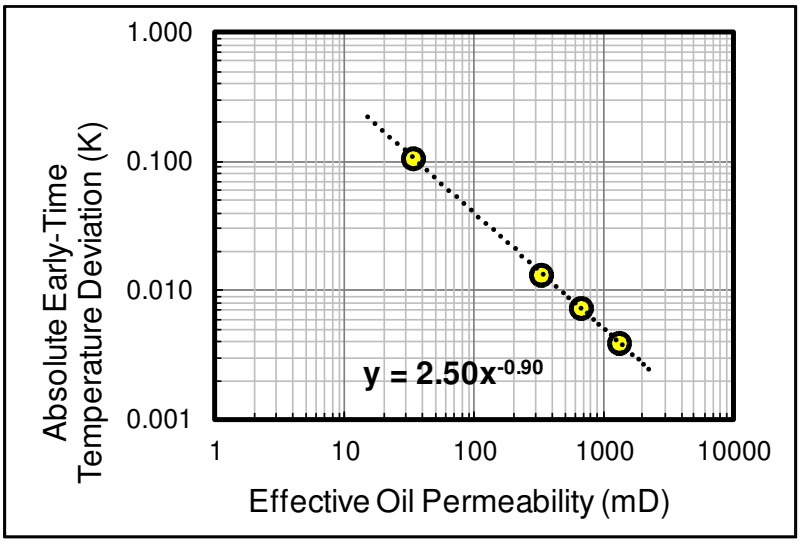


Figure 5.4: Absolute Early-Time Temperature Deviation vs. Effective Permeability

Another analysis can be performed in terms of the relative early-time deviation, defined as the ratio of the analytical solution temperature difference to the simulator temperature difference.

$$(\Delta T/\Delta T)_{deviation} = \frac{\left(T_{max} - T_{wf}\right)_{(an.\ solution)}}{\left(T_{max} - T_{wf}\right)_{(simulator)}}. \tag{5.5}$$

This analysis isolates the early-time $\partial \Delta p/\partial \Delta t$ impact, as shown in Figure 5.5.

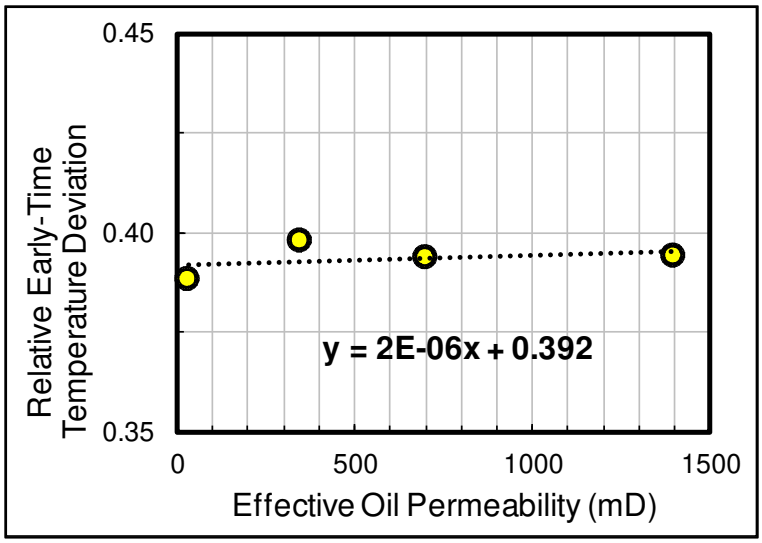


Figure 5.5: Relative Early-Time Temperature Deviation vs. Effective Permeability

The relative early-time temperature deviation is 40%, regardless of the value of permeability. Both analyses show that deviations are systematic.

In real well-testing operations, the downhole tester valve is usually placed near the bottom of the test string, reducing the WBS effect during buildup. Hence, real downhole data should be well described by the analytical solution.

Apart from the wellbore storage impact on temperature, the proposed solution presents a good match with the non-isothermal simulator. Furthermore, results show that the analytical solution can be applied to a wide range of permeabilities, given the wellbore/reservoir system and operational conditions adopted in Example 1. Additionally, the solution presents a good match even for long shut-in times, making the solution valid for conventional test sequences.

Regarding the magnitude of the drawdown rate, the proposed solution presents a good match for low rates at early times, however it fails to describe temperature changes at intermediate and late times due to the adopted assumptions. For the wellbore/reservoir system presented in Example 1, the match is good for rates above 300 m³/d, from early to late shut-in times.



## 5.2. Validation of Analytical Transient-Wellbore-Temperature Solutions

This section verifies the transient-wellbore-temperature solutions derived in this work. The production-casing drawdown and buildup solutions are expressed in Eqs. (3.41) and (3.78), and cased-tubing solutions are given by Eqs. (3.51) and (3.79).

It is noteworthy to state that buildup wellbore-temperature solutions are only coupled with the buildup-sandface solution at $\Delta t = 0^+$. After this instant, wellbore solutions no longer depend on reservoir data (except at $z = 0$). This feature is important to be clear, because wellbore solutions are not restricted to the limitations of the buildup-sandface solution and can be applied to low rate scenarios and to low permeability reservoirs.

To the best of the author's knowledge, the simulator finite wellbore completion model does not account for expansion joints. Therefore, this chapter assumes no tubing expansion or contraction. This effect will be evaluated in Chapter 6.

The proposed solution will be compared to the rigorous non-isothermal simulator response. Analyses will be performed by evaluating both temperature and

pressure data from simulated gauges placed inside the finite wellbore model. Table 5.9 presents the gauge locations.

Table 5.9: Gauge Locations in Example 2

| Case | Gauge Distance From the Producing Horizon $z_g$ (m) | Gauge Location |
|---|---|---|
| Case 2.1 | 0.0 | Production Casing |
| Case 2.2 | 100.0 | Production Casing |
| Case 2.3 | 137.5 | Tubing |
| Case 2.4 | 287.5 | Tubing |
| Case 2.5 | 512.5 | Tubing |

The reservoir permeability is set at 100 mD and the reservoir thickness is 50 meters. The simulated test sequence comprises 48 hours of production at a constant downhole rate of 800 m³/d followed by a 48-hour buildup.

Recalling Figure 5.1, the schematic gauge location is presented as follows:

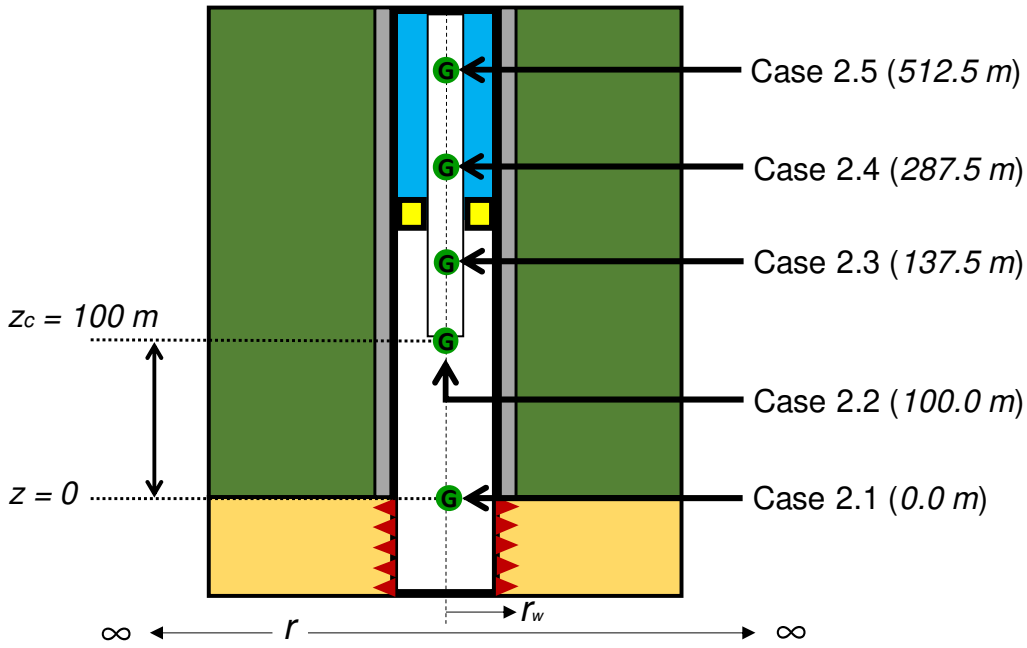


Figure 5.6: Schematic Gauge Location in Example 2

Besides the comparison with the non-isothermal simulator, the proposed solution will be compared to other two analytical transient-wellbore-temperature solutions, proposed by Hasan et al. (2005) and Onur et al. (2017). These solutions do not model temperature changes in a cased tubing, therefore they will only be addressed in cases 2.1 and 2.2.

This work assumes a constant volumetric production rate, which is a reasonable assumption regarding the wellbore/reservoir and operational properties adopted in the examples. Hence, the solutions proposed by Hasan et al. (2005) and Onur et al. (2017) will be computed under the same assumption. In addition, a constant fluid mass density will be adopted for these solutions.

**Case 2.1 ($z_g$ = 0 m)**

The objective of this case is to evaluate the wellbore-temperature solutions at $z = 0$, i.e., at sandface. Hence, Case 2.1 uses the same finite wellbore simulation model of Example 1.

Figure 5.7 presents the drawdown response of the wellbore-temperature solutions at $z = 0$, together with the sandface solution proposed by Onur and Cinar (2017a) and the non-isothermal simulator response.

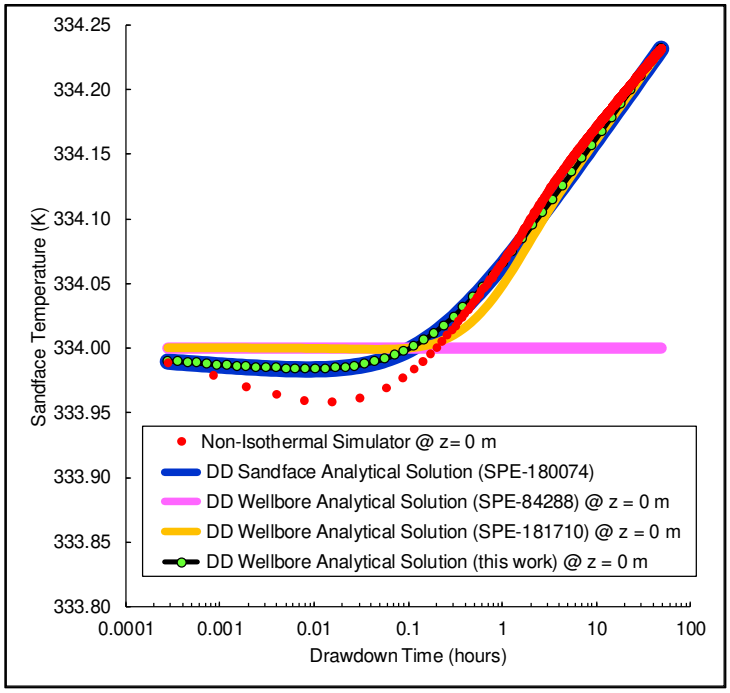


Figure 5.7: Drawdown Solutions at $z = 0$

The analytical sandface solution (blue curve) proposed by Onur and Cinar (2017a) presents a good match with the non-isothermal simulator at $z = 0$ (red curve). The minor differences at early times have been previously discussed and they are due to WBS impacts on the fluid adiabatic expansion effect.

The proposed analytical wellbore-temperature solution (green curve) is fully coupled with sandface-temperature changes (blue curve), yielding the exact same

response at $z = 0$. Recalling Eq. (3.35), Onur and Cinar (2017a) sandface-temperature solution (blue curve) is an imposed boundary condition to solve the transient problem.

The wellbore solution proposed by Onur et al. (2017) (yellow curve) presents deviations at early and intermediate times due to the approximation of the term $\partial T/\partial z$. This is a consequence of using the sandface-temperature boundary condition to solve the steady-state problem, not making it available for the transient problem. The impacts of this assumption along the wellbore will be discussed in Case 2.2.

Hasan et al. (2005) adopt the same simplification and, in addition, the reservoir is assumed isothermal, therefore no temperature changes occur at $z = 0$ (pink curve).

The buildup-sandface response has been assessed in Example 1 and will not be addressed in this case.



**Case 2.2 ($z_g$ = 100 m)**

First, the proposed analytical wellbore-temperature solution will be compared to the non-isothermal simulator response. Then, a comparison with the solutions proposed by Hasan et al. (2005) and Onur et al. (2017) will be performed.

Figure 5.8 presents the drawdown and the buildup curves at a gauge placed 100 meters above the producing horizon in a production casing. In addition, the blue and green curves are the drawdown- and buildup-sandface temperatures, respectively.

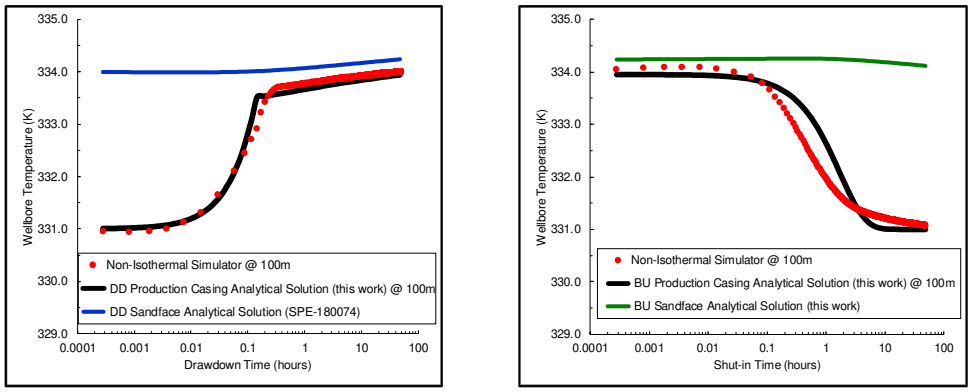


(a) (b)

Figure 5.8: Case 2.2 – (a) Drawdown; (b) Buildup

In Figure 5.8 (a), there is an interesting transition in the drawdown behavior at 0.2 hours, when the proposed analytical solution (black curve) and the simulated response (red curve) present a change in the heating profile. When the well is opened to flow, the fluid below the gauge starts flowing upwards, heating the gauge by a simple process of fluid elevation, i.e., a deeper and warmer fluid continuously reaches the gauge over time. This heating mechanism dominates gauge-temperature changes until the fluid originally at sandface reaches the gauge depth, suddenly ceasing the process of heating by vertical lifting. At this moment, there is no longer any fluid from deeper horizons to keep the mechanism active. From this point on, gauge-temperature changes are governed by Joule-Thomson heating effects (both in the wellbore and reservoir), and by the heat loss to surroundings caused by radial diffusion.

The proposed analytical solution is able to accurately describe the heating caused by the fluid elevation process. In Eqs. (3.42) and (3.43), when the Heaviside Step functions are "turned on", the lifting effect ceases and the heating behavior suffers the change depicted in Figure 5.8 (a).

Figure 5.8 (b) presents the buildup period that follows the drawdown in Figure 5.8 (a). The wellbore temperature at late times approaches the constant value of the Earth temperature at the gauge location. The intermediate-time mismatch stems from the neglect of axial conduction effects along the wellbore. Nonetheless, the overall behavior has been successfully reproduced.

The drawdown thermal-storage coefficient was set to 0.3 and the value for the buildup period was set to 0.0.

The analytical modeling of transient-temperature changes due to vertical fluid elevation is one of the main contributions of this work. This effect has been successfully assessed because the transient wellbore energy-balance equation was treated as a true partial-differential equation, and not simplified to an ordinary-differential equation.

As mentioned before, the solutions proposed by Hasan et al. (2005) and Onur et al. (2017) adopted a simplification for the wellbore-temperature gradient $\partial T/\partial z$. Figure 5.9 compares the proposed analytical solution in this work to these two other analytical solutions at $z = 100$ m.

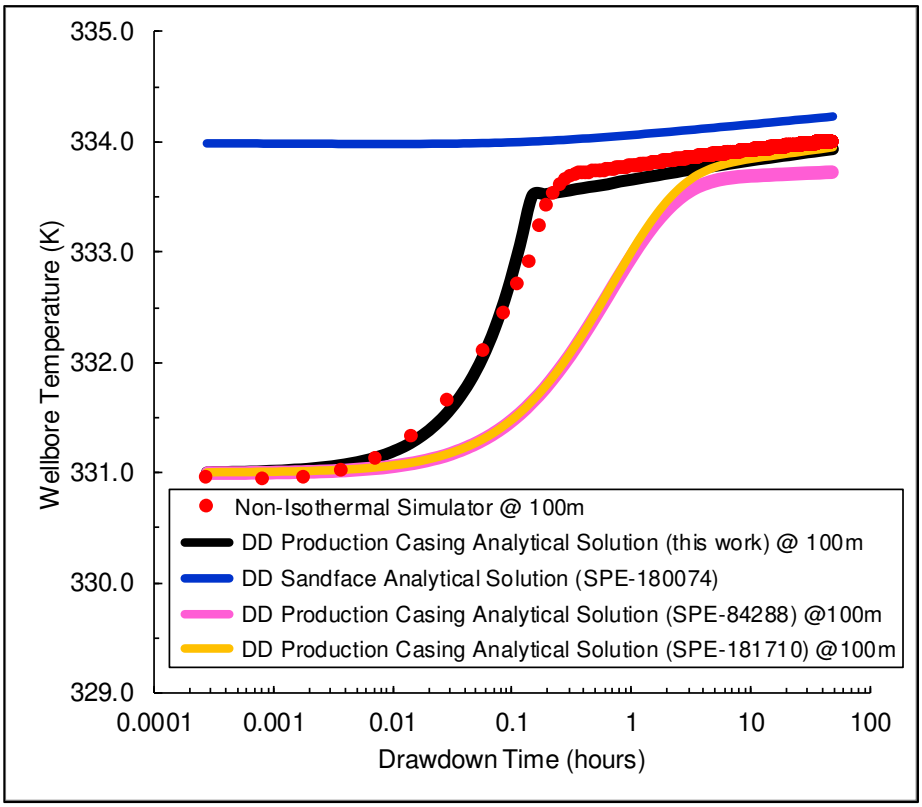


Figure 5.9: Drawdown Solutions

In Figure 5.9, the solutions proposed by Hasan et al. (2005) (pink curve) and Onur et al. (2017) (yellow curve) do not provide a good match with the non-isothermal simulator at intermediate times. The mismatch is rooted in the assumption of using the steady-state $\partial T/\partial z$ to solve the transient flow problem. Hasan et al. (2005) also noted the impacts of this simplification in their work when translating pressures within the wellbore.

The solution proposed by Hasan et al. (2005) also does not present a good match at late times, due to the assumption of an isothermal reservoir in their work. As expected, at late times the solution proposed by Onur et al. (2017) (yellow curve) converges to the non-isothermal simulator response, when the system is closer to a steady-state condition.

Regarding thermal-storage coefficients, Hasan et al. (2005) and Onur et al. (2017) solutions were computed with a null value. Higher values provided curves further apart from the non-isothermal simulator response.

**Case 2.3 ($z_g$ = 137.5 m)**

Case 2.3 presents the first analysis of flow in a cased tubing (see Figure 5.6).

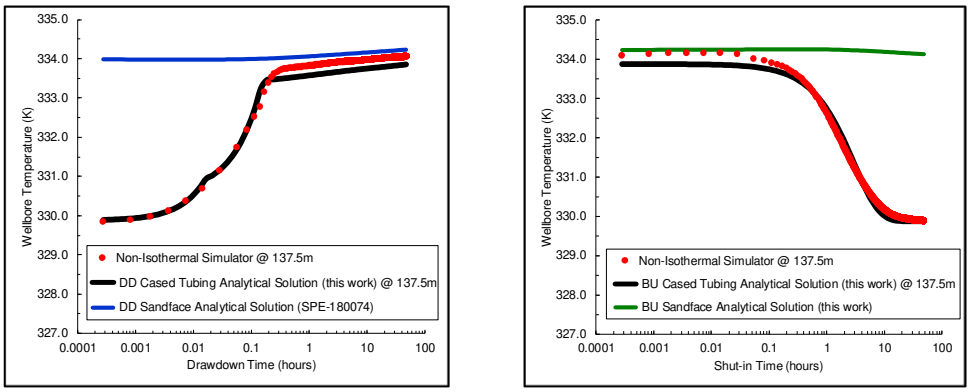


(a) (b)

Figure 5.10: Case 2.3 – (a) Drawdown; (b) Buildup

In Figure 5.10 (a), the change in the heating profile due to fluid elevation described in Case 2.2 happens twice. The first change (0.02 h) is due to the elevation of the fluid originally at the bottom of the tubing string. The second change (0.25 h) is caused by the elevation of the fluid originally at sandface. The event happens twice because there is a change in pipe area, yielding two different flowing velocities for the same volumetric rate.

The additional heating in the simulated curve (Figure 5.10 (a)) may be caused by some sort of numerical effect or due to viscous dissipation effects. Nevertheless, the deviation is small, 5% considering the temperature change in the 48-hour drawdown period.

As for the buildup period in Figure 5.10 (b), the match is good and the minor deviations are due to the lack of an axial diffusion model.

In this case, both casing and tubing thermal-storage coefficients were set to 0.3 for the drawdown period, and buildup coefficients were 0.2.

To the best of the author's knowledge, the analytical modeling of a coupled reservoir/casing/tubing thermal system has not yet been addressed in Literature. This is another contribution of this work.

**Case 2.4 ($z_g$ = 287.5 m)**

Case 2.4 presents the flow in a cased tubing at a different gauge location. All previous observations and conclusions apply to this case, including the description of the fluid elevation phenomenon.

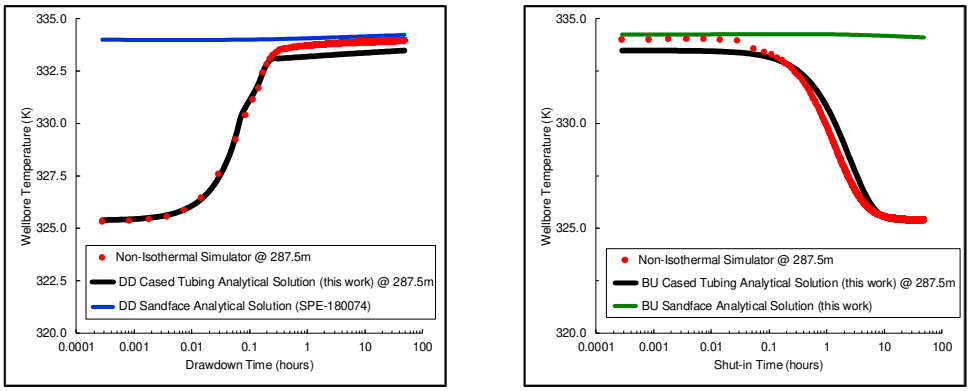


(a) (b)

Figure 5.11: Case 2.4 – (a) Drawdown; (b) Buildup

In Figure 5.11 (a), as expected, the farther the distance from the bottom of the tubing string, the longer it takes for the first change in the heating profile to happen. At this depth, it occurred at approximately 0.1 hours. For the same reason, the second change also occurred further in time.

In this case, both casing and tubing thermal-storage coefficients were set to 0.2 for the drawdown period, and buildup coefficients were 0.0.

The next case investigates an even farther location from the producing horizon.

**Case 2.5 ($z_g$ = 512.5 m)**

Case 2.5 presents the flow in a cased tubing at a location 512.5 m above the producing horizon. Like in the previous cases, the same observations and conclusions apply here.

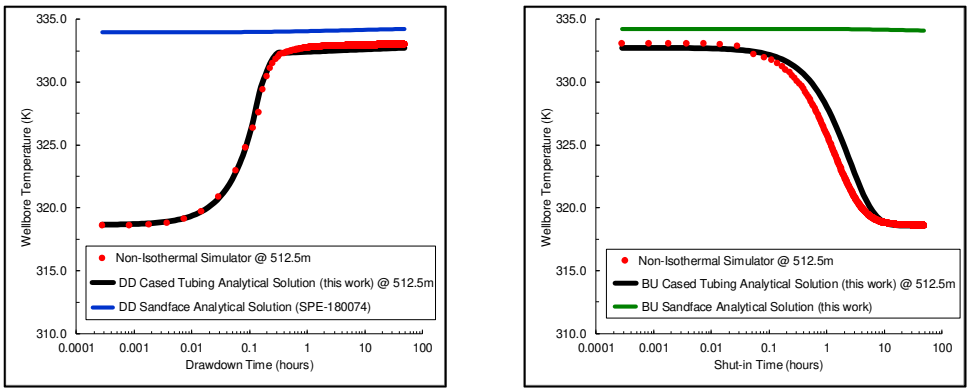


(a) (b)

Figure 5.12: Case 2.5 – (a) Drawdown; (b) Buildup

In Figure 5.12 (a), both heating-profile changes occurred further in time when compared to the previous case. The drawdown thermal-storage coefficients were set to 0.0 and 0.2 for the production casing and the tubing, respectively. The buildup coefficients were 0.0.

The proposed analytical model successfully reproduced the non-isothermal simulator temperature response for drawdown and buildup tests at different depths, in both casing and tubing strings.

A discussion on the validity of the solutions will be addressed at the end of this chapter.

## 5.3. Validation of Analytical Solutions for Thermal Impacts on Wellbore Pressure

The non-isothermal simulator finite wellbore model does not account for change in tubing length. Therefore, this section verifies the constant pipe-length solutions. The variable pipe-length solutions are examined in the next chapter, where impacts on interpretation results are addressed.

Example 3 evaluates the cased-tubing solution and the expressions for $\Delta t_{mp}$ and $\Delta z_{max}$, given by Eqs. (4.16), (4.33) and (4.50), respectively. Analyses will be performed by comparing the solutions to the non-isothermal simulator response.

This section adopts a null value for the parameters $C_{Tc}$ and $C_{Tt}$ and all analyses are performed by assessing the buildup periods.

### 5.3.1. Validation of Cased-Tubing Solution

In this example, the effective oil flow capacity (*kh*) is 450,000 mD.m. The simulated test sequence comprises 24 hours of production at a constant downhole rate of 1400 m³/d followed by a 48-hour buildup.

The buildup pressure computed from the analytical solution will be compared to the non-isothermal simulator response along the wellbore. The schematic gauge location is presented as follows:

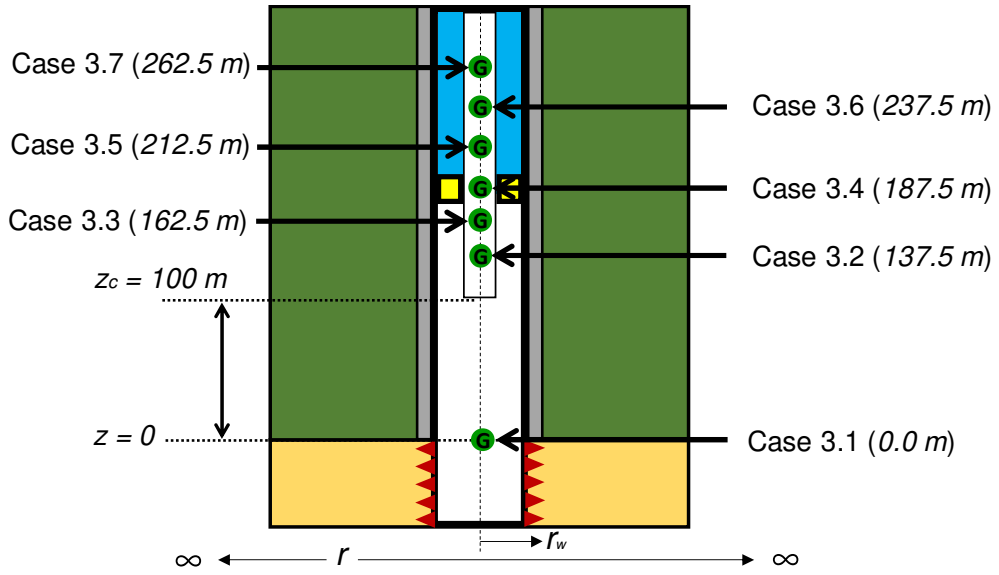


Figure 5.13: Gauge Location in Example 3

Figure 5.14 presents the wellbore-temperature changes for the six gauges placed inside the tubing string.

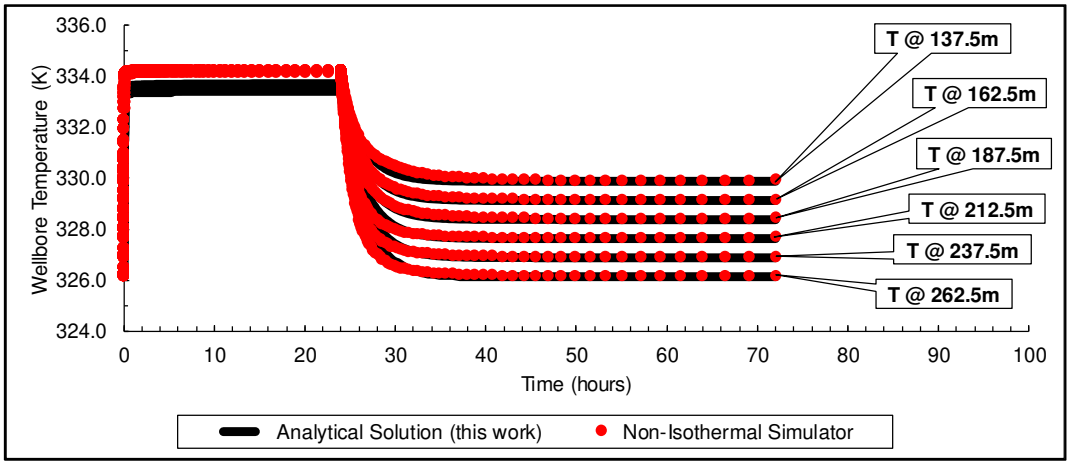


Figure 5.14: Wellbore-Temperature Changes in Example 3

As mentioned before, the proposed analytical solution does not account for a friction model, therefore the non-isothermal simulator drawdown temperatures are slightly higher. Nonetheless, this effect entails minor effects on buildup temperature changes.

Recalling Eq. (4.16), the buildup-sandface pressure $\Delta p_{sf}$ for Example 3 is given by the infinite-acting homogeneous reservoir line sink solution in absence of skin and WBS effects. Besides, it will be adopted the log approximation of $\mathrm{Ei}(-x)$.

$$\Delta p_{sf}(\Delta t) = \frac{1}{2} C_2 \frac{Q_o B_o \mu_o}{k_o h} \left[ \ln\left( \frac{t_p \Delta t}{t_p + \Delta t} \right) + \ln\left( \frac{4 C_1 k_o}{\phi \mu_o c_t r_w^2 e^{\gamma}} \right) \right]. \tag{5.6}$$

### Case 3.1: Buildup at $z_g$ = 0 m

Case 3.1 ($z = 0$) comprises the buildup-sandface pressure response.

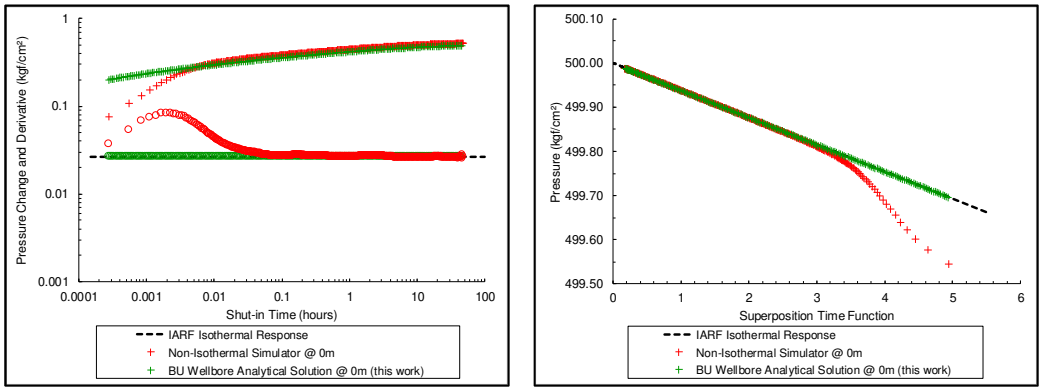


(a) (b)

Figure 5.15: Case 3.1 – (a) Log-Log Plot; (b) Horner Plot

Figure 5.15 (a) presents the log-log plot and Figure 5.15 (b) shows the Horner plot. The dashed lines in both plots represent the isothermal infinite-acting radial flow regime (IARF). WBS effects and/or numerical effects are evident in the non-isothermal simulator data (red curves), ceasing at 0.05 hours of shut-in time.

Results for this case indicate that buildup sandface-pressure solutions under non-isothermal flow are well represented by the corresponding isothermal-flow solutions, a condition also observed by Onur and Cinar (2017a).

Case 3.1 is the base case for this example. All deviations from the dashed lines in the following analyses are due to thermal effects. All plots present the same pressure scale, in order to allow easy comparisons among the cases.

### Case 3.2: Buildup at $z_g$ = 137.5 m

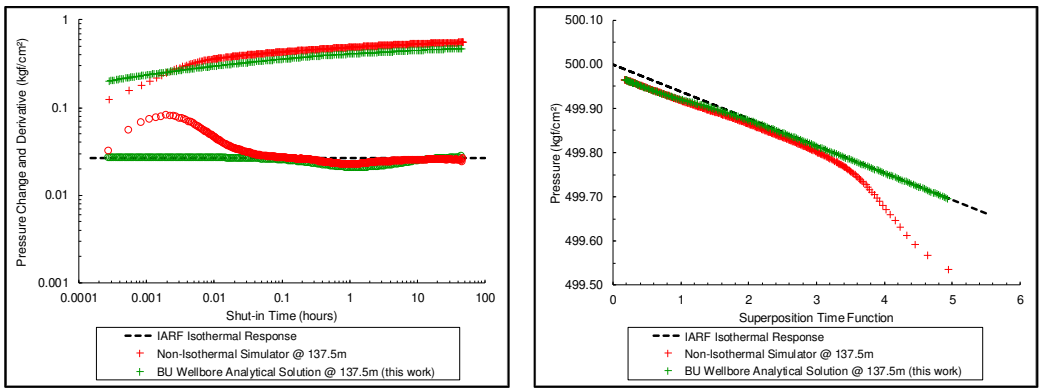


(a) (b)

Figure 5.16: Case 3.2 – (a) Log-Log Plot; (b) Horner Plot

As mentioned before, the proposed analytical solution does not account for a friction model. The effect on pressure is an additional pressure drop, which is evident in the simulated pressure-change curve. Friction losses do not influence the buildup derivative shape and cause no impact to flow diagnosis.

Apart from friction loss and early-time effects, the proposed analytical solution presents a good match with the non-isothermal simulator in both plots.

Impacts on reservoir characterization due to deviations from the IARF dashed line will be addressed in Chapter 6.

**Case 3.3: Buildup at $z_g$ = 162.5 m**

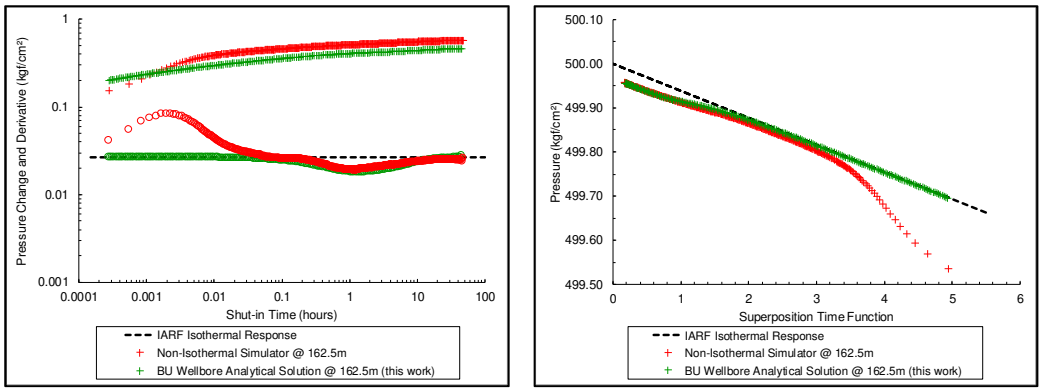


(a) (b)

Figure 5.17: Case 3.3 – (a) Log-Log Plot; (b) Horner Plot

As expected, thermal effects provided a stronger deviation from the isothermal response. The derivative reached a lower value than in the previous case and the friction loss effect was greater.

The proposed analytical solution presents a good match in both plots, being able to reproduce the deviation from the IARF dashed lines with great accuracy.

**Case 3.4: Buildup at $z_g$ = 187.5 m**

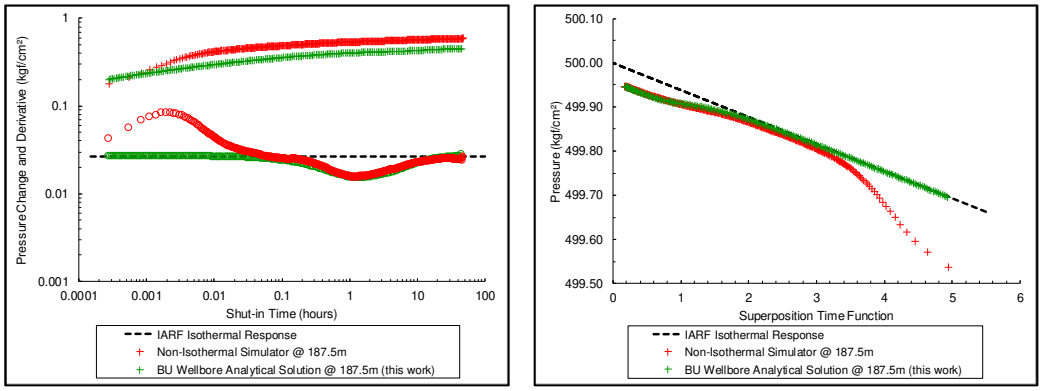


(a) (b)

Figure 5.18: Case 3.4 – (a) Log-Log Plot; (b) Horner Plot

There is a good match in both plots and all conclusions previously discussed apply to this case. As expected, the derivative reached lower values and the friction loss was stronger.

**Case 3.5: Buildup at $z_g$ = 212.5 m**

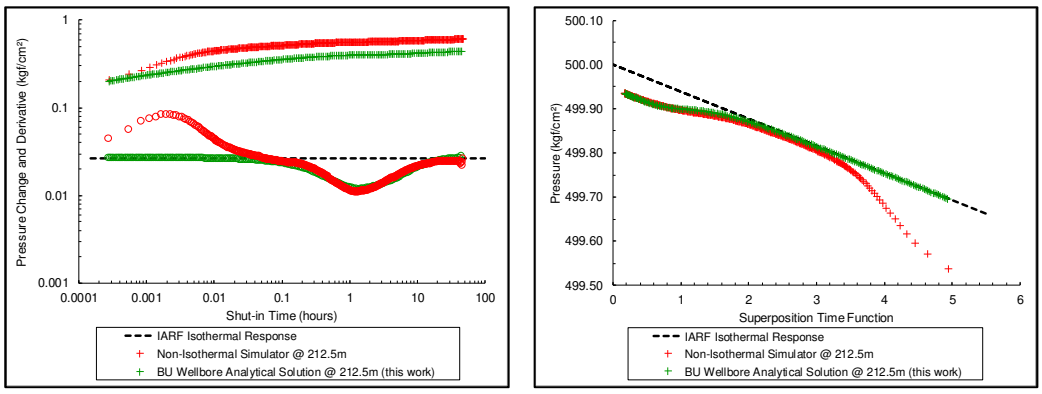


(a) (b)

Figure 5.19: Case 3.5 – (a) Log-Log Plot; (b) Horner Plot

In Figure 5.19 (a), the derivative valley reached the value of 0.01 kgf/cm² and will continue to reach even lower values in the cases to come. As expected, the friction loss continues to grow stronger with depth.

Again, the proposed analytical solution provides a good match with the simulator in both plots.

The evolution of derivative valleys in the last cases makes it clear the concept of the *Time of Maximum Impact on Pressure* $\Delta t_{mp}$, addressed in Chapter 4. It is easy to see a pattern in the derivative curves, where there is time when data are most

impacted by thermal effects, represented by the inflections. At the end of this example, the expression for $\Delta t_{mp}$ will be evaluated, as well as the expression for the maximum gauge distance $\Delta z_{max}$.

**Case 3.6: Buildup at $z_g$ = 237.5 m**

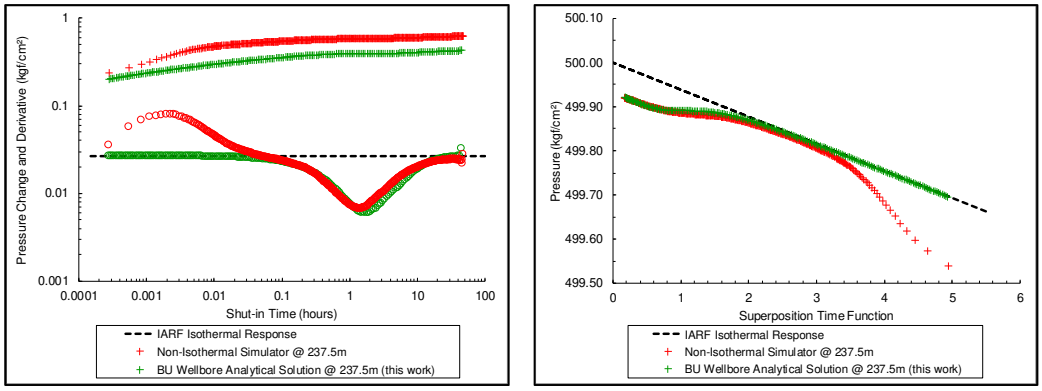


(a) (b)

Figure 5.20: Case 3.6 – (a) Log-Log Plot; (b) Horner Plot

In this case, the analytical solution derivative presents minor deviations from the non-isothermal simulator data. The mismatch is mainly caused by the lack of a wellbore axial diffusion model. Nevertheless, the match is still good in both plots.

**Case 3.7: Buildup at $z_g$ = 262.5 m**

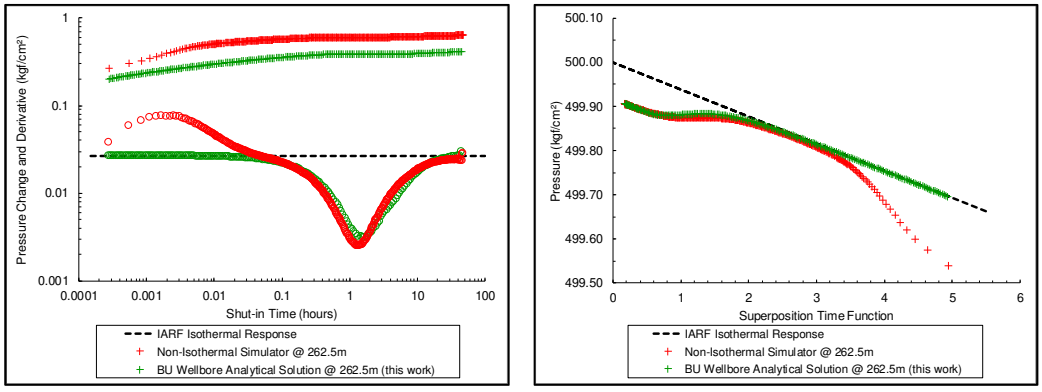


(a) (b)

Figure 5.21: Case 3.7 – (a) Log-Log Plot; (b) Horner Plot

All previous conclusions apply to this case. As mentioned before, the lack of an axial diffusion model is responsible for minor deviations. That apart, the match is good in both plots.

The proposed analytical solution in this work was able to reproduce the non-isothermal simulator data with great accuracy. In addition to the cases presented, farther gauge locations have been assessed, also providing a good match with simulated data.

The next sections evaluate the expressions for the *Time of Maximum Impact on Pressure* $\Delta t_{mp}$ and the maximum gauge distance from the producing horizon $\Delta z_{max}$.

### 5.3.2. Validation of $\Delta t_{mp}$ – Time of Maximum Impact on Pressure

The *Time of Maximum Impact on Pressure* $\Delta t_{mp}$, given by Eq. (4.33), calculates when pressure derivate data are most influenced by thermal effects. Under the adopted assumptions, it will be shown that $\Delta t_{mp}$ does not depend on the gauge distance from the producing horizon, on reservoir properties, on the drawdown duration nor on the rate magnitude. Hence, four analyses will be performed. The value of $\Delta t_{mp}$ also does not depend on tubing length, however this feature cannot be tested because the non-isothermal simulator does account for pipe-contraction effects.

The first analysis evaluates the response for different rates given a fixed gauge location. The second analysis extends the conclusions to the response of $\Delta t_{mp}$ over depth. The third analysis investigates different durations for the preceding drawdown period. Finally, the fourth analysis presents the simulated results for different reservoir transmissibilities.

All analyses make use of the same input data used for Example 3. Changes on parameters will be performed to verify the aforementioned statements.

The parameter $z_c$ is 100 meters, therefore $\Delta t_{mp}$ will be computed with casing properties. The analytical expression in Eq. (4.33) yields $\Delta t_{mp} = 1.47$ hours and it will be shown that all analyses provide similar values, regardless of changes in parameters.

**First Analysis – Rate Magnitude**

Given the gauge location of 187.5 m, three different downhole rates were used to compute the simulated data, which were 1400 m³/d, 1050 m³/d and 700 m³/d.

Table 5.10 presents the measured $\Delta t_{mp}$ for each pressure derivative curve. Each measure is obtained simply by reading when derivative data assume the smallest value during the buildup period.

Table 5.10: Time of Maximum Impact on Pressure (hours)

| Gauge Location (m) | Measured $\Delta t_{mp}$ 1400 m³/d | Measured $\Delta t_{mp}$ 1050 m³/d | Measured $\Delta t_{mp}$ 700 m³/d |
|---|---|---|---|
| **187.5** | 1.33 | 1.36 | 1.36 |

The average value in Table 5.10 is 1.35 hours. The minor difference to the analytical result of 1.47 hours is due to the conditions assumed in the derivation of Eq. (4.33).

Figure 5.22 presents the simulated curves log-log diagnostic plot. The red curves are associated to the rate of 1400 m³/d, the yellow curves to 1050 m³/d and the green curves to 700 m³/d. Curves are not rate-normalized.

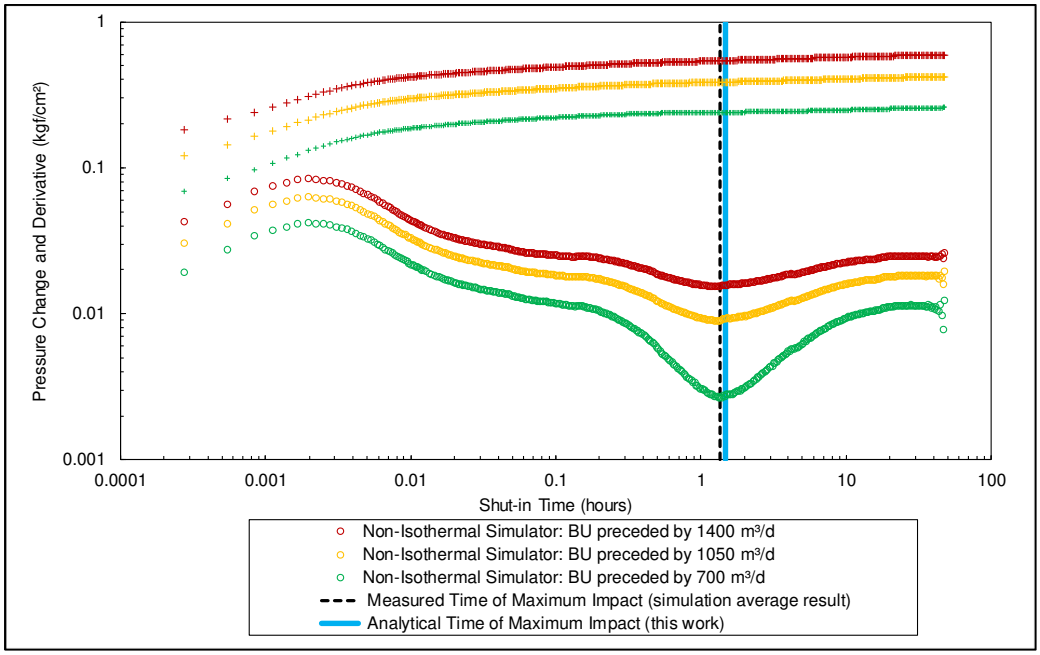


Figure 5.22: First Analysis Log-Log Plot

The dashed vertical line is the average value of 1.35 hours and the blue vertical line is the analytical result of 1.47 hours computed from Eq. (4.33).

As expected, the lower the drawdown rate (green curve), the more influenced by thermal effects are pressure data. Nonetheless, the time when the inflection occurs was not influenced by the rate magnitude.

**Second Analysis – Gauge Distance from the Producing Horizon**

The second analysis evaluates $\Delta t_{mp}$ for six different gauge locations combined with three different drawdown rates, providing eighteen curves. Table 5.11 presents the measured $\Delta t_{mp}$ for each pressure derivative curve.

Table 5.11: Time of Maximum Impact on Pressure (hours)

| Gauge Location (m) | Measured $\Delta t_{mp}$ 1400 m³/d | Measured $\Delta t_{mp}$ 1050 m³/d | Measured $\Delta t_{mp}$ 700 m³/d |
|---|---|---|---|
| **137.5** | 1.05 | 1.00 | 0.95 |
| **162.5** | 1.24 | 1.18 | 1.30 |
| **187.5** | 1.33 | 1.36 | 1.36 |
| **212.5** | 1.36 | 1.36 | 1.36 |
| **237.5** | 1.40 | 1.40 | 1.46 |
| **262.5** | 1.30 | 1.30 | 1.33 |

The average value in Table 5.11 is 1.28 hours. Again, simulation results are close to the analytical result of 1.47 hours.

The second analysis extends the previous conclusion to different gauge locations. Figure 5.23 presents the log-log diagnostic plot of all eighteen curves.

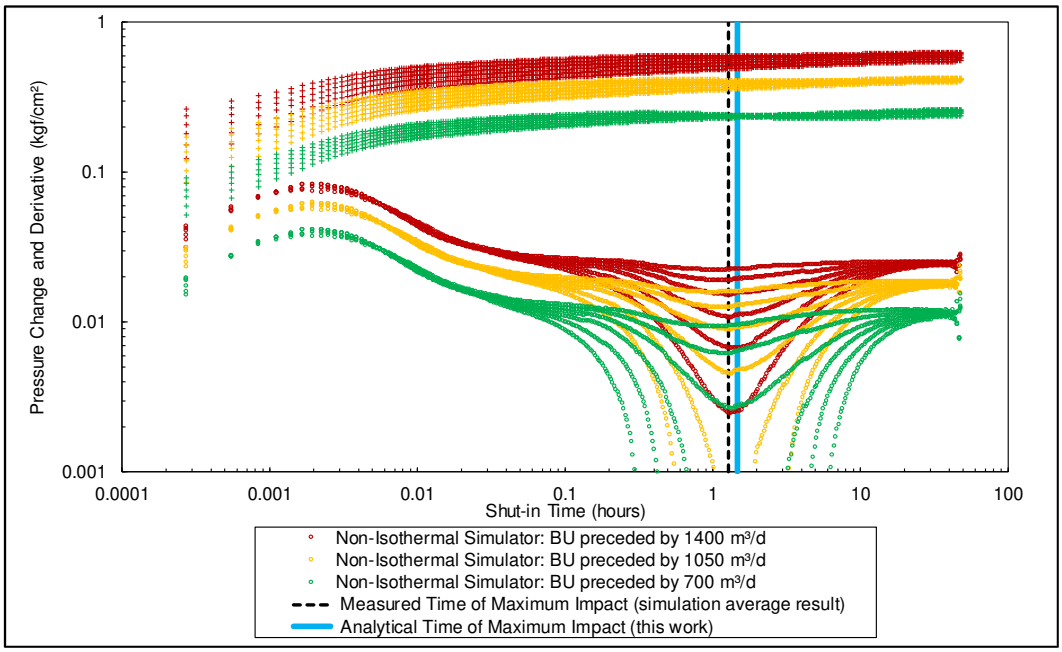


Figure 5.23: Second Analysis Log-Log Plot

In Figure 5.23, each color refers to a different rate and vertical lines are analogous to the previous plot. Though Figure 5.23 presents a dense plot, it is easy to verify that all inflections fall approximately at the same point in time. The magnitude of thermal impacts depend on gauge location and on the preceding drawdown rate, nonetheless the time when the inflection occurs does not depend on these parameters.

**Third Analysis – Drawdown Period Duration**

This analysis investigates different drawdown durations. Table 5.12 presents the measured values of $\Delta t_{mp}$ for two different producing times, given the same downhole rate of 1400 m³/d.

Table 5.12: Time of Maximum Impact on Pressure (hours)

| Gauge Location (m) | Measured $\Delta t_{mp}$ 12 h DD | Measured $\Delta t_{mp}$ 24 h DD |
|---|---|---|
| **137.5** | 1.10 | 1.05 |
| **162.5** | 1.30 | 1.24 |
| **187.5** | 1.36 | 1.33 |
| **212.5** | 1.40 | 1.36 |
| **237.5** | 1.54 | 1.40 |
| **262.5** | 1.40 | 1.30 |

The average value in Table 5.12 is 1.33 hours, and again the result of 1.47 hours is in line with simulated data. Figure 5.24 presents the twelve simulated curves.

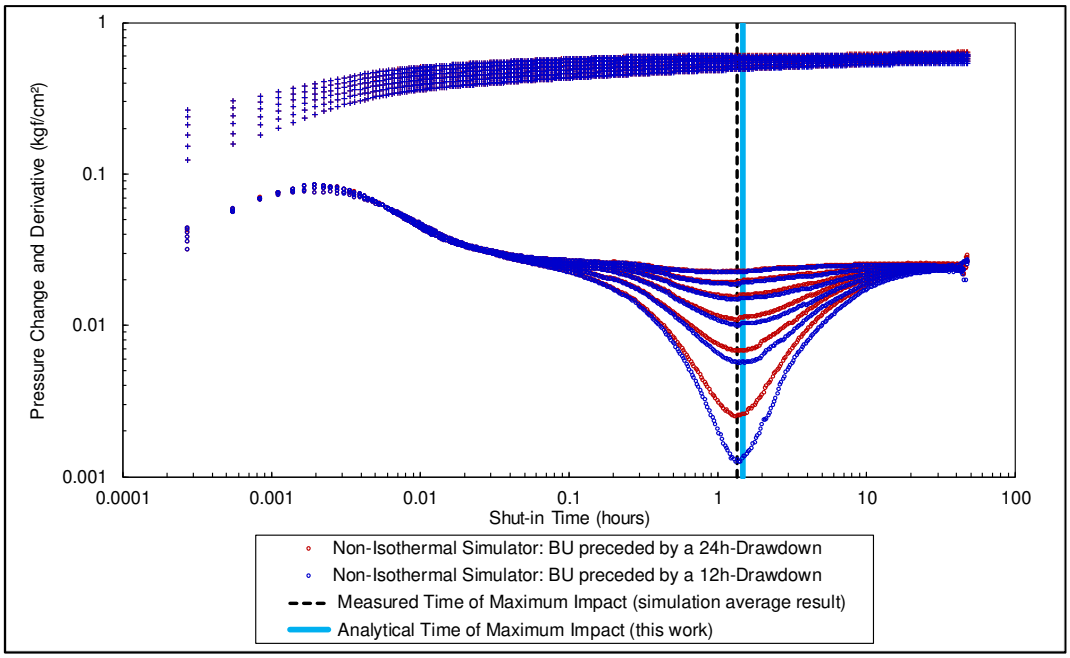


Figure 5.24: Third Analysis Log-Log Plot

Figure 5.24 shows that the time when the inflection occurs does not depend on the preceding drawdown duration.

**Fourth Analysis – Reservoir Parameters**

The fourth analysis investigates $\Delta t_{mp}$ for two different transmissibilities, subject to a 24-hour drawdown under a rate of 1050 m³/d. Results are presented in Table 5.13.

Table 5.13: Time of Maximum Impact on Pressure (hours)

| Gauge Location (m) | Measured $\Delta t_{mp}$ 500,000.0 mD.m/cP | Measured $\Delta t_{mp}$ 167,000.0 mD.m/cP |
|---|---|---|
| **137.5** | 1.00 | 0.93 |
| **162.5** | 1.18 | 1.10 |
| **187.5** | 1.36 | 1.36 |
| **212.5** | 1.36 | 1.30 |
| **237.5** | 1.40 | 1.36 |
| **262.5** | 1.30 | 1.36 |

The average value in this case is 1.25 hours. Figure 5.25 presents the twelve simulated curves.

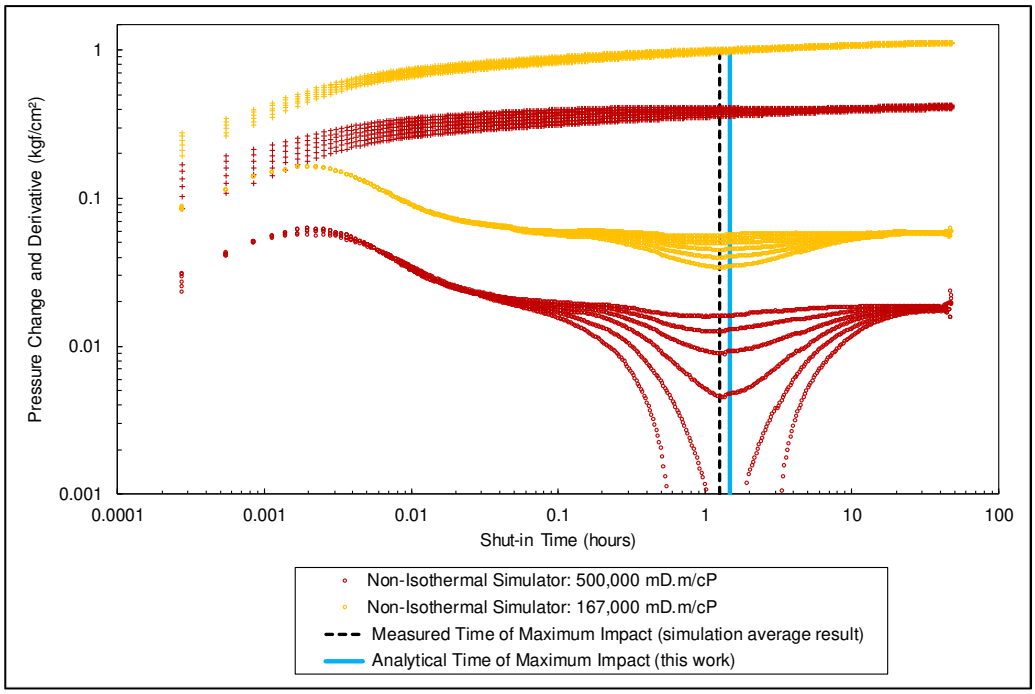


Figure 5.25: Fourth Analysis Log-Log Plot



Figure 5.25 shows that the time when the inflection occurs does not depend on reservoir parameters.

Buildup tests performed in infinite-acting homogeneous reservoirs will always comprise at least one valley in the derivative curve, assuming a sufficiently long shut-in time. Impacts on pressure due to thermal effects depend on rate magnitude, producing time, gauge distance and reservoir parameters. Nonetheless, under the adopted assumptions, this section showed that the time when the inflection occurs does not depend on these parameters. It only depends on radial diffusion (heat loss) to surroundings and on some wellbore and fluid properties, such as inside-tubing radius and fluid heat capacity, as shown in Eqs. (4.33) and (4.34). The value of $\Delta t_{mp}$ also does not depend on tubing length. This feature could not be assessed, because the non-isothermal simulator finite wellbore model does not account for change in pipe length. This feature will be addressed in Chapter 6.

### 5.3.3. Validation of $\Delta z_{max}$ – Maximum Gauge Distance from the Producing Horizon

The maximum gauge distance from the producing horizon $\Delta z_{max}$ calculates the farthest location a pressure gauge can be placed in order to let the isothermal

hypothesis be valid. In other words, it determines the maximum distance that thermal effects can be neglected and conventional PTA interpretation methods can be applied.

The expressions to be verified in this section are presented in Eqs. (4.50) and (4.52). The term dependent on tubing length ($L_0$) has been discarded, because the non-isothermal simulator does not account for pipe-contraction effects.

It will be adopted a signal-to-noise ratio (SNR) of 5.0 and the same input data used for Example 3. Considering a downhole rate of 1400 m³/d, the result for $\Delta z_{max}$ computed from Eq. (4.50) is 105 meters. Hence, it is expected the pressure response at this distance not to be sufficiently impacted by thermal effects, allowing the application of the isothermal hypothesis.

Figure 5.26 presents the simulated curves at 0.0 m, 100.0 m and 137.5 m.

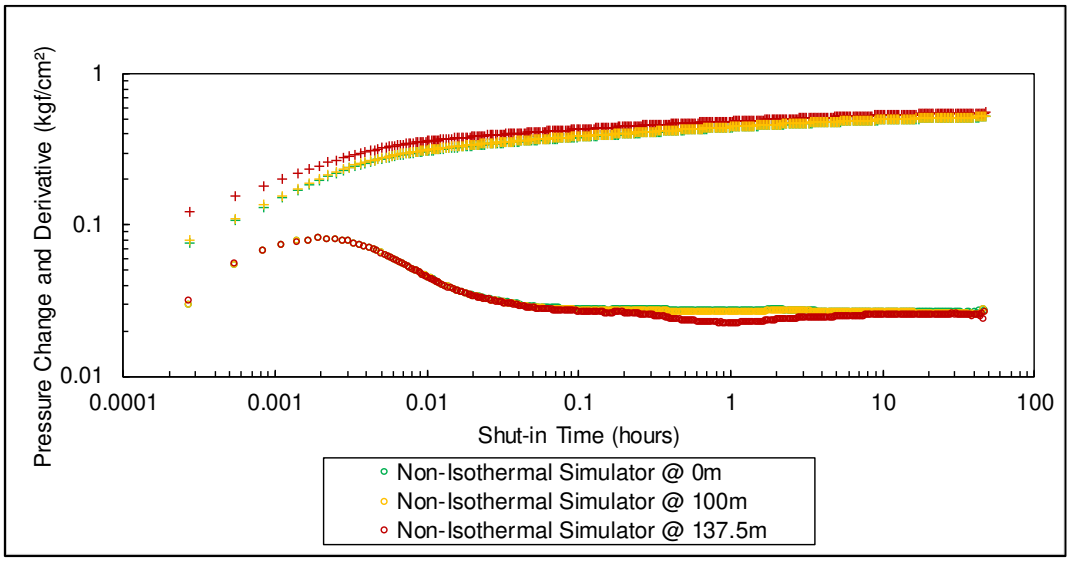


Figure 5.26: Log-Log Plot

The green curve is the sandface pressure and the yellow curve is the response at 100.0 m, not sufficiently impacted by thermal effects. The red curve (137.5 m) shows a deviation from the sandface response and interpretation results may be compromised if the isothermal hypothesis is applied. Gauges placed farther present even deeper derivative valleys, as shown in the previous section.

The result of 105 meters for $\Delta z_{max}$ successfully predicted this condition. It is noteworthy to state that the simplified solution in Eq. (4.52) resulted in a maximum distance of 113 meters.

## 5.4. Discussion on the Validity of the Model Solutions

The proposed solutions assume single-phase flow of a slightly compressible fluid, where the fluid mass density in the wellbore is a function of temperature. Other fluid properties are treated as constants at their values computed at initial conditions. Consequently, the analytical solutions are not applicable under multiphase flow.

Regarding wellbore configuration, solutions are designed to address the general case of a cased tubing completion. The model encompasses the resistance to heat flow offered by the fluid inside the tubing, tubing wall, fluids in the annulus, casing wall and cement. Moreover, additional resistances may be included, e.g., the resistance to heat flow caused by an intermediate casing. Yet, the model does not account for viscous dissipation effects, therefore the additional heating caused by these effects cannot be described. Besides, the model neglects axial conduction effects.

The aim of this study is to investigate transient temperature and pressure measurements made within the wellbore at a given gauge depth in the context of transient testing in oil wells. That is to say, only single-phase-liquid flow occurs, producing and shut-in times are in the order of hours and flow rates range from hundreds to few thousands of $m^3/d$. Under these conditions, the proposed analytical solutions were able to reproduce the non-isothermal simulator data with great accuracy. Therefore, the use of the proposed model for this investigation should be acceptable.

The next chapter investigates thermal impacts on PTA results, where interpretation models are used to fit thermal-distorted data.

# 6
# Impacts on PTA Interpretation – Synthetic Case Studies

This chapter evaluates impacts on PTA interpretations due to neglecting thermal effects in well tests under a non-isothermal condition. Chapter 5 verified the analytical solutions derived in this work by comparing them to the rigorous response of a commercial non-isothermal simulator, hence the simulator response will not be assessed in the case studies to be appraised.

Case Study 1 investigates possible interpretation models for two curves presented in Example 3. Besides, the additional effect of pipe contraction is addressed.

Case Study 2 reproduces a typical drill stem test (DST). It will be shown that a different wellbore configuration can cause a time-shift in the inflection of the pressure derivative curve. Additional analyses are performed to evaluate the sensitivity to the isobaric-thermal-expansion coefficient ($\beta_o$) and to the preceding drawdown rate.

Case Study 3 investigates the necessary conditions for the occurrence of more than one inflection in pressure derivative curves. Additional analyses regarding the sensitivity to thermal-storage coefficients are also provided.

Both constant and variable pipe-length configurations will be examined. The wellbore completions will be described in details in the following sections, since each case study comprises a different configuration.

The conceptual model of an infinite-acting homogeneous reservoir with uniform thickness is adopted in all case studies, differing only in the effective oil flow capacity ($kh$). The schematic reservoir model is presented in Figure 6.1.

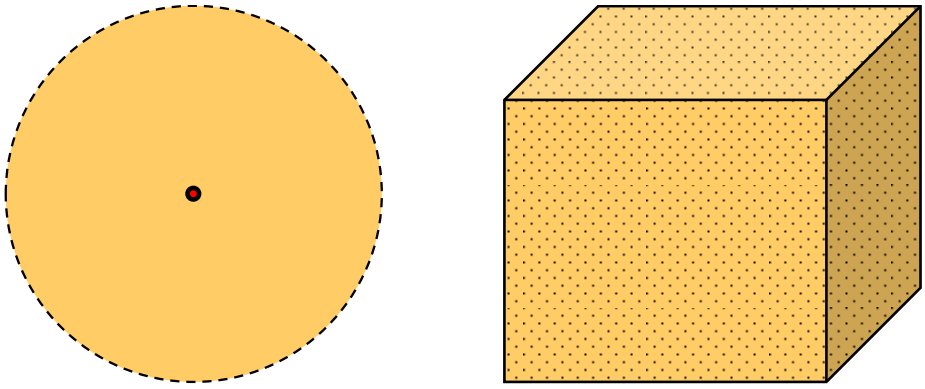

(a) (b)

Figure 6.1: (a) Infinite-Acting Reservoir; (b) Homogeneous Matrix

The dashed contour in Figure 6.1 (a) indicates the absence of reservoir boundaries and Figure 6.1 (b) illustrates the homogeneous matrix.

The main objective of the case studies is to show how thermal-distorted data can affect interpretation results.



## 6.1. Synthetic Case Study 1

This case study makes use of the same input data used in Example 3. The simulated test sequence comprises 24 hours of production at a constant downhole rate of 1400 m³/d followed by a 48-hour buildup. Two gauges have been placed in the tubing string (Figure 6.2):

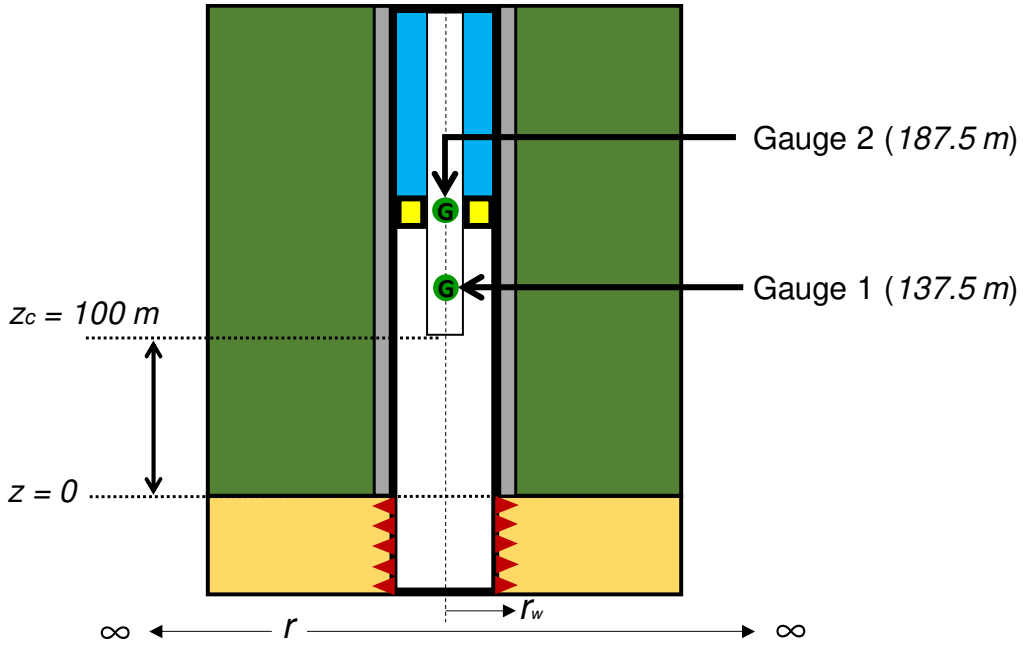


Figure 6.2: Case Study 1 – Wellbore/Reservoir System

As mentioned in Chapter 3, perforations are assumed to be a point source. Therefore, the location of $z = 0$ at the top of the completed interval in Figure 6.2 is merely schematic. The field case study in Chapter 7 provides an approach to cope with finite intervals.

First, the case study will evaluate the impact on interpretation results under the constant pipe-length configuration. Then, the variable length configuration will be addressed.

### 6.1.1. Case Study 1: Constant Pipe-Length Configuration

The interpreted data in this section are the same data presented in Figure 5.16 (a) and Figure 5.18 (a). Regarding the plot size, from this point on all log-log diagnostic plots present symmetrical axes. Like in Example 3, all deviations from the IARF isothermal dashed line are due to thermal effects.



**Gauge 1: 137.5 m**

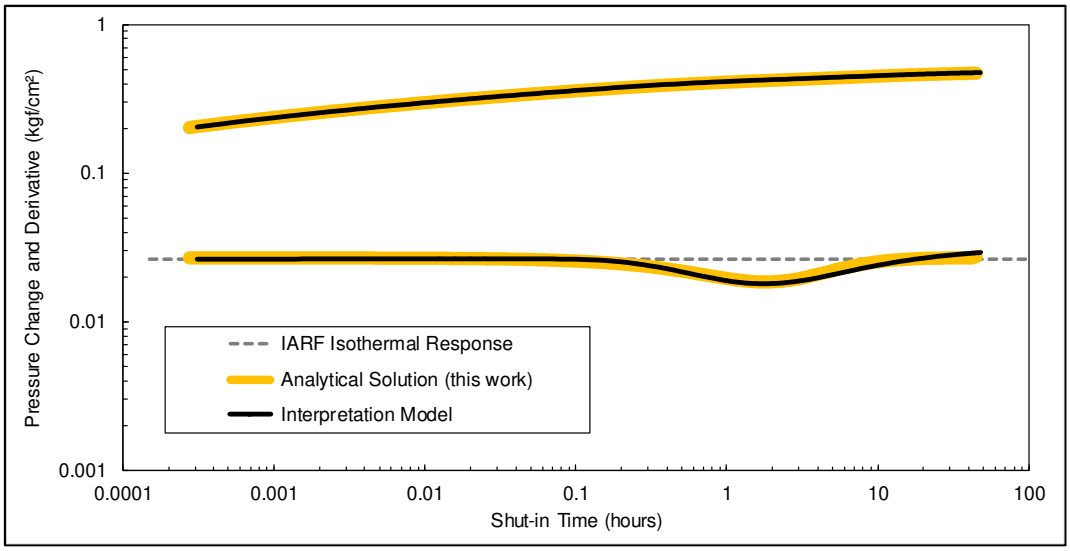


Figure 6.3: Case Study 1 (137.5 m) – Gauge Data and Interpretation Model

Figure 6.3 presents the thermal-distorted gauge data in yellow and the adopted interpretation model (black curve) used to fit the data.

The adopted model has the following parameters:

- Homogeneous matrix;
- Radial Composite Reservoir: 450,000 mD.m near the wellbore, followed by an increase in permeability yielding 750,000 mD.m at a distance of 230 meters from the well;
- Presence of a flow barrier 800 meters away from the well.

Figure 6.4 illustrates the resulting interpretation model.

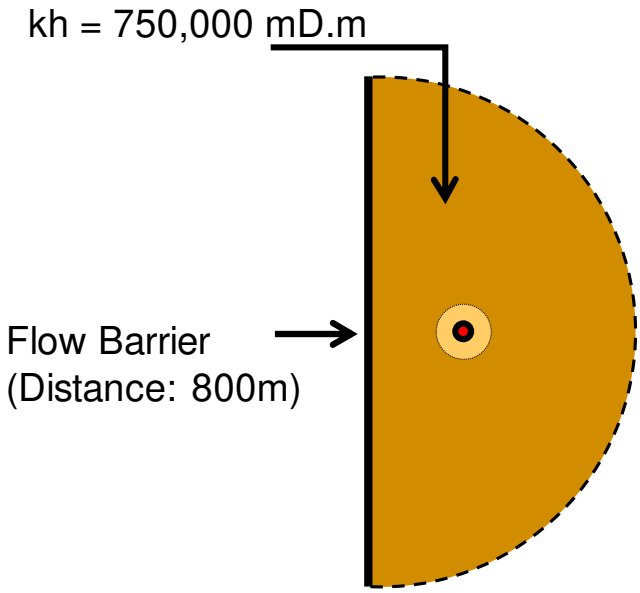


Figure 6.4: Case Study 1 (137.5 m) – Schematic Interpretation Model

Impacts on a development plan could imply a change in the injector/producer strategy, in order to avoid the unreal flow barrier 800 m from the well, represented by the thick vertical line in Figure 6.4. The light brown color represents the near-wellbore region and the dark brown color refers to the false increased permeability.

Indeed, PTA interpretations carry an implicit non-uniqueness, i.e., this is one of the possible solutions that match well with the thermal-distorted data in Figure 6.3. Nevertheless, the applied model is one of the simplest models that provides a good match. Other possible models would bring additional false heterogeneities.

**Gauge 2: 187.5 m**

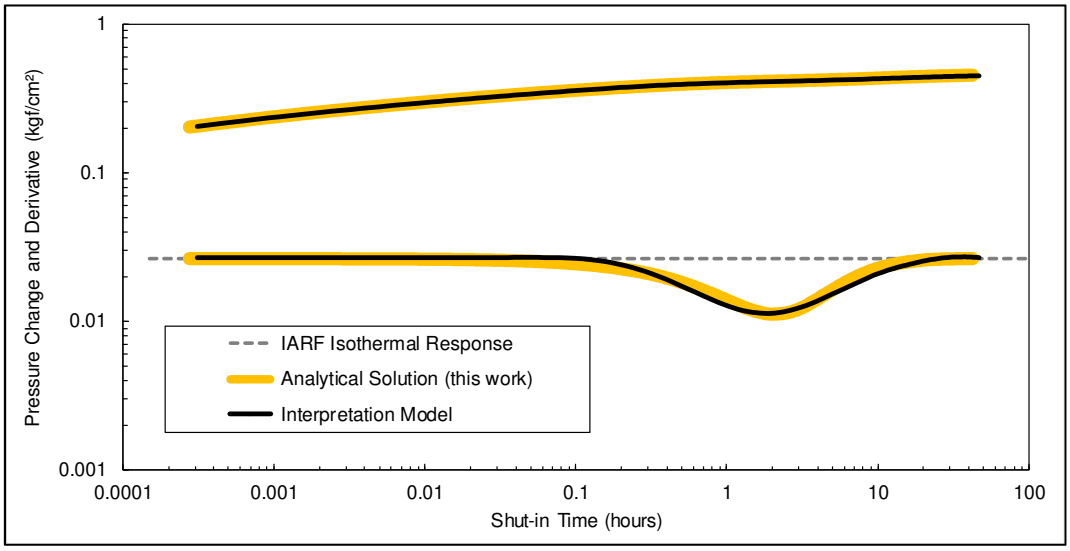


Figure 6.5: Case Study 1 (187.5 m) – Gauge Data and Interpretation Model

As expected, in this case the derivative valley reaches a deeper value. The model used to fit the data has the following parameters:

- Homogeneous matrix;
- Radial Composite Reservoir: 450,000.0 mD.m near the wellbore, followed by an increase in permeability yielding 1,215,000.0 mD.m at a distance of 220 meters from the well;
- Presence of perpendicular faults 700 m and 4000 m meters away from the well.

Figure 6.6 illustrates the resulting interpretation model.

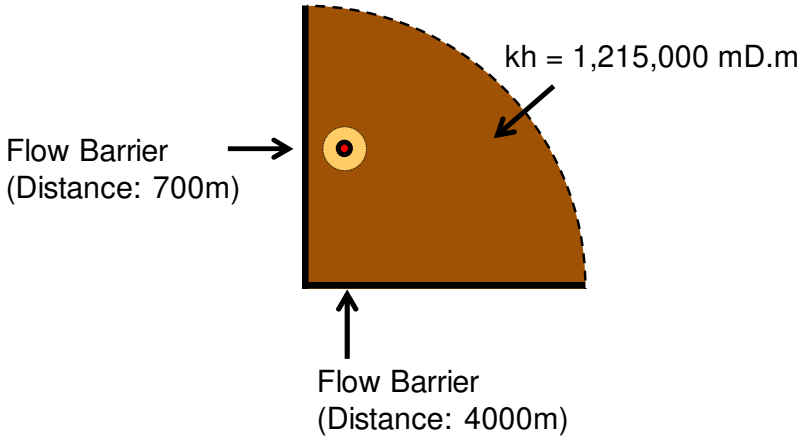


Figure 6.6: Case Study 1 (187.5 m) – Schematic Interpretation Model

In this case, the interpretation model is even more distant from reality. Instead of an infinite-acting reservoir, the interpreter found two perpendicular flow barriers, where the dark brown color refers to the false increase in permeability.

Due to the aforementioned non-uniqueness feature, the same data in this case could be interpreted with a different model. In Figure 6.7, the double-porosity model (Warren and Root, 1963) is used.

**Gauge 2: 187.5 m (double-porosity model)**

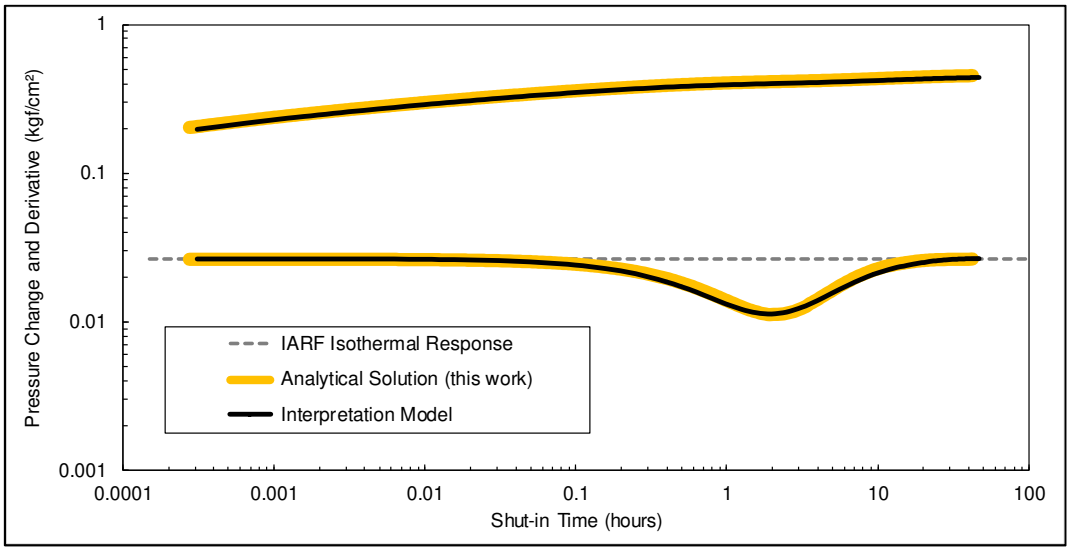


Figure 6.7: Case Study 1 (187.5 m) – Gauge Data and Double-Porosity Model

The double-porosity model in Figure 6.7 also provides a good match. Figure 6.8 presents the heterogeneous fracture/matrix system assumed in double-porosity models.

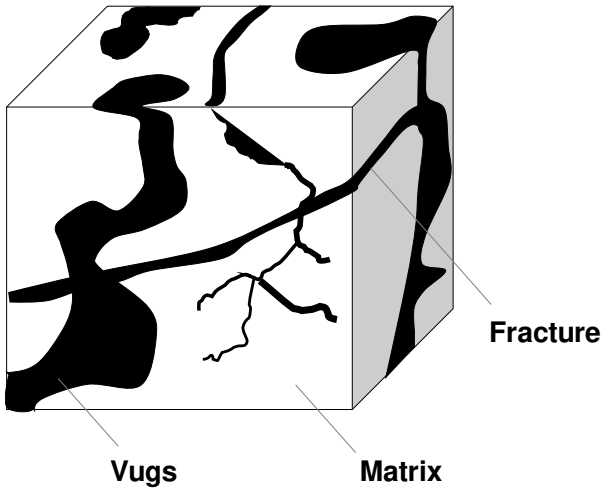


Figure 6.8: Heterogeneous Double-Porosity System (adapted from Warren and Root, 1963)

The system presented in Figure 6.8 completely fails to describe the real matrix system presented in Figure 6.1 (b), which is perfectly homogeneous.

The double-porosity model divides the pore space into a matrix of lower transmissibility and a medium composed by fractures with high permeability. The model assumes that fluid flows to the wellbore through fractures and the matrix only feeds the fracture network.

The model accounts for two additional parameters, *omega* and *lambda*. Omega is the storativity ratio, which is the fraction of the pore volume occupied by the fractures to the total interconnected pore volume. Lambda is the interporosity flow coefficient, which models the ability of the matrix to feed the fractures.

Regarding pressure derivative data, the double-porosity response is similar to the resulting thermal impacted data of an infinite-acting homogeneous medium. It comprises a valley in the derivative, which intensity is a function of omega and the transition time is a function of lambda.

The double-porosity model in Figure 6.7 yields an omega of 0.18, indicating that 18% of the volume is contained within fractures. The value of lambda depends on the system geometry and on the ratio of matrix permeability to fracture network permeability. The model in Figure 6.7 resulted in a lambda of 5.5E-8, which entails a rather low matrix permeability.

Instead of a homogeneous high permeability reservoir, the interpretation resulted in a fracture dominated system, with a low matrix permeability. Impacts on waterflooding strategy could be severe, since breakthrough calculations would yield results distant from reality. Moreover, reserves estimates would also suffer a negative impact.



### 6.1.2. Case Study 1: Variable Pipe-Length Configuration

This section investigates additional impacts caused by tubing contraction during buildup, considering the packer in Figure 6.2 not to be a fixed point. It considers a tubing linear thermal expansion coefficient ($\alpha_{LTE}$) of 1.3E-5 $K^{-1}$ and a free tubing length ($L_0$) of 1000 meters to expand/contract affecting both gauges.

The analytical expression for change in tubing length is given by Eq. (4.21). At the end of the 48-hour buildup, the total tubing contraction was approximately 0.21 m. The transient tubing contraction $\Delta L(\Delta t)$ is presented in Figure 6.9.

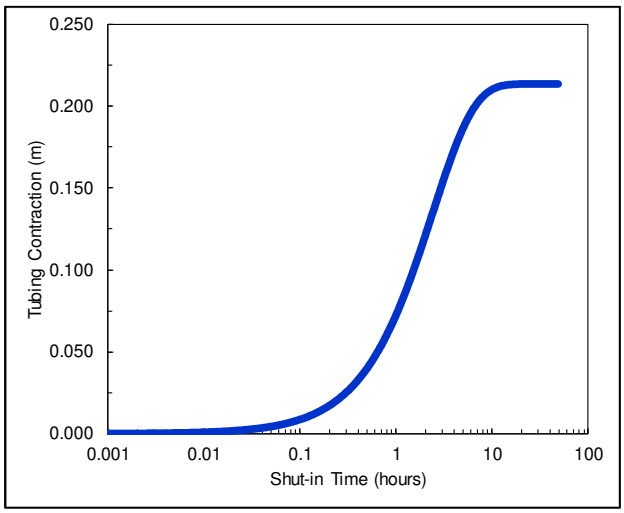


Figure 6.9: Case Study 1 – Transient Tubing Contraction

The transient change in pipe length is used in Eq. (4.20) to compute the transient impact on pressure due to tubing contraction $\Delta p_{cont}(z_g, \Delta t)$.

The next analyses show the additional tubing contraction effect on pressure derivative data. The blue curves are the complete solution, comprising the pipe-contraction effect.

**Gauge 1: 137.5 m**

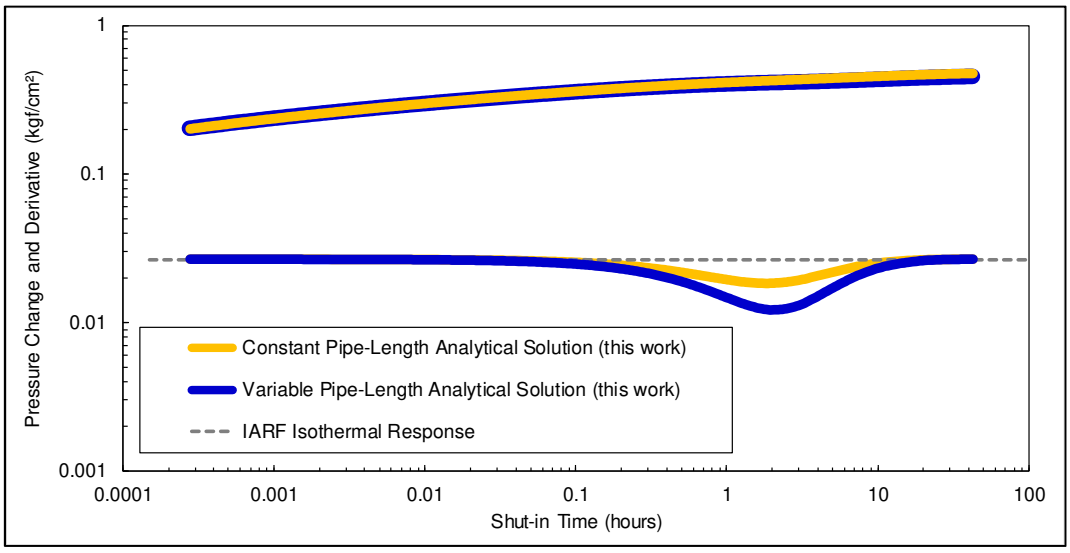


Figure 6.10: Case Study 1 (137.5 m) – Constant and Variable Pipe-Length Solutions

In Figure 6.10, the blue curve presents a deeper valley, further away from the IARF dashed line. Resulting impacts on the interpretation model presented in Figure 6.3 would entail a higher outer permeability and closer flow barriers.

**Gauge 2: 187.5 m**

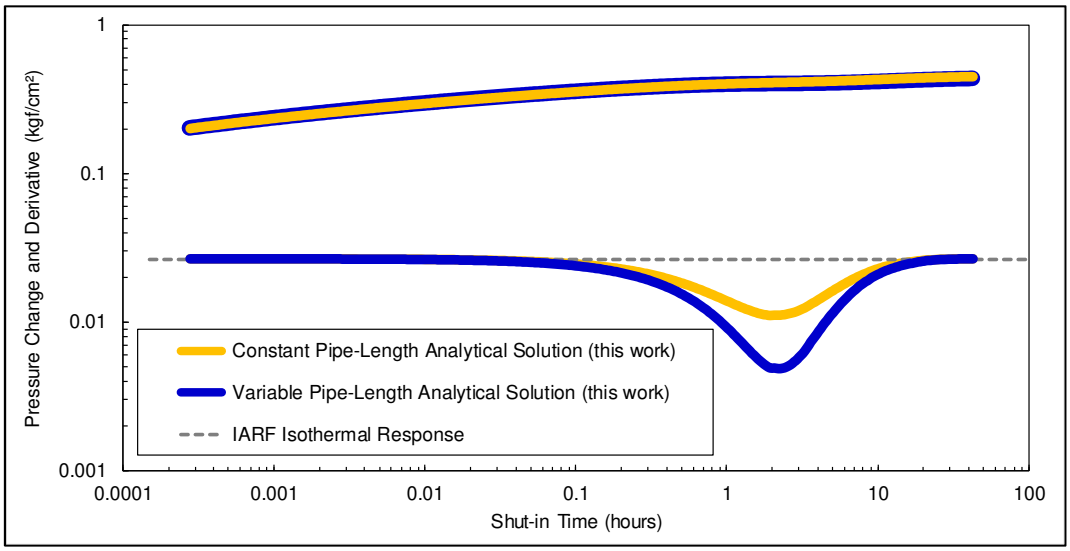


Figure 6.11: Case Study 1 (187.5 m) – Constant and Variable Pipe-Length Solutions

Like in the previous case, the pipe-contraction effect would indicate additional heterogeneities in the interpretation model, represented by the deeper derivative valley in the blue curve.

## 6.2. Synthetic Case Study 2

Case Study 2 investigates potential impacts on pressure derivative data caused by typical DST wellbore configurations. The adopted test string has an ID of 2.25”, an OD of 5” and a length of 1300 meters. Moreover, the annular fluid is brine. Additional analyses regarding sensitivity to the isobaric-thermal-expansion coefficient ($\beta_o$) and drawdown rate magnitude are also addressed.

Some test strings are designed with gauge adapters placed below expansion joints, hence their locations are fixed. Conversely, some test strings may account for packers that compensate for string movement (Sidorova et al., 2014). Therefore, both constant and variable pipe-length solutions will be assessed.

The bottom of the test string is usually placed near the perforations. In this case study, the distance from the producing horizon is 40 meters and the first gauge is located 40 meters above, i.e., 80 meters from the producing horizon. A second gauge is placed farther, at a distance of 200 meters. Figure 6.12 presents a schematic of the wellbore/reservoir system.

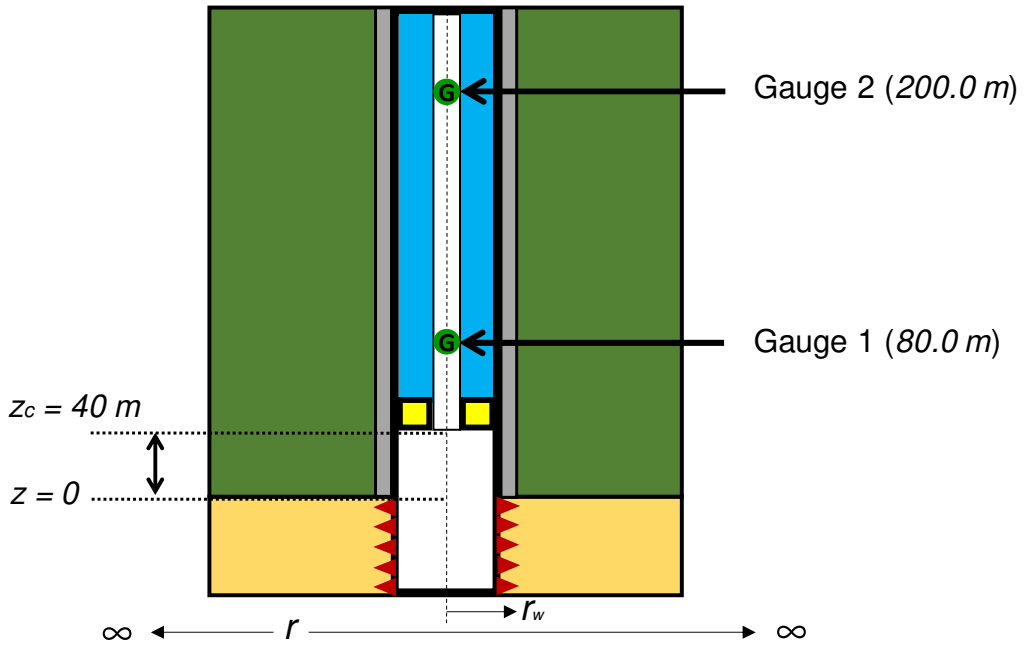


Figure 6.12: Case Study 2 – Wellbore/Reservoir System

The effective oil flow capacity is 270,000 mD.m and all other reservoir and fluid input data are presented in Table 5.1, Table 5.2, Table 5.5 and Table 5.6. Wellbore parameters for this case study are presented in Table 6.1.

Table 6.1: Wellbore Parameters for Case Study 2

| Property | Value |
|---|---|
| $r_w$ (m) | 0.156 |
| $\lambda_{cem}$ (J/m/h/K) | 6.833E+3 |
| $r_{co}$ (m) | 0.12224 |
| $r_{ci}$ (m) | 0.10839 |
| $r_{to}$ (m) | 0.06350 |
| $r_{ti}$ (m) | 0.028575 |
| $\lambda_{an}$ (J/m/h/K) | 2.229E+3 |
| Skin Factor | 0 |
| $\theta$ (degree) | 90° |
| $z_c$ (m) | 40.0 |
| $L_0$ (m) | 1300 |
| $C_{Tc}$ (dimensionless) | 0 |
| $C_{Tt}$ (dimensionless) | 0 |



For simplicity, the tubing length $L_0$ is the same for both gauges. The simulated test sequence comprises 24 hours of production at a constant downhole rate of 1400 m³/d followed by a 48-hour buildup. The transient tubing contraction during the 48-hour buildup is presented in Figure 6.13.

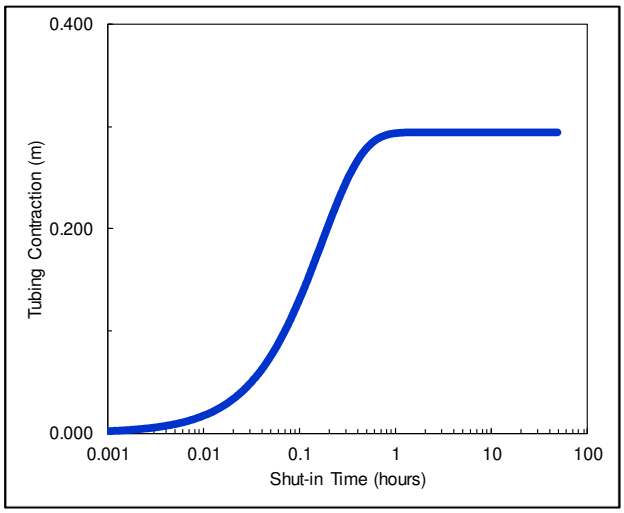


Figure 6.13: Case Study 2 – Transient Tubing Contraction

The total contraction was 0.29 m. The contraction profile is different from Case Study 1 (see Figure 6.9), due to a smaller pipe ID and to a higher annular fluid thermal conductivity.

It will be adopted a signal-to-noise ratio of 4.5 to compute $\Delta z_{max}$ from Eq. (4.50). For the constant pipe-length configuration, the value is 150 meters, hence it is expected Gauge 1 (80 m) not to be impacted by thermal effects and Gauge 2 (200 m) to present deviations from the IARF regime. For the variable pipe-length configuration, the value is 50 meters, therefore it is expected both gauges to be impacted.

The test string is close to perforations, therefore the parameter $\Delta t_{mp}$ has been computed from Eq. (4.33) with test string properties, yielding the value of 0.168 hours.

**Gauge 1: 80.0 m**

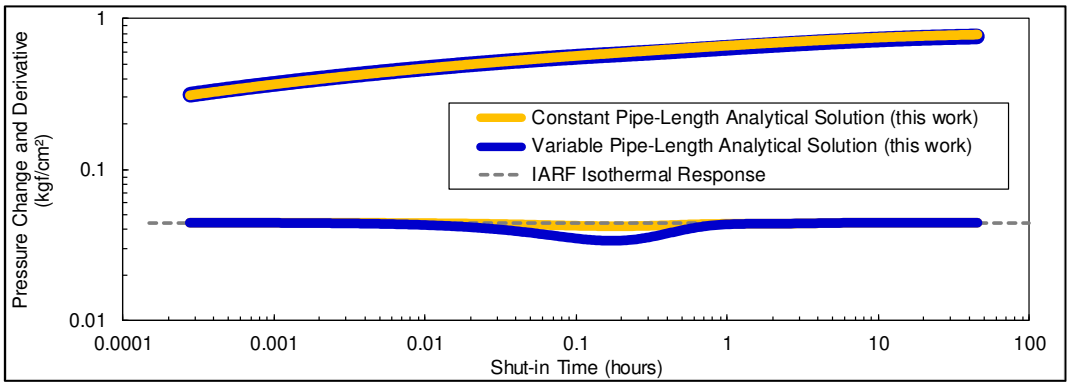


Figure 6.14: Case Study 2 (80.0 m) – Constant and Variable Pipe-Length Solutions

In Figure 6.14, the yellow curve is the constant pipe-length solution and the blue curve comprises the additional effect of pipe contraction. The dashed line is the IARF isothermal response.

As predicted by the results of $\Delta z_{max}$, fixed gauge data are not sufficiently impacted by thermal effects and variable pipe-length data suffered visible distortions. The maximum impact occurred at 0.173 hours for the blue curve, close to the expected value of 0.168 hours.

A possible interpretation model for the blue curve is presented in Figure 6.15.

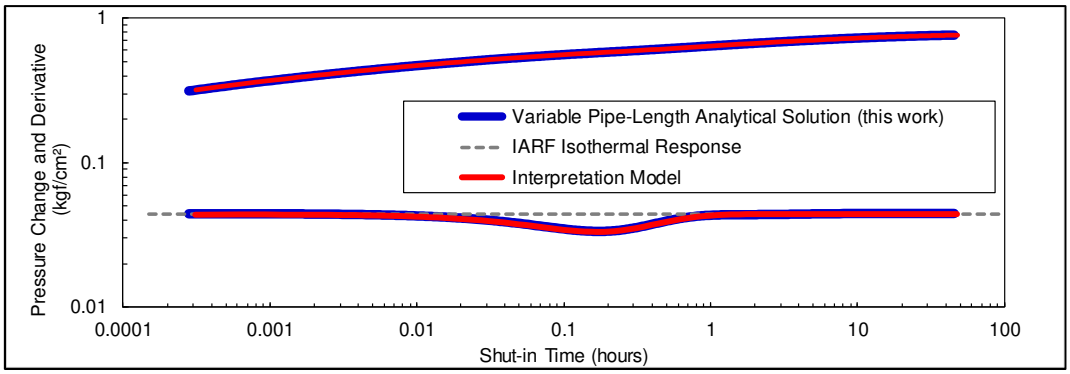


Figure 6.15: Case Study 2 (80.0 m) – Gauge Data and Interpretation Model

The interpretation model (red curve) is a double-porosity reservoir, as described in the previous section. Parameters include an omega of 0.50 and a lambda of 1.1E-6. Instead of a high permeability homogeneous reservoir, thermal-distorted data have led to a fractured dominated system, where 50% of reserves are contained within the fracture network. Moreover, the matrix presents low permeability. As previously discussed, these false results could provide severe impacts on a field development plan.

**Gauge 2: 200.0 m**

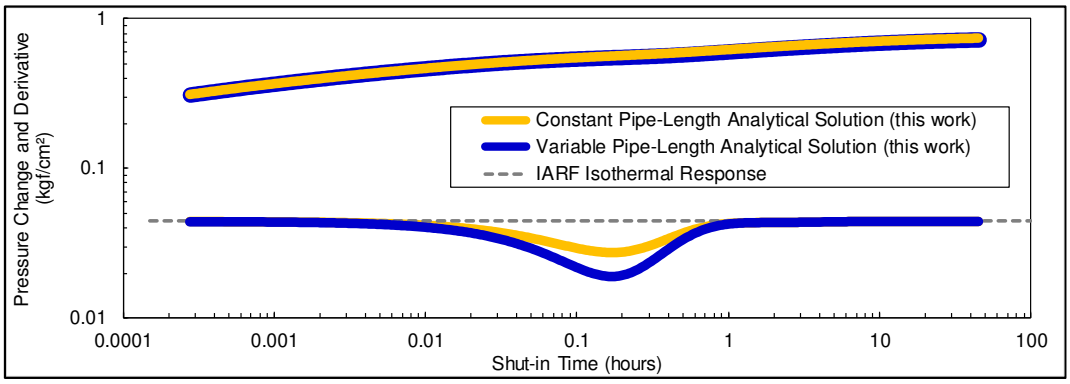


Figure 6.16: Case Study 2 (200.0 m) – Constant and Variable Pipe-Length Solutions

As predicted by the results of $\Delta z_{max}$, both data sets are affected by thermal effects at this depth. The maximum impact occurred at 0.173 hours in both curves, close to the expected value of 0.168 hours.

A possible interpretation model for the blue curve is presented in Figure 6.17.

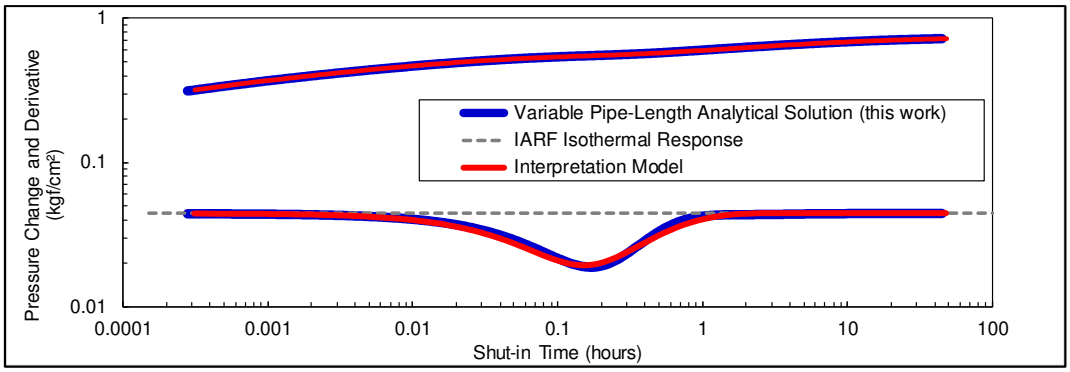


Figure 6.17: Case Study 2 (200.0 m) – Gauge Data and Interpretation Model

Again, the chosen interpretation model (red curve) is a double-porosity reservoir. In this case, parameters include an omega of 0.18 and a lambda of 1.1E-6. Note that lambda presented the same value as in the previous case. This condition was expected, because $\Delta t_{mp}$ is the same for both gauges and lambda models the derivative curve transition time.

Indeed, the interpretation models presented in this section could not find geological support in a real field test. Recalling the purpose of this chapter, the idea is to show how far from reality thermal effects can lead an interpreter to yield invalid conclusions.

**Sensitivity to Isobaric-Thermal-Expansion Coefficient ($\beta_o$)**

The following analysis investigates impacts of the isobaric-thermal-expansion coefficient ($\beta_o$) on pressure derivative curves. The parameter is present in both thermal mass density and pipe-contraction effects, providing a minor influence on the latter.

The value of 1.11E-3 $K^{-1}$ has been adopted for $\beta_o$ in the synthetic examples and changes of $\pm 20\%$ shall be made in order to perform this investigation. Figure 6.18 presents three buildup curves, all computed from the variable pipe-length solution at 200 m, preceded by a drawdown rate of 1400 m³/d.

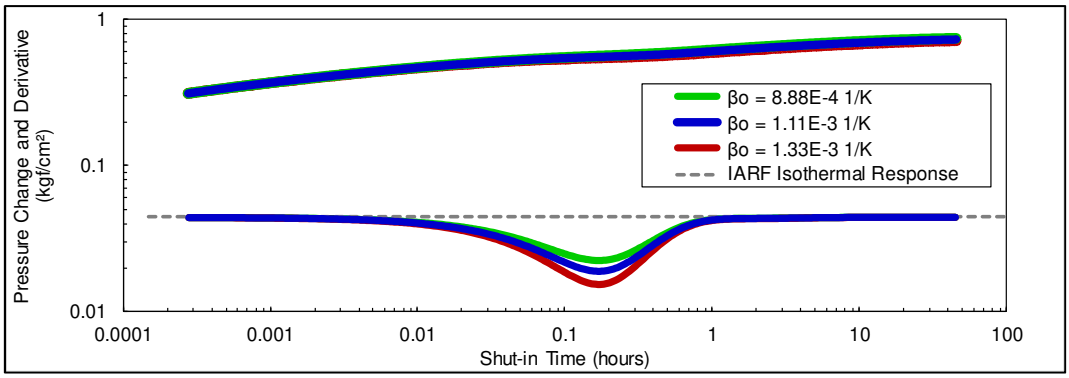


Figure 6.18: Case Study 2 (200.0 m) – Sensitivity to $\beta_o$

The blue curve in Figure 6.18 is equal to the one shown in Figure 6.16. As predicted by Eq. (4.55), the lower the coefficient $\beta_o$, the better the signal-to-noise ratio (SNR). Additionally, the value of $\Delta t_{mp}$ did not change, as expected.

The measured SNR for each curve is presented in Table 6.2.

Table 6.2: $\beta_o$ vs SNR in Case Study 2

| $\beta_o$ ($K^{-1}$) | Measured SNR | Computed SNR (Analytical Solution in Eq. (4.55)) |
|---|---|---|
| 8.88E-4 | 2.01 | 1.92 |
| 1.11E-3 | 1.74 | 1.66 |
| 1.33E-3 | 1.53 | 1.47 |

The minor differences are due to the assumptions adopted to derive Eq. (4.55).

**Sensitivity to Drawdown Rate**

The last feature to be analyzed is the preceding drawdown rate. Given a gauge depth and a desired SNR, the minimum rate can be determined.

Assuming that a SNR of 4.5 is good enough to allow the application of the isothermal hypothesis, the minimum downhole rate for the variable pipe-length configuration at 200 meters is 3800 m³/d, computed from Eq. (4.53).

Figure 6.19 shows the rate-normalized comparison between the buildup curves preceded by the rates of 1400 m³/d and 3800 m³/d.

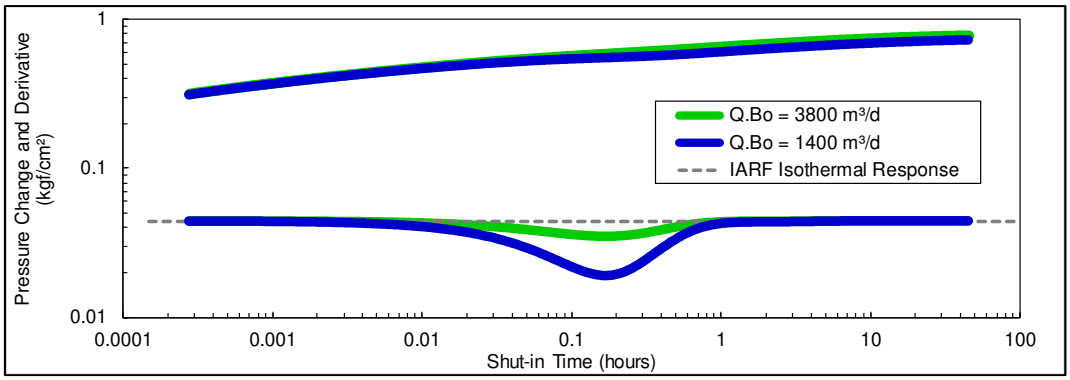


Figure 6.19: Case Study 2 (200.0 m) – Different Downhole Rates

The deviation from the isothermal IARF dashed line is smaller for the rate of 3800 m³/d. As for tubing contraction, this condition yielded a total change in length of 0.31 m, similar to the 0.29 m in the previous case.

An important conclusion can be drawn from the analysis. The change in rate magnitude can be used in well test design and operations to identify whether pressure data are impacted by thermal effects. If the buildup pressure derivative is not sensitive to different preceding drawdown rates, then thermal effects should not be relevant.

## 6.3. Synthetic Case Study 3

This case study investigates the required conditions for the occurrence of two valleys in the pressure derivative curve. The assumptions for deriving Eq. (4.33) comprise similar pipe diameters for casing and tubing, as well as similar thermal-storage coefficients. Under these conditions, only one inflection occurs in the pressure derivative curve.

In this case study, the wellbore is designed to provide three inflections in the derivative curve, i.e., two valleys. The tubing ID and OD are 2.25” and 5.0”, respectively. As for the production casing, values are 8.535” and 9.625”, respectively. Moreover, thermal-storage coefficients will have different values and the distance from the bottom of the test string to the producing horizon is 150 meters. Figure 6.20 presents a schematic of the wellbore/reservoir system for Case Study 3.

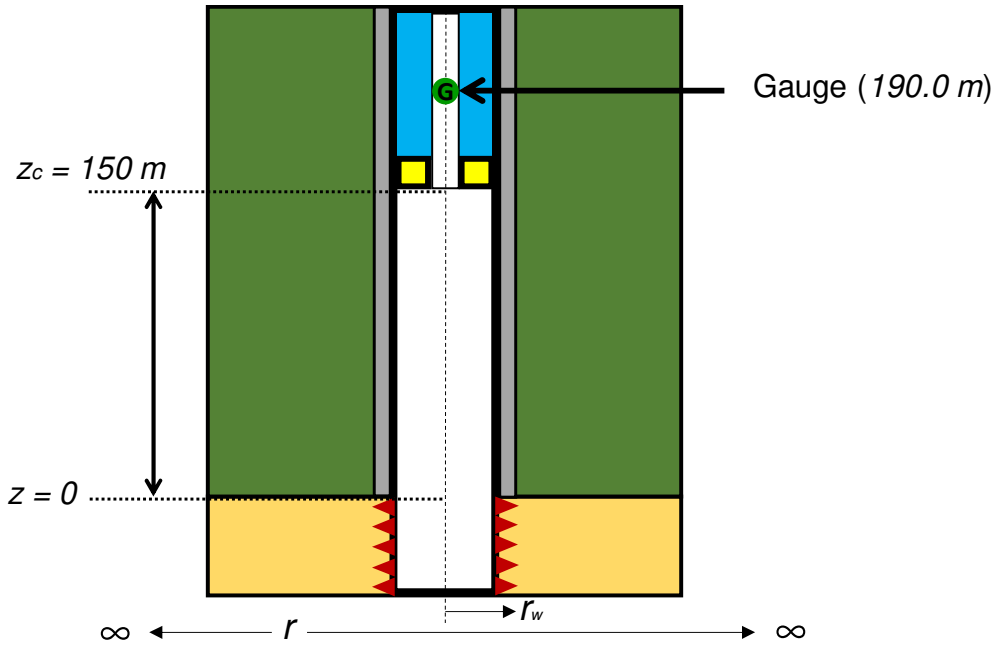


Figure 6.20: Case Study 3 – Wellbore/Reservoir System

The reservoir effective oil flow capacity is 450,000 mD.m and all other reservoir and fluid input data are presented in Table 5.1, Table 5.2, Table 5.5 and Table 5.6. Wellbore parameters for this case study are presented in Table 6.3.

Table 6.3: Wellbore Parameters for Case Study 3

| Property | Value |
|---|---|
| $r_w$ (m) | 0.156 |
| $\lambda_{cem}$ (J/m/h/K) | 6.833E+3 |
| $r_{co}$ (m) | 0.12224 |
| $r_{ci}$ (m) | 0.10839 |
| $r_{to}$ (m) | 0.06350 |
| $r_{ti}$ (m) | 0.028575 |
| $\lambda_{an}$ (J/m/h/K) | 2.229E+3 |
| Skin Factor | 0 |
| $\theta$ (degree) | 90° |
| $z_c$ (m) | 150.0 |
| $L_0$ (m) | 1500 |
| $C_{Tc}$ (dimensionless) | 4.0 and 12.0 |
| $C_{Tt}$ (dimensionless) | 0.0 – 12.0 |

The first analysis considers $C_{Tc} = 4.0$ and a null value for $C_{Tt}$. The second analysis investigates the sensitivity to the parameter $C_{Tt}$. A third analysis investigates the impacts of high thermal-storage coefficients.

The simulated test sequence comprises 24 hours of production at a constant downhole rate of 1400 m³/d followed by a 48-hour buildup. In this case study, the total tubing contraction was approximately 0.50 m.

Like in Case Study 2, both constant and variable pipe-length solutions will be assessed.

**Analysis 1: Two-Valley Pressure Derivative Curve**

The total thermal noise is the sum of three effects: fluid mass density variation in casing, fluid mass density variation in tubing and tubing contraction. Figure 6.21 shows the transient behavior of each effect and the total thermal noise.

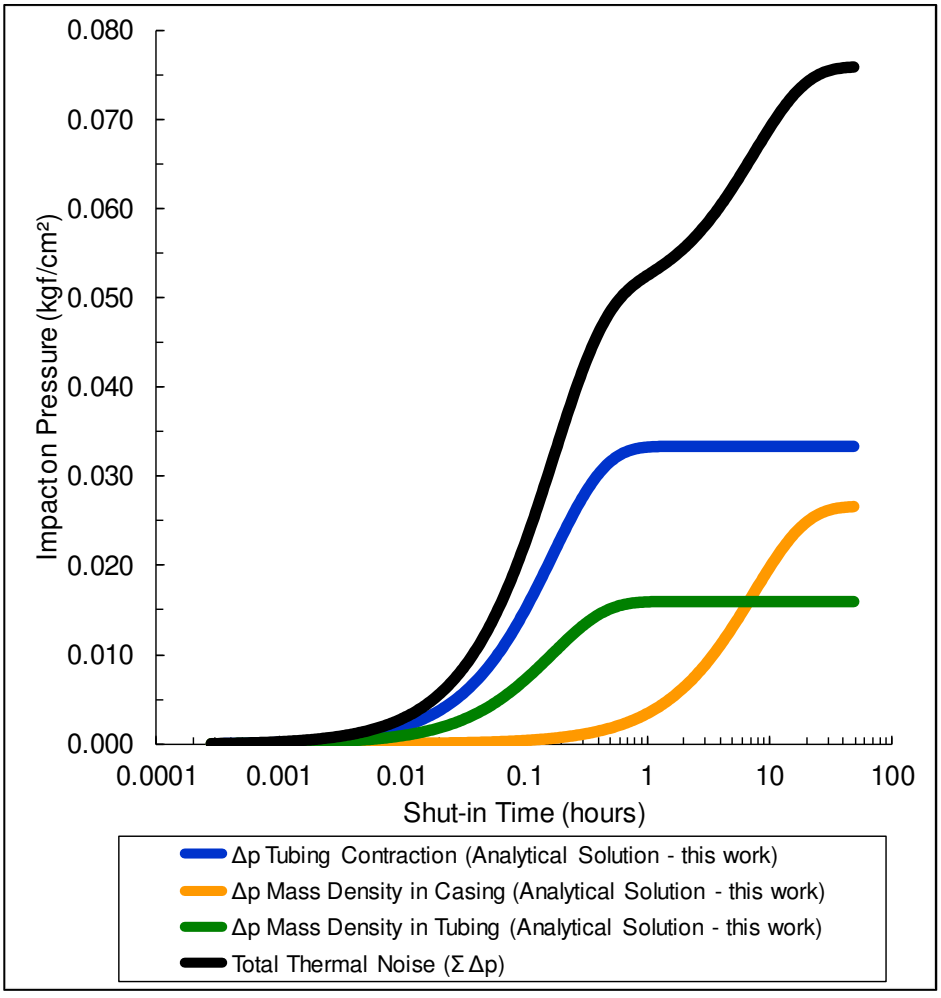


Figure 6.21: Case Study 3 – Thermal Noise Separate Effects

The black curve in Figure 6.21 is the total thermal noise, i.e., the sum of the other three curves. The measured gauge data comprise the formation signal $\Delta p_{sf}$ minus the black curve (see Eq. (4.19)). The resulting derivative curve is presented in Figure 6.22.

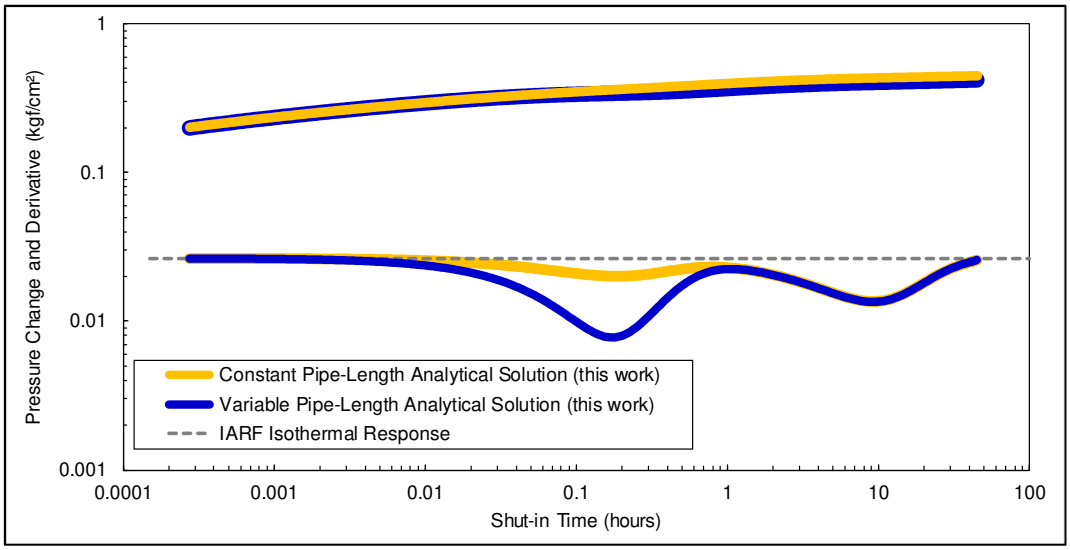


Figure 6.22: Constant and Variable Pipe-Length Solutions

The difference between the blue and yellow curves is the intensity of the first valley, due to tubing contraction. Note that the third inflection (second valley) is the same for both solutions.

In this case study, the concept of a single time of maximum impact on pressure is no longer applicable, given the presence of more than one valley in the pressure derivative curve.

In Figure 6.22, the elapsed times when inflections occur can be estimated from Eq. (4.31).

Table 6.4: Shut-in Times

| Inflection | Measured Shut-in Time (hours) | Computed Time (hours) (Analytical Solution in Eq. (4.31)) |
|---|---|---|
| 1 | 0.17 | 0.17 |
| 2 | 1.04 | 1.07 |
| 3 | 9.04 | 7.31 |

The assumption of a constant buildup-pressure derivative with respect to $\ln \Delta t$ is responsible for the increasing error over time. Yet, for practical purposes, the error is not significant, due to the logarithmic scale.

Double-permeability models can be used to interpret pressure derivative data with more than one inflection. These models comprise even more heterogeneities than the double-porosity model described in Case Study 1, leading to interpretations even further from reality.

**Analysis 2: Sensitivity to Thermal-Storage Coefficient**

Thermal storage represents the capacity of the wellbore to store or release heat and its value depends on a series of thermal, dimensional and operational parameters.

Figure 6.23 shows curves computed from the variable pipe-length solution with different values for the tubing thermal storage.

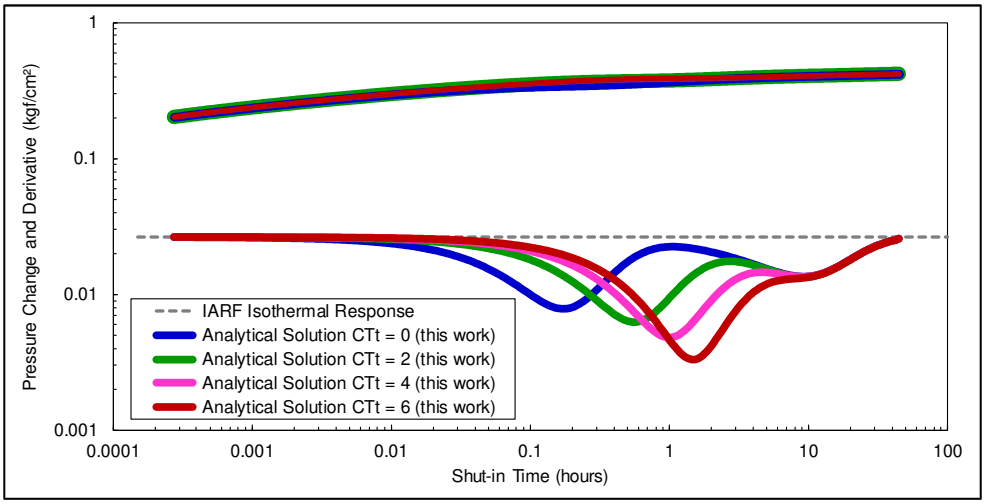


Figure 6.23: Sensitivity to the Thermal-Storage Coefficient

The greater the tubing thermal storage, the further in time the first inflection occurs. The second valley remains unchanged due to the fixed value of $C_{Tc}$.

Figure 6.23 illustrates how far from reality thermal distorted data can affect pressure transient analysis. In the derivative curves, each change in slope could be interpreted as an additional false heterogeneity. Interpretation results could yield a model with several false geological features in the reservoir, which in this case is homogeneous infinite-acting.

**Analysis 3: High Thermal-Storage Wellbores**

In cases of high thermal storage, inflections in derivative curves are pushed to right even further in time, not making it possible to observe the return to the

initial IARF line during typical well-testing times. This condition may lead to the false interpretation of a continuous increase in reservoir flow capacity.

To illustrate the effect, Figure 6.24 shows the constant pipe-length solution curve computed with thermal-storage coefficients of 12 for both tubing and casing.

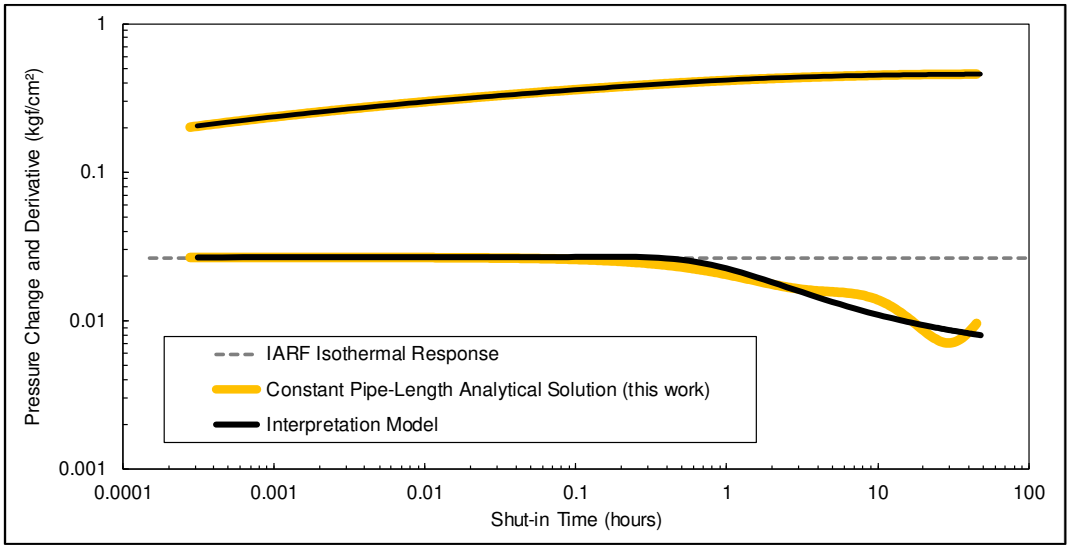


Figure 6.24: High Thermal-Storage Wellbore: Constant Pipe-Length Solution and Interpretation Model

Inflections in the yellow curve at late times could easily be mistaken for the well-known tidal effect. The interpretation model in Figure 6.24 accounts for a linear increase in reservoir thickness in one direction only, yielding a final flow capacity 3 times the value near the wellbore. Figure 6.25 presents a schematic of the interpretation model.

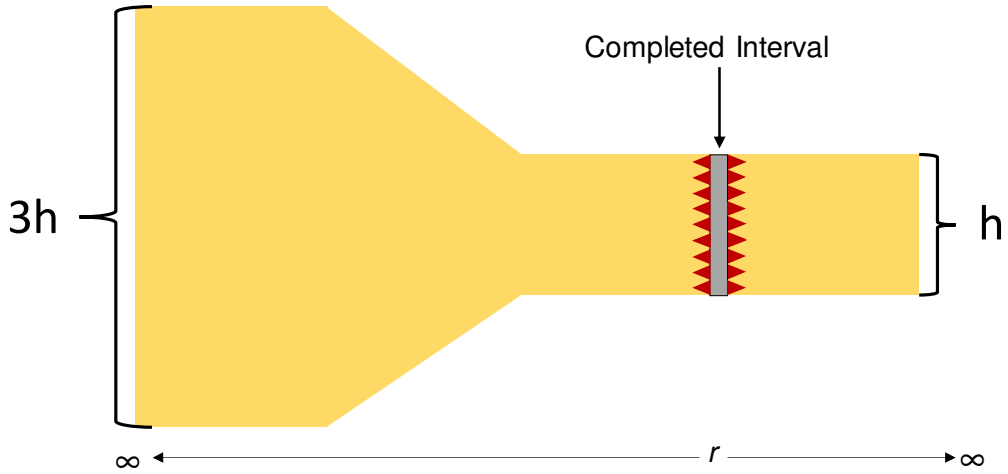


Figure 6.25: High Thermal-Storage Wellbore – Schematic Interpretation Model

The high thermal-storage condition particularly occurs when a buildup test is preceded by a variable surface-rate history. The preceding drawdown periods distort the initial condition for this problem, which is the Earth temperature at $t = 0$. This is the result of temperature superposition effects. Another operational feature that changes the capacity of the wellbore to store or release heat is the additional heating caused by viscous dissipation effects.

## 6.4. Discussion on Results

Thermal impacts on far-field parameter characterization can provide an unrealistic improvement on permeability and the identification of inexistent flow barriers. Moreover, the heat loss during buildup periods can make a homogeneous reservoir be wrongly interpreted as a double-porosity reservoir.

Chapter 7 presents a field case study. It will be shown that thermal-storage coefficients can be used to cope with viscous dissipation and temperature superposition effects.

# 7
# Field Case Study

This chapter presents a field case study. A conventional DST was conducted in a high productivity offshore vertical well with a complete suite of surface and downhole measurements. Early-time pressure transient analysis resulted in a near-wellbore effective oil transmissibility in the order of 500,000 mD.m/cP and a skin factor close to zero.

The well test was conducted prior to any production in the field, consisting of three producing periods, each followed by a buildup period. Fluid production above bubblepoint occurred in all producing periods. The minimum flowing pressure at the furthest gauge location was 200 kgf/cm² above the bubblepoint pressure. The well was shut-in downhole in the first and second buildup periods.

Shown in Figure 7.1 is the log-log diagnostic plot of the first buildup.

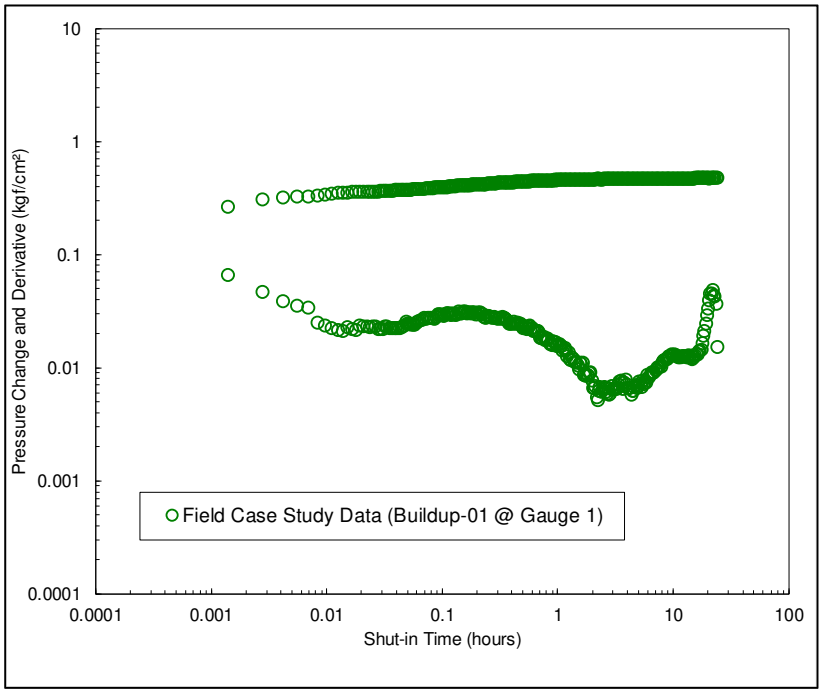


Figure 7.1: Field Case Study - Buildup 1 at Gauge 1 Log-Log Plot

In Figure 7.1, under the isothermal hypothesis, interpretation of pressure-transient data would possibly entail strong heterogeneities on far-field reservoir characterization. The objective of this case study is to evaluate potential thermal

impacts on the measured buildup pressure data and provide the real reservoir characterization.

Figure 7.2 presents the schematic of the wellbore/reservoir system, where two gauges at different depths are placed in the test string.

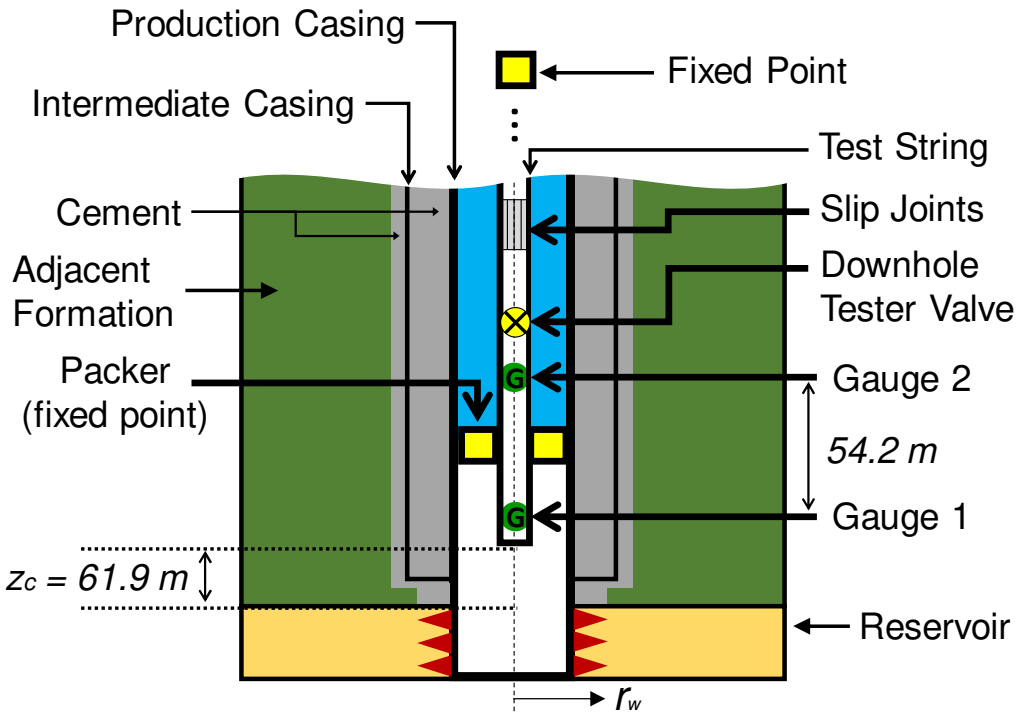


Figure 7.2: Field Case Study Schematic of the Wellbore/Reservoir System

Besides the test string and the production casing, the wellbore comprises an intermediate casing. The expression for the overall heat-transfer coefficient in Eq. (3.5) has been adapted to account for this additional heat-flow resistance. Borehole and pipe dimensions are presented in Table 7.4.

The annular fluid is brine and regarding the first gauge, it is placed below the packer, being exposed only to the formation fluid. The packer provides a fixed point and both gauges are located below slip joints, which compensate for pipe movement. Hence, measured data are not exposed to pipe contraction effects during the buildup period. The data displayed in Figure 7.1 were acquired at Gauge 1.

A production logging tool assessed the perforations during the third drawdown period. Figure 7.3 presents the production logging flow profile and the corresponding temperature curve.

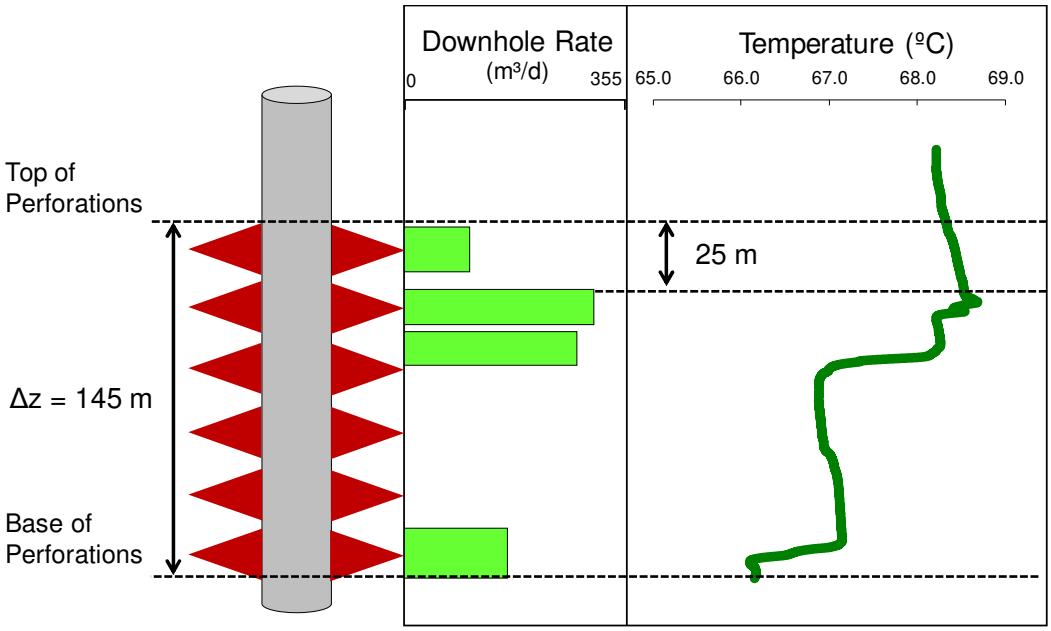


Figure 7.3: Field Case Study - Production Logging Flow Profile

In Figure 7.3, the flow profile indicates a relevant contribution to well productivity from the base of the completed interval. Moreover, the wellbore flowing temperature is dominated by the producing zone at the top of perforations. Therefore, the real problem can be viewed as a point-source problem coupled with a finite-perforated-interval problem. As mentioned before, a finite perforated interval is out of the scope of this work, hence to make use of the derived solutions, pressure and temperature assessments have to be addressed differently.

Pressure data recorded at the gauges are exposed to the entire wellbore-fluid column, including thermal impacts within the 145 m perforated interval. As for temperature, data must be governed by the stronger signal from top of perforations. Hence, temperature data will be analyzed considering the producing horizon located at the main producing zone (25 meters below the top of perforations in Figure 7.3) and pressure analyses will account for the entire completed interval, assuming the producing horizon to be located at the base of perforations.

## 7.1. Thermal Effects on PTA

The proposed analytical solution describes transient temperature changes along the wellbore and computes the impacts on buildup pressure at the gauges. The transient thermal noise comprises the description of changes in fluid mass density and change in pipe length over time and depth. The result is a transient pressure exerted by the wellbore-fluid column between the gauges and the producing horizon.

The proposed solution will be evaluated under the same operational conditions of the field well test. Real data will be compared to the complete analytical solution presented in Eq. (4.19), discarding the term $\Delta p_{cont}$ due to the fixed gauge locations shown in Figure 7.2.

The test sequence is presented in Table 7.1.

Table 7.1: Field Case Study Flow and Shut-in Periods

| Period | Duration (hours) | Oil Rate (std m³/d) |
|---|---|---|
| Cleanup + DD-01 | 24.7 | 850 |
| BU-01 | 24.6 | 0 |
| DD-02 | 9.0 | 820 |
| BU-02 | 9.5 | 0 |
| DD-03 (Production Logging Job) | 9.3 | 580 |
| BU-03 (Shut-in at Surface) | 30.7 | 0 |



In Eq. (4.19), the input formation signal $\Delta p_{sf}(\Delta t)$ is defined by

$$\Delta p_{sf}(\Delta t) = p_{ws}(t_p + \Delta t) - p_{wf}(t_p). \tag{7.1}$$

The pressure difference in Eq. (7.1) must account for pressure superposition effects. Therefore, the final flowing pressures $p_{wf}$ and the buildup pressures $p_{ws}$ will be computed by use of the well-known infinite-acting radial flow variable-rate expression

$$p_w(t) = p_i - C_2 \frac{1}{2}\frac{B_o \mu_o}{k_o h}\left[ Q_1 \left( \ln t + \ln\left(\frac{4C_1\eta_o}{r_w^2 e^{\gamma}}\right) + S \right) + \sum_{j=2}^{N} (Q_j - Q_{j-1}) \left( \ln(t - t_{j-1}) + \ln\left(\frac{4C_1\eta_o}{r_w^2 e^{\gamma}}\right) + S \right) \right], \tag{7.2}$$

where $Q_j$ is the flow step between the elapsed times $t_{j-1}$ and $t_j$, and $N$ is the number of constant step changes in flow rate.

The additional input data to compute the proposed analytical solution are presented in the following tables.

Table 7.2: Field Case Study Fluid Properties

| Property | Oil |
|---|---|
| $B_o$ (m³/std m³) | 1.47 |
| $c_o$ (cm²/kgf) | 1.10E-4 |
| $\mu_o$ (cP) | 1.30 |
| $\lambda_o$ (J/m/h/K) | 5.832E+2 |
| $\rho_{oi}$ (kg/m³) | 768.4 |
| $\beta_o$ (K$^{-1}$) | 9.200E-4 |
| $\varepsilon_{JTo}$ (K/(kgf/cm²)) | -3.3172E-2 |
| $\varphi_o$ (K/(kgf/cm²)) | 2.29294E-2 |
| $c_{po}$ (J/kg/K) | 2274.90 |

In Table 7.2, some fluid properties were obtained from the PVT analysis and other property values were estimated by use of CMG-STARS (2017) fluid models.

Table 7.3: Field Case Study Reservoir Properties

| Property | Value |
|---|---|
| $(kh)_o$ (mD.m) | 615,000.0 |
| $\phi$ (fraction) | 0.128 |
| $c_r$ (cm²/kgf) | 3.0E-5 |
| $s_w$ (fraction) | 0.189 |
| $g_G$ (K/m) | 0.03 |
| $c_{pr}$(J/m³/K) | 2.366E+6 |
| $\lambda_r$ (J/m/h/K) | 8.100E+3 |
| $\lambda_e$ (J/m/h/K) | 8.100E+3 |

Table 7.4: Field Case Study Wellbore Parameters

| Property | Value |
|---|---|
| $r_{w,16"}$ (m) | 0.2032 |
| $r_{int,co}$ (intermediate casing) (m) | 0.17780 |
| $r_{int,ci}$ (intermediate casing) (m) | 0.15718 |
| $r_{w,12.25"}$ (at reservoir) (m) | 0.156 |
| $r_{prod,co}$ (production casing) (m) | 0.12224 |
| $r_{prod,ci}$ (production casing) (m) | 0.10839 |
| $r_{to}$ (m) | 0.065151 |
| $r_{ti}$ (m) | 0.048006 |
| $\lambda_{cem}$ (J/m/h/K) | 3.060E+3 |
| $\lambda_{an}$ (J/m/h/K) | 2.229E+3 |
| Skin Factor | 0 |
| $\theta$ (degree) | 90° |
| $z_c^{PTA}$ (m) | 206.9 |
| $z_{g1}$ (m) | 208.6 |
| $z_{g2}$ (m) | 262.8 |
| $C_{Tc}$ (dimensionless) | 0.5 – 1.7 |
| $C_{Tt}$ (dimensionless) | 3.0 |

The parameter $z_c^{PTA}$ is the distance from the bottom of the test string to the base of perforations.

The periods to be analyzed are BU-01 and BU-03. The first analysis addresses BU-01 and investigates the response of both gauges. The second analysis investigates different producing times and rates by comparing BU-01 to BU-03 at Gauge 1. All analyses and comparisons are performed in the corresponding rate-normalized log-log diagnostic plots.

**Pressure Transient Analysis 1: BU-01 Data at Gauge 1 and Gauge 2**

Analysis 1 assesses BU-01 at two different depths. Figure 7.4 presents the log-log diagnostic plot of Gauge 1 data (in green) and the proposed analytical solution (in yellow).

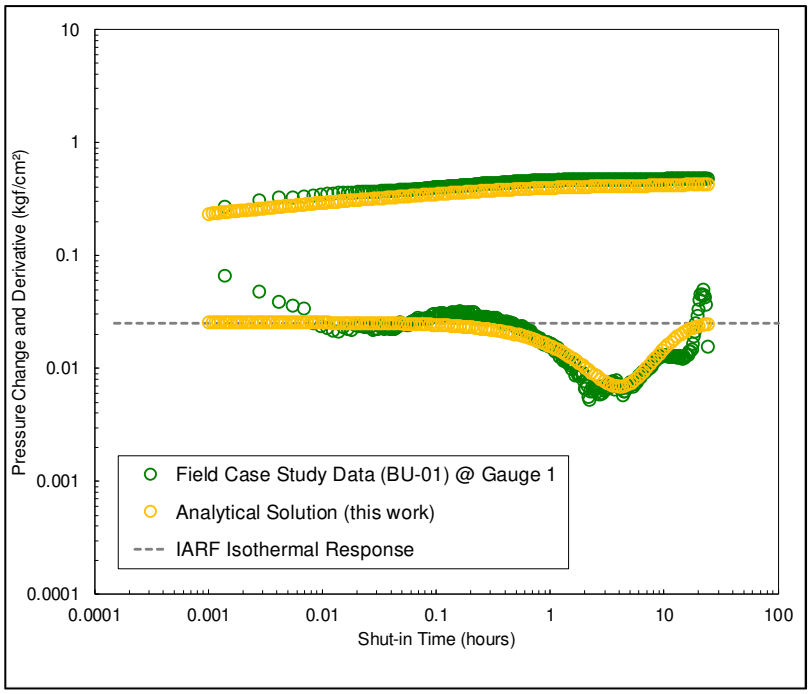


Figure 7.4: Field Pressure Data (BU-01 at Gauge 1) and Analytical Solution



Early-time data are not impacted by any kind of thermal effect, a condition systematically observed in all analytical and numerical results presented in this work. Therefore, the IARF isothermal line has been set at the radial plateau identified between 0.01 – 0.1 hours.

In Figure 7.4, both pressure derivative curves began to drop at approximately 0.2 hours and reached a minimum value at approximately 3 hours, when the inflection occurred in both curves. After that, the return of both data sets towards the IARF line is also in good agreement. The proposed analytical solution presents a good match with the field gauge data in Figure 7.4.

The adopted value for $C_{Tc}$ was 0.5. In this case, $C_{Tt}$ is not relevant to calculations, since the gauge is located at the bottom of the test string (see Figure 7.2). Conversely, $C_{Tt}$ plays an important role for Gauge 2 data. Figure 7.5 presents the same buildup period at Gauge 2, placed farther from perforations.

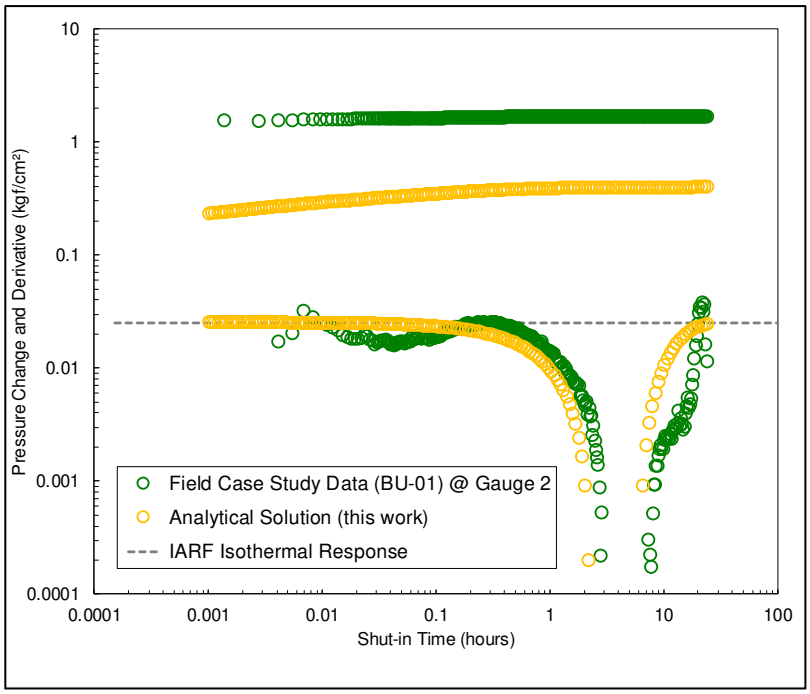


Figure 7.5: Field Pressure Data (BU-01 at Gauge 2) and Analytical Solution



As expected, the farther the gauge, the more impacted by thermal effects are the measured data.

As mentioned before, the analytical solution does not account for a friction model, thus it is not able to represent the additional pressure drop due to friction loss. This effect is evident in the field data pressure-change curve in Figure 7.5. Consequently, the impact of the additional heating due to viscous dissipation has altered the capacity of the wellbore to store and release heat, making it necessary to set $C_{Tt}$ at the value of 3.0 to reproduce Gauge 2 data. The value of $C_{Tc}$ was kept at 0.5.

The IARF isothermal line has been set at the same plateau of Figure 7.4. Apart from the total skin, the proposed analytical solution match well with field data. Moreover, at this depth the thermal noise overcame the formation signal between 3 and 7 hours of shut-in time, providing negative values, which cannot be plotted on a log-log graph paper. This harsh condition has also been reproduced by the proposed analytical solution.

**Pressure Transient Analysis 2: Gauge 1 Data during BU-01 and BU-03**

The second analysis compares BU-01 to BU-03 at Gauge 1 and evaluates the proposed analytical solution in both periods. The differences between the two buildup periods are listed as follows:

1. In BU-03, the well was shut in at surface, thus it is expected the wellbore storage effect to be noticeable;
2. DD-03 and BU-03 were preceded by a series of flow and shut-in periods. Hence, wellbore surroundings have been heated;
3. DD-03 was shorter than DD-01 and the production rate was 32% lower (see Table 7.1). Therefore, thermal impacts on BU-03 derivative should be more evident.

Shown in Figure 7.6 is a comparison of BU-01 and BU-03 at Gauge 1.

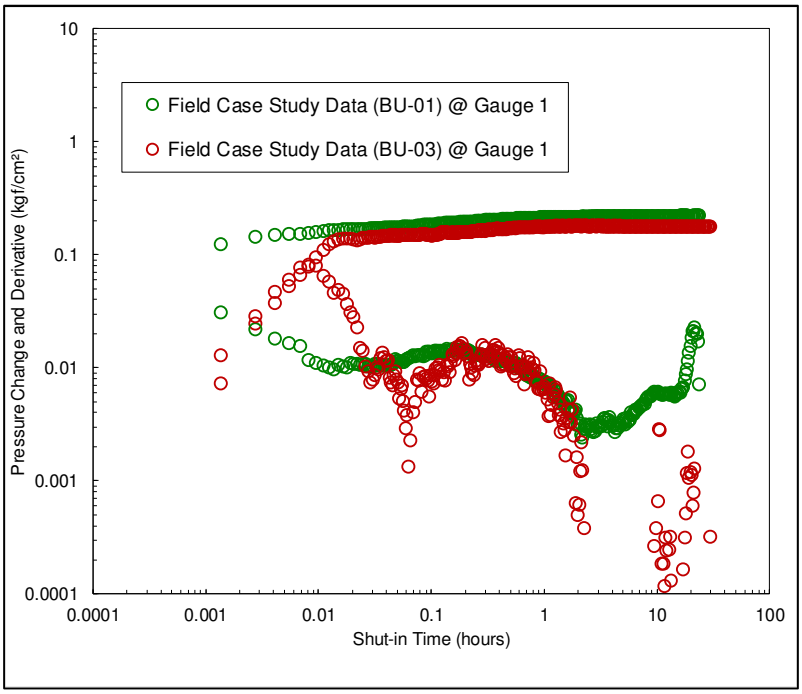


Figure 7.6: Field Pressure Data (BU-01 and BU-03 at Gauge 1)

As expected, the wellbore storage effect is evident in BU-03 (red curve). Regarding thermal impacts, it is clear that BU-03 was more influenced due to the lower preceding flow rate and the shorter drawdown duration.

BU-03 minimum derivative value occurred at approximately 4 hours, further in time when compared to BU-01. The preceding drawdown periods have heated the formation adjacent to the wellbore, causing a change in the capacity of the

wellbore to store and release heat. Therefore, the adopted value for the casing thermal-storage coefficient has been updated to 1.7.

Figure 7.7 presents the proposed analytical solution (yellow curve) compared to Gauge 1 data during BU-03 (green curve).

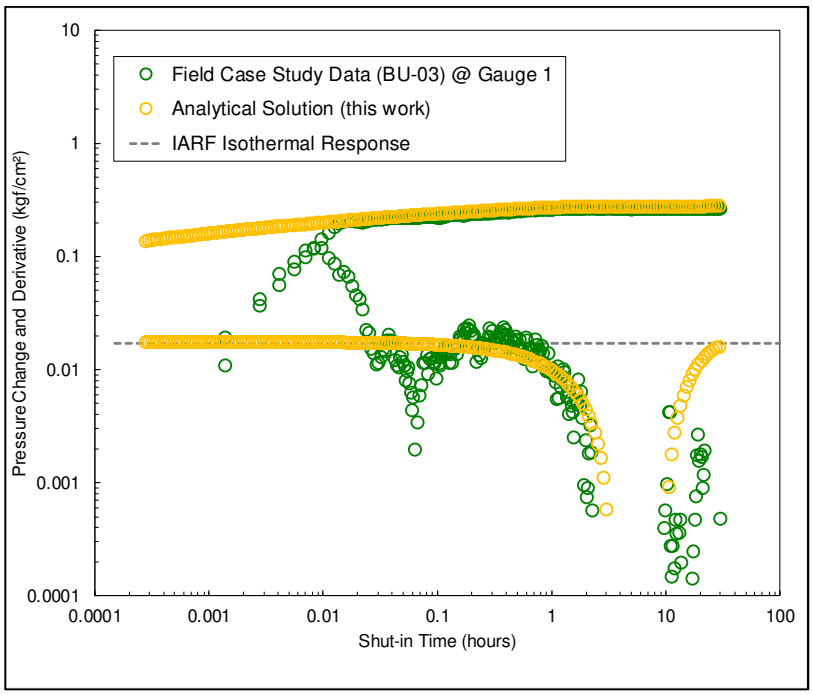


Figure 7.7: Field Pressure Data (BU-03 at Gauge 1) and Analytical Solution

Apart from wellbore storage effects and from the inherent noise of shutting in the well at surface, the analytical model successfully reproduced the field data.

Under the given conditions, the thermal noise overcame the formation signal between 3 and 9 hours of shut-in time, providing negative values. Again, the proposed analytical solution successfully represented this harsh condition.

## 7.2. Temperature Analyses

Analyses will be performed by comparing buildup-temperature changes, defined by Eq. (3.58). Figure 7.8 shows a comparison of the proposed analytical solution (yellow curve) and Gauge 1 data during BU-01 (green curve).

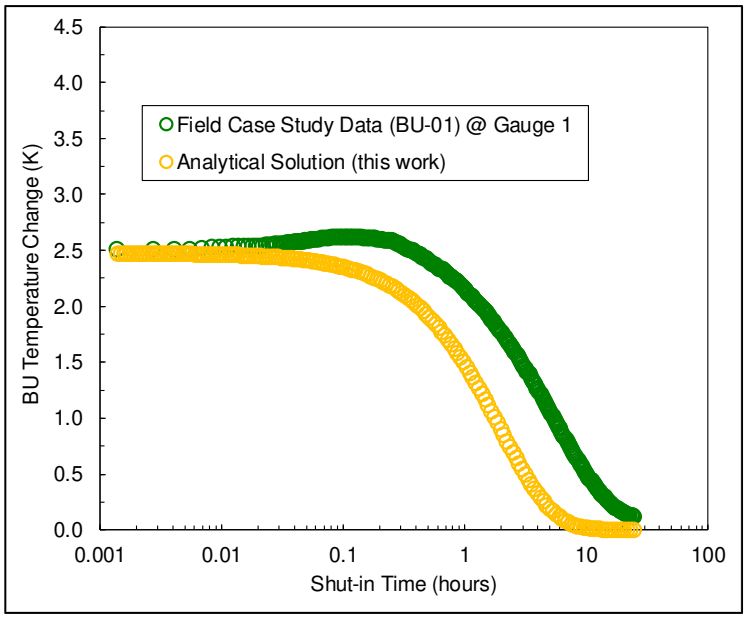


Figure 7.8: Field Temperature Data (BU-01 at Gauge 1) and Analytical Solution

Both early- and late-time matches are good. The intermediate-time mismatch is caused by afterflow and axial conduction effects in the wellbore, which retard the cooling response. Though not shown here, an increase in the thermal-storage coefficient yields a better match.

Figure 7.9 presents Gauge 2 data.

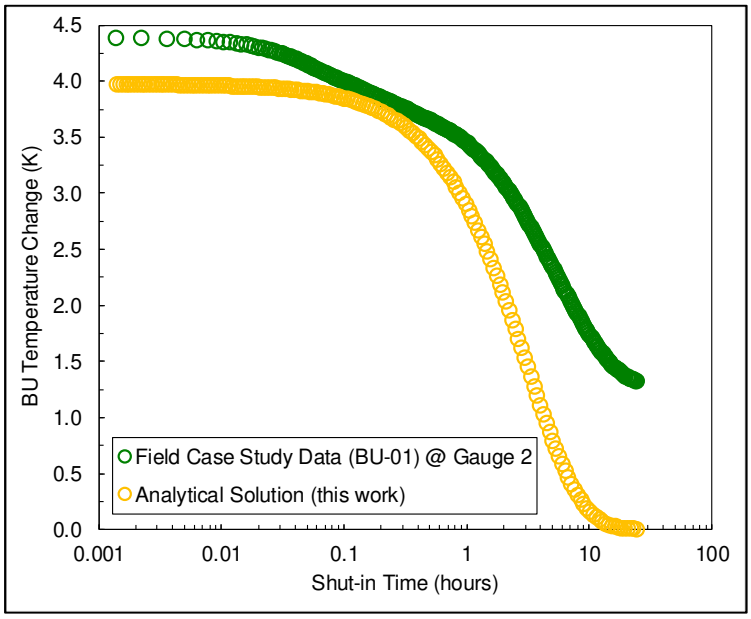


Figure 7.9: Field Temperature Data (BU-01 at Gauge 2) and Analytical Solution

This is indeed an expected result. The mismatch is rooted in neglecting viscous dissipation effects. The over-heated gauge requires more time to approach

the constant value of the Earth temperature at this location. The other possible source of error stems from the neglect of axial conduction effects along the wellbore. Again, although not shown here, the assumption of a high thermal-storage condition can provide a better match, especially with late-time data.

Mismatches on pressure data are less dramatic than in temperature data due to the integration procedure used for computing the former (see Eq. (B.11)). Fortunately, the required integration tends to smooth temperature-distribution particularities along the wellbore, thus the resulting pressure data are less influenced by local factors.

## 7.3. Field Case Study Conclusions

In light of the foregoing, the proposed analytical model successfully reproduced the field data at different depths and for different preceding drawdown rates and durations. Moreover, analyses showed that thermal-storage coefficients can be used to describe two phenomena:

- The additional heating caused by the viscous dissipation effects, as shown in BU-01 at Gauge 2;
- The effect of previous producing periods, which heat the wellbore surroundings, as shown in BU-03 at Gauge 1.

Most important, the proposed solution revealed that the reservoir is dominated by an infinite-acting homogeneous behavior and mitigated the risk of incorporating false geological heterogeneities to the interpretation model. In particular, a double-porosity model could have been used to interpret the data if thermal effects were neglected. Less drastic than interpreting thermal-distorted data, but also unfortunate, one could have discarded the acquired data, due to the apparent limited value from a test-interpretation viewpoint.

The proposed solution provided the correct far-field reservoir characterization, avoiding potential impacts on the geological model and on the field development plan.

# 8
# Conclusions and Final Remarks

This work provided a new coupled transient-wellbore/reservoir thermal analytical model, consisting of a reservoir/casing/tubing combined system. The analytical solutions consider flow of a slightly compressible, single-phase fluid in a homogeneous infinite-acting reservoir, accounting for Joule-Thomson, adiabatic fluid-expansion, conduction and convection effects. The wellbore fluid mass density is modeled as a function of temperature and the wellbore-temperature gradient $\partial T/\partial z$ is not a known input to solve the transient problem.

Analytical solutions for thermal impacts on pressure are derived from the temperature model. Buildup pressure solutions are obtained for different wellbore completions, accounting for the change in pipe length due to temperature changes.

Though some of the derived expressions are long, they encompass an intrinsic simplicity in that one can compute temperatures and pressures on a spreadsheet. Solutions are easily adaptable by simply modifying the input parameter values.

Both temperature and pressure analytical solutions were verified through use of a commercial non-isothermal simulator and impacts on PTA interpretations were thoroughly investigated. This work shows that thermal effects can induce an infinite-acting homogeneous reservoir to be wrongly interpreted as a double-porosity system.

A field case study was presented and the proposed analytical model successfully reproduced the field data of a well undergoing a drill stem test subject to a strong non-isothermal condition. The proposed solution avoided potential impacts on the geological model by providing the correct reservoir characterization, adding value to the field development plan.

This work provides the means to understand and interpret well tests under non-isothermal conditions, where inflections may occur in pressure derivative curves. The proposed analytical model mitigates the risk of interpreting thermal impacts on pressure as geological heterogeneities. The derived solutions should also prove useful for designing well tests.

## 8.1. Contributions of This Work

The main contributions of this work are listed as follows:

1. A new analytical buildup sandface-temperature solution that applies from early to late shut-in times (Chapter 2);
2. New drawdown and buildup analytical transient-wellbore-temperature solutions for flow in a cased tubing (Chapter 3);
3. A new analytical expression for the transient change in pipe length due to temperature changes (Chapter 4);
4. A new analytical solution for transient thermal impacts on buildup pressure in a cased tubing, accounting for tubing contraction effects (Chapter 4);
5. Derivation of analytical and easy to compute metrics for determining the farthest gauge location under a non-isothermal condition and the shut-in time of maximum impact on pressure (Chapter 4);
6. Successful validation of the proposed solutions and derived metrics through use of a commercial non-isothermal simulator (Chapter 5);
7. A thorough investigation of thermal impacts on PTA interpretations, with special attention to the misuse of double-porosity models (Chapter 6);
8. Use of the proposed model to appraise a real field case study. The proposed solutions successfully reproduced field-test data at different gauge depths and for different flowing rates (Chapter 7).

The derived metrics and solutions combined with the drawdown sandface-temperature solution provided by Onur and Cinar (2017a) comprise the proposed coupled reservoir/casing/tubing analytical model. The proposed solutions are fully analytical, requiring no iterative or numerical methods to be computed.

## 8.2. Future Work

This work consisted of an effort to better understand both transient temperature and pressure behaviors in a coupled reservoir/casing/tubing system. To further extend the proposed model, there are important steps that deserve attention for future works, such as:

1. Friction model. The proposed analytical model does not account for viscous pressure drop and thermal dissipation effects. Therefore, the next suggested step is to include a friction model in the transient wellbore energy and momentum balance;
2. Finite perforated intervals. The proposed analytical model assumes perforations to be a point source. Although the adopted approach in the field case study was successful, the modeling of a finite completed interval should improve accuracy of results;
3. Skin effect. The incorporation of skin effects will better describe the sandface-temperature changes in cases of damaged/stimulated wells;
4. Variable surface-rate history. The proposed analytical model was derived for constant-volumetric-rate drawdown and buildup tests. Therefore, the modeling of variable-rate production histories will enable the incorporation of temperature superposition effects;
5. Wellbore-fluid-flow model. The modeling of WBS and momentum effects will provide important generalizations to the proposed solutions;
6. Layered heterogeneous reservoirs. Layered reservoirs present different permeabilities over depth, therefore the modeling of non-uniform flow distribution along perforations shall provide a significant generalization to the model;
7. Water injection wells and gas wells. The modeling of injection tests and gas flow will provide additional generalizations to the model;
8. Dimensionless approach. From a dimensionless perspective, the primary dimensionless parameters that affect the solutions should arise, possibly providing new insights.

# Bibliography


AGARWAL, R. G. A New Method to Account for Producing Time Effects When Drawdown Type Curves are used to Analyze Pressure Buildup and Other Test Data. *In:* **SPE Annual Technical Conference and Exhibition**. Society of Petroleum Engineers. doi:10.2118/9289-MS, 1980.

ALVES, I. N.; ALHANATI, F. J. S.; SHOHAM, O. A Unified Model for Predicting Flowing Temperature Distribution in Wellbores and Pipelines. **SPE Production Engineering, v. 7**(04), p. 363-367. doi:10.2118/20632-PA, 1992.

APP, J. F. Field Cases: Nonisothermal Behavior Due to Joule-Thomson and Transient Fluid Expansion/Compression Effects. *In:* **SPE Annual Technical Conference and Exhibition.** Society of Petroleum Engineers. doi:10.2118/124338-MS, 2009.

APP, J. F. Nonisothermal and Productivity Behavior of High-Pressure Reservoirs. **SPE Journal, v. 15**(01), p. 50-63. doi:10.2118/114705-PA, 2010.

BOURDET, D.; AYOUB, J. A.; PIRARD, Y. M. Use of Pressure Derivative in Well Test Interpretation. **SPE Formation Evaluation, v. 4**(02), p. 293-302. doi:10.2118/12777-PA, 1989.

CHEVARUNOTAI, N.; HASAN, A. R.; KABIR, C. S. Transient Flowing-Fluid Temperature Modeling in Oil Reservoirs for Flow Associated with Large Drawdowns. *In:* **SPE Annual Technical Conference and Exhibition.** Society of Petroleum Engineers. doi:10.2118/175008-MS, 2015.

COMPUTER MODELLING GROUP (CMG). **CMG-STARS** v2017.10.6504.34460, Advanced Process and Thermal Simulator. Calgary: CMG, 2017.

CURTIS, M. R.; WITTERHOLT, E. J. Use of the Temperature Log for Determining Flow Rates in Producing Wells. *In:* **Fall Meeting of the Society of Petroleum Engineers of AIME**. Society of Petroleum Engineers. doi:10.2118/4637-MS, 1973.

DURU, O. O.; HORNE, R. N. Modeling Reservoir Temperature Transients and Reservoir-Parameter Estimation Constrained to the Model. **SPE**

**Reservoir Evaluation & Engineering, v. 13**(06), p. 873-883. doi:10.2118/115791-PA, 2010a.

DURU, O. O.; HORNE, R. N. Joint Inversion of Temperature and Pressure Measurements for Estimation of Permeability and Porosity Fields. *In:* **SPE Annual Technical Conference and Exhibition.** Society of Petroleum Engineers. doi:10.2118/134290-MS, 2010b.

DURU, O. O.; HORNE, R. N. Simultaneous Interpretation of Pressure, Temperature, and Flow-Rate Data Using Bayesian Inversion Methods. **SPE Reservoir Evaluation & Engineering, v. 14**(02), p. 225-238. doi:10.2118/124827-PA, 2011a.

DURU, O. O.; HORNE, R. N. Combined Temperature and Pressure Data Interpretation: Applications to Characterization of Near-Wellbore Reservoir Structures. *In:* **SPE Annual Technical Conference and Exhibition.** Society of Petroleum Engineers. doi:10.2118/146614-MS, 2011b.

GRINGARTEN, A. C.; BOURDET, D. P.; LANDEL, P. A.; KNIAZEFF, V. J. A Comparison Between Different Skin And Wellbore Storage Type-Curves For Early-Time Transient Analysis. *In:* **SPE Annual Technical Conference and Exhibition.** Society of Petroleum Engineers. doi:10.2118/8205-MS, 1979.

GRINGARTEN, A. C. From straight lines to deconvolution: the evolution of the state-of-the art in well test analysis. *In:* **SPE Annual Technical Conference and Exhibition.** Society of Petroleum Engineers. doi:10.2118/102079-MS, 2006.

HASAN, A. R.; KABIR, C. S. Heat Transfer During Two-Phase Flow in Wellbores; Part I-Formation Temperature. *In:* **SPE Annual Technical Conference and Exhibition.** Society of Petroleum Engineers. doi:10.2118/22866-MS, 1991.

HASAN, A. R.; KABIR, C. S. **Fluid Flow and Heat Transfer in Wellbores.** 1st ed. Richardson, Texas: Society of Petroleum Engineers, 2002. 181 p., p. 64-68. ISBN 1-55563-094-4.

HASAN, A. R.; KABIR, C. S.; LIN, D. Analytic Wellbore Temperature Model for Transient Gas-Well Testing. **SPE Reservoir Evaluation & Engineering, v. 8**(03), p. 240-247. doi:10.2118/84288-PA, 2005.

HASAN, A. R.; KABIR, C. S.; WANG, X. Development and Application of a Wellbore/Reservoir Simulator for Testing Oil Wells. **SPE Formation Evaluation, v. 12**(03), p. 182-188. doi: 10.2118/29892-PA, 1997.

HORNE, R. N.; SHINOHARA, K. Wellbore Heat Loss in Production and Injection Wells. **Journal of Petroleum Technology, v. 31**(01), p. 116-118. doi:10.2118/7153-PA, 1979.

HORNER, D. R. Pressure Build-up in Wells. *In:* **Third World Petroleum Congress**. WPC-4135, 1951.

IZGEC, B.; KABIR, C. S.; ZHU, D.; HASAN, A. R. Transient Fluid and Heat Flow Modeling in Coupled Wellbore/Reservoir Systems. **SPE Reservoir Evaluation & Engineering, v. 10**(03), p. 294-301. doi:10.2118/102070-PA, 2007.

MAO, Y.; ZEIDOUNI, M. Accounting for Fluid-Property Variations in Temperature-Transient Analysis. **SPE Journal, preprint**. doi:10.2118/187465-PA, 2017.

MURADOV, K. M.; DAVIES, D. R. Temperature Transient Analysis in a Horizontal, Multi-zone, Intelligent Well. *In:* **SPE Intelligent Energy International.** Society of Petroleum Engineers. doi:10.2118/150138-MS, 2012.

ODEH, A. S.; JONES, L. G. Pressure Drawdown Analysis, Variable-Rate Case. **Journal of Petroleum Technology, v. 17**(08), p. 960-964. doi:10.2118/1084-PA, 1965.

ONUR, M.; CINAR, M. Temperature Transient Analysis of Slightly Compressible, Single-Phase Reservoirs. *In:* **SPE Europec 78th EAGE Conference and Exhibition.** Society of Petroleum Engineers. doi:10.2118/180074-MS, 2016.

ONUR, M.; PALABIYIK, Y.; TUREYEN; I., CINAR; M. Transient Temperature behavior and analysis of single-phase liquid water geothermal reservoirs during drawdown and buildup tests: Part II. Interpretation and analysis methodology with applications. **Journal of Petroleum Science and Engineering, v. 146**, p. 657-669. doi.org/10.1016/j.petrol.2016.08.002, 2016a.

ONUR, M.; ULKER, G.; KOCAK, S.; GOK, I. M. Interpretation and Analysis of Transient Sandface and Wellbore Temperature Data. *In:* **SPE Annual Technical Conference and Exhibition Dubai**. Society of Petroleum Engineers. doi:10.2118/181710-MS, 2016b.

ONUR, M.; CINAR, M. Analysis of Sandface-Temperature-Transient Data for Slightly Compressible, Single-Phase Reservoirs. **SPE Journal, v. 22**(04), p. 1134-1155. doi:10.2118/180074-PA, 2017a.

ONUR, M.; CINAR, M. Modeling and Analysis of Temperature Transient Sandface and Wellbore Temperature Data from Variable Rate Well Test Data. *In:* **SPE Europec featured at 79th EAGE Conference and Exhibition**. Society of Petroleum Engineers. doi:10.2118/185802-MS, 2017b.

ONUR, M.; ULKER, G.; KOCAK, S.; GOK, I. M. Interpretation and Analysis of Transient-Sandface- and Wellbore-Temperature Data. **SPE Journal, v. 22**(04), p. 1156-1177. doi:10.2118/181710-PA, 2017.

ONUR, M. Modeling and Interpretation of the Bottomhole Temperature Transient Data. *In:* **SPE Latin America and Caribbean Petroleum Engineering Conference.** Society of Petroleum Engineers. doi:10.2118/185586-MS, 2017.

PALABIYIK, Y.; ONUR, M.; TUREYEN; I., CINAR; M. Transient Temperature behavior and analysis of single-phase liquid water geothermal reservoirs during drawdown and buildup tests: Part I. Theory, new analytical and approximate solutions. **Journal of Petroleum Science and Engineering, v. 146**, p. 637-656. doi.org/10.1016/j.petrol.2016.08.003, 2016.

RAMEY, H. J. Wellbore Heat Transmission. **Journal of Petroleum Technology, v. 14**(04), p. 427-435. doi:10.2118/96-PA, 1962.

RAMEY, H. J. Short-Time Well Test Data Interpretation in the Presence of Skin Effect and Wellbore Storage. **Journal of Petroleum Technology, v. 22**(01), p. 97-104. doi:10.2118/2336-PA, 1970.

RIBEIRO, P. M.; HORNE, R. N. Pressure and Temperature Transient Analysis: Hydraulic Fractured Well Application. *In:* **SPE Annual Technical Conference and Exhibition.** Society of Petroleum Engineers. doi:10.2118/166222-MS, 2013.

RIBEIRO, P. M.; HORNE, R. N. Detecting Fracture Growth Out of Zone by Use of Temperature Analysis. **SPE Journal, 21**(04), 1263-1278. doi:10.2118/170746-PA, 2016.

RUSSELL, D. G. Determination of Formation Characteristics from Two-Rate Flow Tests. **Journal of Petroleum Technology, v. 15**(12), p. 1347-1355. doi:10.2118/645-PA, 1963.

SAGAR, R.; DOTY, D. R.; SCHMIDT, Z. Predicting Temperature Profiles in a Flowing Well. **SPE Production Engineering, v. 6**(04), p. 441-448. doi:10.2118/19702-PA, 1991.

SIDOROVA, M.; THEUVENY, B.; PIMENOV, V.; SHAKO, V.; GUZMAN-GARCIA, A. G. Do Not Let Temperature Transients Hinder Your Build-up Pressure Interpretation - Proper Gauge Placement in Highly Productive Reservoirs in Well Testing Operations. *In:* **SPE Annual Caspian Technical Conference and Exhibition.** Society of Petroleum Engineers. doi:10.2118/172278-MS, 2014.

SIDOROVA, M.; SHAKO, V.; PIMENOV, V.; THEUVENY, B. The Value of Transient Temperature Responses in Testing Operations. *In:* **SPE Middle East Oil & Gas Show and Conference.** Society of Petroleum Engineers. doi:10.2118/172758-MS, 2015.

SUI, W.; ZHU, D.; HILL, A. D.; EHLIG-ECONOMIDES, C. Model for Transient Temperature and Pressure Behavior in Commingled Vertical Wells. *In:* **SPE Russian Oil and Gas Technical Conference and Exhibition.** Society of Petroleum Engineers. doi:10.2118/115200-MS, 2008a.

SUI, W.; ZHU, D.; HILL, A. D.; EHLIG-ECONOMIDES, C. A. Determining Multilayer Formation Properties from Transient Temperature and Pressure Measurements. *In:* **SPE Annual Technical Conference and Exhibition.** Society of Petroleum Engineers. doi:10.2118/116270-MS, 2008b.

SUI, W.; EHLIG-ECONOMIDES, C. A.; ZHU, D.; HILL, A. D. Determining Multilayer Formation Properties from Transient Temperature and Pressure Measurements in Comingled Gas Wells. *In:* **International Oil and Gas Conference and Exhibition in China.** Society of Petroleum Engineers. doi:10.2118/131150-MS, 2010.

VAN EVERDINGEN, A. F.; HURST, W. The Application of the Laplace Transformation to Flow Problems in Reservoirs. **Journal of Petroleum Technology, v. 1**(12), p. 305-324. doi: 10.2118/949305-G, 1949.

VON SCHROETER, T.; HOLLAENDER, F.; GRINGARTEN, A. C. Deconvolution of Well Test Data as a Nonlinear Total Least Squares Problem. *In:* **SPE Annual Technical Conference and Exhibition**. Society of Petroleum Engineers. doi:10.2118/71574-MS, 2001.

WARREN, J. E.; ROOT, P. J. The Behavior of Naturally Fractured Reservoirs. Society of Petroleum Engineers. **SPE Journal, v. 3**(03), p. 245-255. doi:10.2118/426-PA, 1963.

WILLHITE, G. P. Over-all Heat Transfer Coefficients in Steam and Hot Water Injection Wells. **Journal of Petroleum Technology, v. 19**(05), p. 607-615. doi:10.2118/1449-PA, 1967.

# A
# Adopted Unit System and Conversion Factors

Table A.1: Adopted Unit System

| Quantity Name | Unit |
|---|---|
| Absolute Temperature | $K$ |
| Adiabatic-Expansion Coefficient | $K/(kgf/cm^2)$ |
| Area | $m^2$ |
| Energy | $J$ |
| Joule-Thomson Coefficient | $K/(kgf/cm^2)$ |
| Length | $m$ |
| Liquid Rate | $m^3/d$ |
| Mass | $kg$ |
| Mass Density | $kg/m^3$ |
| Permeability | $mD$ |
| Pressure | $kgf/cm^2$ |
| Specific Heat Capacity | $J/kg/K$ |
| Time | $h$ |
| Thermal Conductivity | $J/m/h/K$ |
| Viscosity | $cP$ |
| Volume | $m^3$ |

Table A.2: Conversion Factors

| Constant | SI | Oil Field | Adopted Unit System |
|---|---|---|---|
| $C_1$ | 1.0 | 0.00026374 | 0.0003484 |
| $C_2$ | $1/2\pi$ | 141.2 | 19.03 |
| $C_4$ | 1.0 | $1/24$ | $1/24$ |
| $C_5$ | 1.0 | $6{,}894.8\frac{Pa}{psi}$ | $98{,}066.5\frac{Pa}{(kgf/cm^2)}$ |
| $C_{iso}$ | $3/2\sqrt{e/\pi}$ | 11,322 | 4,778 |

# B
# Derivation of Thermal Impacts on Buildup Wellbore Pressure

## B.1.
## Production-Casing Solution: Constant Pipe Length

In this particular case, the expression for $\Delta p_{f_c}$ (the subscript $c$ refers to the production-casing solution) is obtained by the combination of Eqs. (3.41), (3.78) and (4.12).

$$\Delta p_{f_c}(z_g, \Delta t) = \beta_o \gamma_{oi} \sin\theta \int_0^{z_g} \left[\Delta T_{wp}(z, t_p) - e^{-\Delta t a_c L_{Rc}} \Delta T_z^{(0+)}\right] dz, \tag{B.1}$$

where the expression for $\Delta T_z^{(0+)}$ is obtained from Eq. (3.59). Hence, the expression for $\Delta p_{f_c}$ can be written as

$$\Delta p_{f_c}(z_g, \Delta t) = \beta_o \gamma_{oi} \sin\theta \int_0^{z_g} \Big[\Delta T_{wp}(z, t_p) - e^{-\Delta t a_c L_{Rc}} \left(\Delta T_{wp}(z, t_p) + \Delta T_{sf}(0^+)\right)\Big] dz. \tag{B.2}$$

The value of $\Delta T_{sf}(0^+)$ is obtained by evaluating Eq. (2.56) for a small $\Delta t$ (1 – 5 seconds). Eq. (B.2) can be rewritten as

$$\Delta p_{f_c}(z_g, \Delta t) = \beta_o \gamma_{oi} \sin\theta \int_0^{z_g} \Delta T_{wp}(z, t_p)(1 - e^{-\Delta t a_c L_{Rc}}) dz - \beta_o \gamma_{oi} \sin\theta \int_0^{z_g} \Delta T_{sf}(0^+) e^{-\Delta t a_c L_{Rc}} dz\,. \tag{B.3}$$

In Eq. (B.3), the second integral in the RHS can be easily solved:

$$\Delta p_{f_c}(z_g, \Delta t) = \beta_o \gamma_{oi} \sin\theta\, (1 - e^{-\Delta t a_c L_{Rc}}) \int_0^{z_g} \Delta T_{wp}(z, t_p) dz - z_g \sin\theta\, \beta_o \gamma_{oi} \Delta T_{sf}(0^+) e^{-\Delta t a_c L_{Rc}}. \tag{B.4}$$

As for the integral of $\Delta T_{wp}(z, t_p)$, it can be written as

$$\int_0^{z_g} \Delta T_{wp}(z, t_p) dz = \int_0^{z_g} \left(F_{(DD,c)}^{BC}(z, t_p) + F_{(DD,c)}(z, t_p)\right) dz, \tag{B.5}$$

where $F_{(DD,c)}^{BC}$ and $F_{(DD,c)}$ are functions defined by Eqs. (3.42) and (3.43), respectively.

The integrals in Eq. (B.5) are definite integrals and can be easily solved. Let the corresponding of values of $W_{(DD,c)}^{BC}$ and $W_{(DD,c)}$ be defined by:

$$W_{(DD,c)}^{BC}(z_g, t_p) = \int_0^{z_g} F_{(DD,c)}^{BC}(z, t_p)dz, \tag{B.6}$$

and

$$W_{(DD,c)}(z_g, t_p) = \int_0^{z_g} F_{(DD,c)}(z, t_p)dz. \tag{B.7}$$

Following the same idea as in the temperature solution, $W_{(DD,c)}^{BC}(z_g, t_p)$ depends on the boundary condition and $W_{(DD,c)}(z_g, t_p)$ does not.

Before solving Eqs. (B.6) and (B.7), let the following simplification be made:

$$\Delta T_{sf}\left(t_p - \frac{z}{a_c}\right) \sim \Delta T_{sf}(t_p). \tag{B.8}$$

For typical well-testing operations, this assumption is valid after a few hours of producing time. The solution of Eq. (B.6) is given by

$$W_{(DD,c)}^{BC}(z_g, t_p) = \\ = \frac{\Delta T_{sf}(t_p)}{L_{\beta c}}\Big[(1 - e^{-a_c t_p L_{\beta c}}) \\ + \Theta\left(t_p - \frac{z_g}{a_c}\right)(e^{-a_c t_p L_{\beta c}} - e^{-z_g L_{\beta c}})\Big], \tag{B.9}$$

where $\Delta T_{sf}(t_p)$ is obtained by evaluating Eq. (2.22) at $r = r_w$ and $t = t_p$.

As for the value of $W_{(DD,c)}(z_g, t_p)$:

$$
\begin{aligned}
\mathrm{W}_{(DD,c)}(z_g,t_p) = \\
&= \left\{ -\frac{1}{2L_{\beta c}^3} \left( \Theta\left(t_p - \frac{z_g}{a_c}\right) \right.\right. \\
&\times e^{-a_c t_p L_{\beta c}} \left[ \Omega\left( \left( (a_c t_p - z_g) L_{\beta c} \right)^2 \right.\right. \\
&+ 2\left( (a_c t_p - z_g) L_{\beta c} \right) - 2e^{\left( (a_c t_p - z_g) L_{\beta c} \right)} + 2 \Big) \\
&+ 2\psi L_{\beta c} \left( (a_c t_p - z_g) L_{\beta c} - e^{\left( (a_c t_p - z_g) L_{\beta c} \right)} + 1 \right) \Big] \\
&- \left( e^{-a_c t_p L_{\beta c}} \left( \Omega\left( \left( a_c t_p L_{\beta c} \right)^2 + 2 a_c t_p L_{\beta c} - 2e^{a_c t_p L_{\beta c}} \right.\right.\right. \\
&+ 2 \Big) + 2\psi L_{\beta c} \left( a_c t_p L_{\beta c} - e^{a_c t_p L_{\beta c}} + 1 \right) \Big) \Big) \Big) \Big\} \\
&+ \left\{ \frac{z_g e^{-a_c t_p L_{\beta c}}}{2L_{\beta c}^2} \left( \Omega\left( \left( 2 - z_g L_{\beta c} \right) e^{a_c t_p L_{\beta c}} - 2 a_c t_p L_{\beta c} \right.\right.\right. \\
&+ z_g L_{\beta c} - 2 \Big) + 2\psi L_{\beta c} \left( e^{a_c t_p L_{\beta c}} - 1 \right) \Big) \Big\}.
\end{aligned}
\tag{B.10}
$$

The constant pipe-length production-casing solution is given by Eq. (4.14).

## B.2. Cased-Tubing Solution: Constant Pipe Length

In this case, the expression for the buildup-pressure difference is obtained by the combination of Eqs. (3.51), (3.79) and (4.12).

$$
\begin{aligned}
\Delta p_{f_t}(z_g, \Delta t) = \beta_o \gamma_{oi} \sin\theta \int_0^{z_c} \left[ \Delta T_{wp}(z, t_p) - e^{-\Delta t a_c L_{Rc}} \Delta T_z^{(0+)} \right] dz \\
+ \beta_o \gamma_{oi} \sin\theta \int_{z_c}^{z_g} \left[ \Delta T_{wp}(z, t_p) - e^{-\Delta t a_t L_{Rt}} \Delta T_z^{(0+)} \right] dz,
\end{aligned}
\tag{B.11}
$$

where the subscript $t$ refers to the cased-tubing solution.

The first term in the RHS of Eq. (B.11) is the solution for $\Delta p_{f_c}$ derived in the previous section evaluated at $z = z_c$ and the expression for $\Delta T_z^{(0+)}$ is obtained from Eq. (3.59). The expression for $\Delta p_{f_t}$ can be written as

$$\Delta p_{f_t}(z_g, \Delta t) = \Delta p_{f_c}(z_c, \Delta t) + \beta_o \gamma_{oi} \sin\theta \int_{z_c}^{z_g} \left[\Delta T_{wp}(z, t_p) - e^{-\Delta t a_t L_{Rt}} \left(\Delta T_{wp}(z, t_p) + \Delta T_{sf}(0^+)\right)\right] dz. \quad \text{(B.12)}$$

The value of $\Delta T_{sf}(0^+)$ is obtained by evaluating Eq. (2.56) for a small $\Delta t$ (1 – 5 seconds). Eq. (B.12) can be rewritten as

$$\Delta p_{f_t}(z_g, \Delta t) = \Delta p_{f_c}(z_c, \Delta t) + \beta_o \gamma_{oi} \sin\theta \int_{z_c}^{z_g} \Delta T_{wp}(z, t_p)(1 - e^{-\Delta t a_t L_{Rt}}) dz - \beta_o \gamma_{oi} \sin\theta \int_{z_c}^{z_g} \Delta T_{sf}(0^+) e^{-\Delta t a_t L_{Rt}} dz. \quad \text{(B.13)}$$

In Eq. (B.13), the second integral can be easily solved:

$$\Delta p_{f_t}(z_g, \Delta t) = \Delta p_{f_c}(z_c, \Delta t) + \beta_o \gamma_{oi} \sin\theta \,(1 - e^{-\Delta t a_t L_{Rt}}) \int_{z_c}^{z_g} \Delta T_{wp}(z, t_p) dz - \beta_o \gamma_{oi} \sin\theta \, \Delta T_{sf}(0^+) e^{-\Delta t a_t L_{Rt}} (z_g - z_c). \quad \text{(B.14)}$$

Now the solution only depends on the integral of $\Delta T_{wp}(z, t_p)$, which can be written in terms of the variable $z_t$ defined by Eq. (3.47).

$$\int_{z_c}^{z_g} \Delta T_{wp}(z, t_p) dz = \int_0^{z_g - z_c} \Delta T_{wp}(z_t, t_p) dz_t = = \int_0^{z_g - z_c} \left(F^{BC}_{(DD,t)}(z_t, t_p) + F_{(DD,t)}(z_t, t_p)\right) dz_t, \quad \text{(B.15)}$$

where $F^{BC}_{(DD,t)}$ and $F_{(DD,t)}$ are functions defined by Eqs. (3.52) and (3.57), respectively.

The integrals in Eq. (B.15) are definite integrals and can be easily solved. Let the corresponding of values of $\mathrm{W}^{BC}_{(DD,t)}$ and $\mathrm{W}_{(DD,t)}$ be defined by:

$$\mathrm{W}^{BC}_{(DD,t)}\left((z_g - z_c), t_p\right) = \int_0^{z_g - z_c} F^{BC}_{(DD,t)}(z_t, t_p) dz_t, \quad \text{(B.16)}$$

and

$$\mathrm{W}_{(DD,t)}\left((z_g - z_c), t_p\right) = \int_0^{z_g - z_c} F_{(DD,t)}(z_t, t_p) dz_t. \quad \text{(B.17)}$$

Following the same idea as in the temperature solution, $\mathrm{W}^{BC}_{(DD,t)}$ depends on the boundary condition and $\mathrm{W}_{(DD,t)}$ does not.

The assumption made in Eq. (B.8) will also be adopted in this case and the calculation of $\mathrm{W}_{(DD,t)}$ is analogous to the production-casing result, with the substitution of the variable $z$ for the variable $z_t$ and tubing properties:

$$\begin{aligned}
&\mathrm{W}_{(DD,t)}\left(\left(z_g - z_c\right), t_p\right) = \\
&= \left\{ -\frac{1}{2L_{\beta t}^3}\left( \Theta\left(t_p - \frac{\left(z_g - z_c\right)}{a_t}\right) e^{-a_t t_p L_{\beta t}} \right.\right. \\
&\times \left[ \Omega\left( \left( \left(a_t t_p - \left(z_g - z_c\right)\right) L_{\beta t}\right)^2 \right.\right. \\
&+ 2\left( \left(a_t t_p - \left(z_g - z_c\right)\right) L_{\beta t}\right) - 2e^{\left( \left(a_t t_p - \left(z_g - z_c\right)\right) L_{\beta t}\right)} \\
&\left.\left. + 2\right) + 2\psi L_{\beta t} \right. \\
&\times \left.\left( \left(a_t t_p - \left(z_g - z_c\right)\right) L_{\beta t} - e^{\left( \left(a_t t_p - \left(z_g - z_c\right)\right) L_{\beta t}\right)} + 1 \right)\right] \\
&- \left( e^{-a_t t_p L_{\beta t}} \left( \Omega\left( \left(a_t t_p L_{\beta t}\right)^2 + 2a_t t_p L_{\beta t} - 2e^{a_t t_p L_{\beta t}} \right.\right.\right. \\
&\left.\left.\left. + 2\right) + 2\psi L_{\beta t}\left(a_t t_p L_{\beta t} - e^{a_t t_p L_{\beta t}} + 1\right)\right)\right)\Bigg\} \\
&+ \left\{ \frac{\left(z_g - z_c\right) e^{-a_t t_p L_{\beta t}}}{2L_{\beta t}^2} \left( \Omega\left( \left(2 - \left(z_g - z_c\right) L_{\beta t}\right) e^{a_t t_p L_{\beta t}} \right.\right.\right. \\
&- 2a_t t_p L_{\beta t} + \left(z_g - z_c\right) L_{\beta t} - 2\Big) \\
&\left.\left.\left. + 2\psi L_{\beta t}\left(e^{a_t t_p L_{\beta t}} - 1\right)\right)\right\}.
\end{aligned} \tag{B.18}$$

Regarding $\mathrm{W}_{(DD,t)}^{BC}$, it is convenient to split the expression into the following sum:

$$\begin{aligned}
&\mathrm{W}_{(DD,t)}^{BC}\left(\left(z_g - z_c\right), t_p\right) = \\
&= \mathrm{w}1_{(DD,t)}^{BC}\left(\left(z_g - z_c\right), t_p\right) + \mathrm{w}2_{(DD,t)}^{BC}\left(\left(z_g - z_c\right), t_p\right) \\
&+ \mathrm{w}3_{(DD,t)}^{BC}\left(\left(z_g - z_c\right), t_p\right) + \mathrm{w}4_{(DD,t)}^{BC}\left(\left(z_g - z_c\right), t_p\right),
\end{aligned} \tag{B.19}$$

where

$$\mathrm{w}_{1_{(DD,t)}}^{BC}\left(\left(z_g - z_c\right), t_p\right) = \int_0^{z_g - z_c} f_{1_{(DD,t)}}^{BC}\left(z_t, t_p\right) dz_t, \tag{B.20}$$

$$\mathrm{w}_{2_{(DD,t)}}^{BC}\left(\left(z_g - z_c\right), t_p\right) = \int_0^{z_g - z_c} f_{2_{(DD,t)}}^{BC}\left(z_t, t_p\right) dz_t, \tag{B.21}$$

$$\mathrm{w}_{3_{(DD,t)}}^{BC}\left(\left(z_g - z_c\right), t_p\right) = \int_0^{z_g - z_c} f_{3_{(DD,t)}}^{BC}\left(z_t, t_p\right) dz_t, \tag{B.22}$$

and

$$\mathrm{w}_{4_{(DD,t)}}^{BC}\left(\left(z_g - z_c\right), t_p\right) = \int_0^{z_g - z_c} f_{4_{(DD,t)}}^{BC}\left(z_t, t_p\right) dz_t. \tag{B.23}$$

The functions $f_{1(DD,t)}^{BC}$, $f_{2(DD,t)}^{BC}$, $f_{3(DD,t)}^{BC}$ and $f_{4(DD,t)}^{BC}$ are defined by Eqs. (3.53) through (3.56).

The corresponding values of $\mathrm{w}_{1_{(DD,t)}}^{BC}$, $\mathrm{w}_{2_{(DD,t)}}^{BC}$, $\mathrm{w}_{3_{(DD,t)}}^{BC}$ and $\mathrm{w}_{4_{(DD,t)}}^{BC}$ are given by, respectively,

$$\begin{aligned}
&\mathrm{w}_{1_{(DD,t)}}^{BC}\left(\left(z_g - z_c\right), t_p\right) = \\
&= \frac{a_t \Omega}{L_{\beta c}\left(a_c L_{\beta c} - a_t L_{\beta t}\right)^2} \Bigg\{ \Theta\left(t_p - \frac{\left(z_g - z_c\right)}{a_t} - \frac{z_c}{a_c}\right) \\
&\times e^{\left(-a_t t_p L_{\beta t} - L_{\beta c} z_c\right)} \Bigg( e^{-\left(z_g - z_c\right) L_{\beta t} + a_t t_p L_{\beta t} + L_{\beta c} z_c - a_c\left(t_p - \frac{\left(z_g - z_c\right)}{a_t}\right) L_{\beta c}} \\
&\times \left( a_c^2 \left( t_p - \frac{\left(z_g - z_c\right)}{a_t} \right) L_{\beta c} + a_c - a_t a_c \left( t_p - \frac{\left(z_g - z_c\right)}{a_t} \right) L_{\beta t} \right) \\
&+ e^{\frac{a_t L_{\beta t} z_c}{a_c}} \left(-a_c - a_c L_{\beta c} z_c + a_t L_{\beta t} z_c\right) \Bigg) \\
&- \Bigg[ \Theta\left(t_p - \frac{z_c}{a_c}\right) e^{\left(-a_t t_p L_{\beta t} - L_{\beta c} z_c\right)} \\
&\times \Bigg( e^{a_t t_p L_{\beta t} + L_{\beta c} z_c - a_c t_p L_{\beta c}} \left(a_c^2 t_p L_{\beta c} + a_c - a_t a_c t_p L_{\beta t}\right) \\
&+ e^{\frac{a_t L_{\beta t} z_c}{a_c}} \left(-a_c - a_c L_{\beta c} z_c + a_t L_{\beta t} z_c\right) \Bigg) \Bigg] \Bigg\},
\end{aligned} \tag{B.24}$$

$$w_{2(DD,t)}^{BC}\left((z_g - z_c), t_p\right) =$$

$$= \frac{\Omega}{L_{\beta c}^2 L_{\beta t}\left(a_t L_{\beta t} - a_c L_{\beta c}\right)} \Bigg\{ \Theta\left(t_p - \frac{(z_g - z_c)}{a_t} - \frac{z_c}{a_c}\right)$$

$$\times e^{\left(-a_t t_p L_{\beta t} - a_c\left(t_p - \frac{(z_g - z_c)}{a_t}\right) L_{\beta c} - L_{\beta c} z_c\right)}$$

$$\times \Bigg( a_t L_{\beta t} \Bigg( -L_{\beta c} z_c e^{\frac{a_t L_{\beta t} z_c}{a_c} + a_c\left(t_p - \frac{(z_g - z_c)}{a_t}\right) L_{\beta c}}$$

$$+ e^{a_t\left(t_p - \frac{(z_g - z_c)}{a_t}\right) L_{\beta t} + a_c\left(t_p - \frac{(z_g - z_c)}{a_t}\right) L_{\beta c}}$$

$$+ \left(L_{\beta c} z_c - 1\right) e^{a_t\left(t_p - \frac{(z_g - z_c)}{a_t}\right) L_{\beta t} + z_c L_{\beta c}} \Bigg)$$

$$- a_c L_{\beta c} e^{a_c\left(t_p - \frac{(z_g - z_c)}{a_t}\right) L_{\beta c}}$$

$$\times \left( e^{a_t\left(t_p - \frac{(z_g - z_c)}{a_t}\right) L_{\beta t}} - e^{\frac{a_t L_{\beta t} z_c}{a_c}} \right) \Bigg)$$

$$- \Bigg[ e^{\left(-a_t t_p L_{\beta t} - a_c t_p L_{\beta c} - L_{\beta c} z_c\right)} \Theta\left(t_p - \frac{z_c}{a_c}\right)$$

$$\times \Bigg( a_t L_{\beta t} \Bigg( -L_{\beta c} z_c e^{\frac{a_t L_{\beta t} z_c}{a_c} + a_c t_p L_{\beta c}} + e^{a_t t_p L_{\beta t} + a_c t_p L_{\beta c}}$$

$$+ \left(L_{\beta c} z_c - 1\right) e^{a_t t_p L_{\beta t} + z_c L_{\beta c}} \Bigg)$$

$$- a_c L_{\beta c} e^{a_c t_p L_{\beta c}} \left( e^{a_t t_p L_{\beta t}} - e^{\frac{a_t L_{\beta t} z_c}{a_c}} \right) \Bigg) \Bigg] \Bigg\}, \tag{B.25}$$

$$
\begin{aligned}
&\mathrm{w}_{3(DD,t)}^{BC}\left(\left(z_g - z_c\right), t_p\right) = \\
&= \frac{1}{L_{\beta c} L_{\beta t}\left(a_t L_{\beta t} - a_c L_{\beta c}\right)} \Bigg\{ \Theta\left(t_p - \frac{\left(z_g - z_c\right)}{a_t} - \frac{z_c}{a_c}\right) \\
&\times e^{\left(-a_t t_p L_{\beta t} - L_{\beta c} z_c\right)} \Bigg( a_c L_{\beta c}\left(L_{\beta c} \Delta T_{sf}\left(t_p\right) - \psi\right) \\
&\times \left( e^{a_t\left(t_p - \frac{\left(z_g - z_c\right)}{a_t}\right) L_{\beta t}} - e^{\frac{a_t L_{\beta t} z_c}{a_c}} \right) \\
&+ a_t L_{\beta t} \Bigg( \left(\psi - L_{\beta c} \Delta T_{sf}\left(t_p\right)\right) e^{\left(a_t\left(t_p - \frac{\left(z_g - z_c\right)}{a_t}\right) L_{\beta t}\right)} \\
&+ L_{\beta c} \Delta T_{sf}\left(t_p\right) e^{\frac{a_t L_{\beta t} z_c}{a_c}} \\
&- \psi e^{\left(a_t\left(t_p - \frac{\left(z_g - z_c\right)}{a_t}\right) L_{\beta t} + z_c L_{\beta c} - a_c\left(t_p - \frac{\left(z_g - z_c\right)}{a_t}\right) L_{\beta c}\right)} \Bigg) \Bigg) \\
&- \Bigg[ \Theta\left(t_p - \frac{z_c}{a_c}\right) e^{\left(-a_t t_p L_{\beta t} - L_{\beta c} z_c\right)} \\
&\times \Bigg( a_c L_{\beta c}\left(L_{\beta c} \Delta T_{sf}\left(t_p\right) - \psi\right) \left( e^{a_t t_p L_{\beta t}} - e^{\frac{a_t L_{\beta t} z_c}{a_c}} \right) \\
&+ a_t L_{\beta t} \Bigg( \left(\psi - L_{\beta c} \Delta T_{sf}\left(t_p\right)\right) e^{\left(a_t t_p L_{\beta t}\right)} \\
&+ L_{\beta c} \Delta T_{sf}\left(t_p\right) e^{\frac{a_t L_{\beta t} z_c}{a_c}} \\
&- \psi e^{\left(a_t t_p L_{\beta t} + z_c L_{\beta c} - a_c t_p L_{\beta c}\right)} \Bigg) \Bigg) \Bigg] \Bigg\},
\end{aligned}
\tag{B.26}
$$

and

$$
\begin{aligned}
&\mathrm{w}4_{(DD,t)}^{BC}\left(\left(z_g - z_c\right), t_p\right) = \\
&= \frac{1}{L_{\beta c}^2 L_{\beta t}\left(a_c L_{\beta c} - a_t L_{\beta t}\right)^2}\Bigg\{\Theta\left(t_p - \frac{z_g - z_c}{a_t}\right) \\
&\times e^{-a_t t_p L_{\beta t} - a_c\left(t_p - \frac{z_g - z_c}{a_t}\right)L_{\beta c}}\Bigg(-a_t^2 L_{\beta t}^2 e^{a_t\left(t_p - \frac{z_g - z_c}{a_t}\right)L_{\beta t}}\Bigg(e^{a_c\left(t_p - \frac{z_g - z_c}{a_t}\right)L_{\beta c}} \\
&- 1\Bigg)\left(-\Omega L_{\beta c} z_c + \Omega + \psi L_{\beta c}\right) + a_c^2 L_{\beta c}^2 \\
&\times\Bigg(-\left(-\Omega L_{\beta c} z_c + \Omega + \psi L_{\beta c}\right)e^{a_t\left(t_p - \frac{z_g - z_c}{a_t}\right)L_{\beta t} + a_c\left(t_p - \frac{z_g - z_c}{a_t}\right)L_{\beta c}} \\
&- a_t\left(t_p - \frac{z_g - z_c}{a_t}\right)\Omega L_{\beta t} e^{a_t\left(t_p - \frac{z_g - z_c}{a_t}\right)L_{\beta t}} \\
&+ e^{a_c\left(t_p - \frac{z_g - z_c}{a_t}\right)L_{\beta c}}\left(-\Omega L_{\beta c} z_c + \Omega + \psi L_{\beta c}\right)\Bigg) \\
&+ a_t a_c L_{\beta c} L_{\beta t}\Bigg(2\left(-\Omega L_{\beta c} z_c + \Omega + \psi L_{\beta c}\right) \\
&\times e^{a_t\left(t_p - \frac{z_g - z_c}{a_t}\right)L_{\beta t} + a_c\left(t_p - \frac{z_g - z_c}{a_t}\right)L_{\beta c}} \\
&+ e^{a_t\left(t_p - \frac{z_g - z_c}{a_t}\right)L_{\beta t}}\left(\Omega\left(a_t\left(t_p - \frac{z_g - z_c}{a_t}\right)L_{\beta t} + L_{\beta c} z_c - 2\right) - \psi L_{\beta c}\right) \\
&+ L_{\beta c}\left(-e^{a_c\left(t_p - \frac{z_g - z_c}{a_t}\right)L_{\beta c}}\right)(\psi - \Omega z_c)\Bigg)\Bigg) \\
&- \Big[e^{-a_t t_p L_{\beta t} - a_c t_p L_{\beta c}} \\
&\times\Big(-a_t^2 L_{\beta t}^2 e^{a_t t_p L_{\beta t}}\left(e^{a_c t_p L_{\beta c}} - 1\right)\left(-\Omega L_{\beta c} z_c + \Omega + \psi L_{\beta c}\right) \\
&+ a_c^2 L_{\beta c}^2\Big(-\left(-\Omega L_{\beta c} z_c + \Omega + \psi L_{\beta c}\right)e^{a_t t_p L_{\beta t} + a_c t_p L_{\beta c}} \\
&- a_t t_p \Omega L_{\beta t} e^{a_t t_p L_{\beta t}} + e^{a_c t_p L_{\beta c}}\left(-\Omega L_{\beta c} z_c + \Omega + \psi L_{\beta c}\right)\Big) \\
&+ a_t a_c L_{\beta c} L_{\beta t}\Big(2\left(-\Omega L_{\beta c} z_c + \Omega + \psi L_{\beta c}\right)e^{a_t t_p L_{\beta t} + a_c t_p L_{\beta c}} \\
&+ e^{a_t t_p L_{\beta t}}\left(\Omega\left(a_t t_p L_{\beta t} + L_{\beta c} z_c - 2\right) - \psi L_{\beta c}\right) \\
&+ L_{\beta c}\left(-e^{a_c t_p L_{\beta c}}\right)(\psi - \Omega z_c)\Big)\Big)\Big]\Bigg\}.
\end{aligned}
\tag{B.27}
$$

The constant pipe-length cased-tubing solution is given by Eq. (4.16).

## B.3. Cased-Tubing Solution: Variable Pipe Length

If the tubing string comprises expansion joints, the expression for the pressure exerted by the wellbore-fluid column between the gauge and the producing horizon during buildup is given by

$$p_{f,a}(z_g, \Delta t) = \int_0^{z_g + \Delta L(\Delta t)} \gamma_o(z, \Delta t) \sin\theta \, dz, \tag{B.28}$$

where $\Delta L(\Delta t)$ is the change in tubing length over the shut-in time, which depends on temperature changes, and $z_g$ is the gauge location at the end of the flowing period. The subscript $a$ refers to the adjustable gauge location.

The expression for the fluid specific weight during buildup is given by

$$\gamma_o(z, \Delta t) = \gamma_{oi} - \gamma_{oi}\beta_o \Delta T_{ws}(z, \Delta t) + \gamma_{oi}\beta_o z g_G \sin\theta. \tag{B.29}$$

The combination of Eqs. (B.28) and (B.29) yields

$$\begin{aligned} p_{f,a}(z_g, \Delta t) = {} & \left(z_g + \Delta L(\Delta t)\right)\gamma_{oi} \sin\theta \\ & - \beta_o \gamma_{oi} \sin\theta \int_0^{z_g + \Delta L(\Delta t)} \Delta T_{ws}(z, \Delta t) dz \\ & + \frac{\left(z_g + \Delta L(\Delta t)\right)^2}{2} \gamma_{oi}\beta_o g_G (\sin\theta)^2. \end{aligned} \tag{B.30}$$

The pressure at the gauge during buildup is given by the combination of Eqs. (4.1) and (B.30)

$$\begin{aligned} p_{g,a}(z_g, \Delta t) = {} & p_{sf}(\Delta t) - \left(z_g + \Delta L(\Delta t)\right) \sin\theta \, \gamma_{oi} \\ & + \beta_o \gamma_{oi} \sin\theta \int_0^{z_g + \Delta L(\Delta t)} \Delta T_{ws}(z, \Delta t) dz \\ & - \frac{\left(z_g + \Delta L(\Delta t)\right)^2}{2} \gamma_{oi}\beta_o g_G (\sin\theta)^2. \end{aligned} \tag{B.31}$$

Eq. (B.31) is equal to Eq. (1.3) for the buildup period, where the integral of mass density has been converted into an integral of the wellbore-temperature distribution. The solution of Eq. (B.31) is the main objective of this work.

Eq. (B.31) can be rearranged as

$$p_{g,a}(z_g,\Delta t) = p_{sf}(\Delta t) - z_g\gamma_{oi}\sin\theta + \beta_o\gamma_{oi}\sin\theta\int_0^{z_g}\Delta T_{ws}(z,\Delta t)dz$$
$$-\frac{z_g^2}{2}\gamma_{oi}\beta_o g_G(\sin\theta)^2 - \gamma_{oi}\Delta L(\Delta t)\sin\theta$$
$$+\beta_o\gamma_{oi}\sin\theta\int_{z_g}^{z_g+\Delta L(\Delta t)}\Delta T_{ws}(z,\Delta t)dz$$
$$-\frac{\left(2z_g\Delta L(\Delta t)+\Delta L^2(\Delta t)\right)}{2}\gamma_{oi}\beta_o g_G(\sin\theta)^2. \quad \text{(B.32)}$$

The first four terms in the RHS of Eq. (B.32) comprise the solution for the constant pipe-length configuration. It is interesting to note that the solution for the variable pipe-length configuration can be written as a function of the constant length solution.

Let the impact on pressure due to the tubing contraction be defined by:

$$\Delta p_{cont}(z_g,\Delta t) = \gamma_{oi}\Delta L(\Delta t)\sin\theta$$
$$-\beta_o\gamma_{oi}\sin\theta\int_{z_g}^{z_g+\Delta L(\Delta t)}\Delta T_{ws}(z,\Delta t)dz$$
$$+\Delta L(\Delta t)\frac{\left(2z_g+\Delta L(\Delta t)\right)}{2}\gamma_{oi}\beta_o g_G(\sin\theta)^2. \quad \text{(B.33)}$$

Then, Eq. (B.32) can be written as

$$p_{g,a}(z_g,\Delta t) = p_g(z_g,\Delta t) - \Delta p_{cont}(z_g,\Delta t), \quad \text{(B.34)}$$

where $p_g(z_g,\Delta t)$ is the solution for the constant pipe-length configuration, given by Eq. (4.9).

The expression for an adjustable gauge location in a cased tubing is obtained by combining Eqs. (4.8), (4.16) and (B.34):

$$\Delta p_{gt,a}(z_g,\Delta t) = \Delta p_{sf}(\Delta t) - \Delta p_{ft}(z_g,\Delta t) - \Delta p_{cont}(z_g,\Delta t), \quad \text{(B.35)}$$

where $\Delta p_{sf}(\Delta t)$ is the sandface pressure and $\Delta p_{f_t}(z_g,\Delta t)$ is the solution for the static-fluid pressure difference between a fixed gauge location and the producing horizon in a cased tubing, given by Eq. (4.17).

Regarding Eq. (B.33), solving the integral is not an easy task due to the implicit relation between the upper limit and the integrand. Nevertheless, a reasonable simplification can be assumed, since the change in tubing length is small when compared to $z_g$:

$$z_g + \Delta L(\Delta t) \approx z_g. \quad \text{(B.36)}$$

This assumption discards the need for iterative methods to solve the integral in Eq. (B.33). Therefore, the expression for $\Delta p_{cont}$ can be written as

$$\Delta p_{cont}(z_g, \Delta t) = \Delta L(\Delta t)\left(\gamma_{oi} \sin\theta + \gamma_{oi} z_g \beta_o g_G (\sin\theta)^2\right). \quad \text{(B.37)}$$

In Eq. (B.37), the term $\Delta L(\Delta t)$ carries the necessary information to describe the transient change in pipe length and the term $z_g$ anchors the spatial location of the contraction.

The next section provides an analytical expression for $\Delta L(\Delta t)$.

## B.4. Change in Pipe Length: Tubing Contraction during Buildup

Sidorova et al. (2014) provided a discrete solution for evaluating the effect of tubing contraction, where the wellbore is divided into discrete sections of equal length and the transient temperature profiles are obtained from a numerical simulator.

Among other contributions, this work presents a continuous, fully analytical and easy to compute solution for the transient tubing contraction $\Delta L(\Delta t)$.

For a uniform heating during drawdown and a uniform cooling during buildup, the classical expression for change in tubing length can be written as (assuming negligible effect of pressure)

$$\Delta L = L_0 \alpha_{LTE} \Delta T_{ave}, \quad \text{(B.38)}$$

where $L_0$ is the pipe length at the moment of shut-in between the gauge and a given fixed point, $\alpha_{LTE}$ is the tubing linear thermal expansion coefficient and $\Delta T_{ave}$ is the average change in temperature.

In this work, both heating and cooling effects are not uniform. Moreover, there is the need to describe the transient behavior, especially during the buildup period. In the integral form, the tubing contraction due to the cooling effect in a buildup period is given by

$$\Delta L(\Delta t) = \alpha_{LTE} \int_0^{L_0} \left[T_{wp}(z_t, t_p) - T_{ws}(z_t, \Delta t)\right] dz_t \,, \quad \text{(B.39)}$$

where $T_{wp}(z_t, t_p)$ is the wellbore-temperature distribution prior to shut-in and $T_{ws}(z_t, \Delta t)$ is the temperature during buildup. The variable $z_t$ is defined by Eq. (3.47).

The expression in Eq. (B.39) is a continuous formulation of the discrete expression proposed by Sidorova et al. (2014). Furthermore, the integrand in Eq. (B.39) can be written in terms of the previously derived analytical solutions in this work, $\Delta T_{wp}$ and $\Delta T_{ws}$:

$$T_{wp}(z_t, t_p) - T_{ws}(z_t, \Delta t) = \Delta T_{wp}(z_t, t_p) - \Delta T_{ws}(z_t, \Delta t). \tag{B.40}$$

Therefore, Eq. (B.39) can be rewritten as

$$\Delta L(\Delta t) = \alpha_{LTE} \int_0^{L_0} \left[\Delta T_{wp}(z_t, t_p) - \Delta T_{ws}(z_t, \Delta t)\right] dz_t \, . \tag{B.41}$$

For the buildup zero-rate case, a similar integral has already been addressed in this work. Following the same steps used in Eqs. (B.11) through (B.14), the change in pipe length expressed in Eq. (B.41) can be written as

$$\begin{aligned}\Delta L(\Delta t) = {} & \alpha_{LTE}\,(1 - e^{-\Delta t a_t L_{Rt}}) \int_0^{L_0} \Delta T_{wp}(z_t, t_p) dz_t \\ & - \alpha_{LTE} \Delta T_{sf}(0^+) e^{-\Delta t a_t L_{Rt}} L_0.\end{aligned} \tag{B.42}$$

The definite integral in Eq. (B.42) is the same integral presented in Eq. (B.15), except for a different upper limit of integration. The solution of Eq. (B.42) is given by

$$\begin{aligned}\Delta L(\Delta t) = {} & \alpha_{LTE}\,(1 - e^{-\Delta t a_t L_{Rt}}) \\ & \times \left[\mathrm{W}_{(DD,t)}(L_0, t_p) + \mathrm{W}^{BC}_{(DD,t)}(L_0, t_p)\right] \\ & - \alpha_{LTE} \Delta T_{sf}(0^+) e^{-\Delta t a_t L_{Rt}} L_0,\end{aligned} \tag{B.43}$$

where the values of $\mathrm{W}^{BC}_{(DD,t)}$ and $\mathrm{W}_{(DD,t)}$ are obtained from Eqs. (B.18) and (B.19) by substituting the value of $(z_g - z_c)$ for $L_0$.

As mentioned before, the solution for $\Delta L(\Delta t)$ in Eq. (B.43) is fully analytical and continuous. Finally, the tubing contraction impact on pressure is given by the combination of Eqs. (B.37) and (B.43)

$$\begin{aligned}\Delta p_{cont}(z_g, \Delta t) = {} & \left(\gamma_{oi} \sin\theta + \gamma_{oi} z_g \beta_o g_G (\sin\theta)^2\right) \\ & \times \left\{\alpha_{LTE}\,(1 - e^{-\Delta t a_t L_{Rt}}) \left[\mathrm{W}_{(DD,t)}(L_0, t_p)\right.\right. \\ & \left.\left. + \mathrm{W}^{BC}_{(DD,t)}(L_0, t_p)\right] - \alpha_{LTE} \Delta T_{sf}(0^+) e^{-\Delta t a_t L_{Rt}} L_0\right\}.\end{aligned} \tag{B.44}$$

The variable pipe-length cased-tubing solution is given by Eq. (4.22).